Possibility of Positive-Pulse Switching in Systems of Nonlinear Fabry-Perot Cavities

by

Kwongchoi Caisy Ho

Dissertation submitted to the faculty of the
Virginia Polytechnic Institute and State University
in partial fulfillment of the requirements for the degree of

DOCTOR OF PHILOSOPHY

in

Physics

APPROVED:

Prof. Guy Indebetouw, Chairman

Prof. R. Arndt

Prof. T. C. Poon

Prof. L. D. Roper

Prof. R. Zallen

December, 1991

Blacksburg, Virginia

Possibility of Positive Pulse Switching in Systems of Nonlinear Fabry-Perot Cavities

by

Kwongchoi Caisy Ho

Committee Chairman: Prof. Guy Indebetouw

Department of Physics

(ABSTRACT)

The conventional way of using a nonlinear Fabry-Perot cavity as an optical memory requires a negative pulse input to reset the state of the cavity. The possibility of using positive pulses to turn a system of nonlinear Fabry-Perot cavities on and off is studied and it was found that positive pulse switching is possible in a system of two coupled nonlinear cavities.

First, Korpel and Lohmann's proposal of using polarization switching in a single nonlinear birefringent cavity was studied. After a detailed investigation of their proposal it was found that positive pulse switching in a single nonlinear Fabry-Perot cavity is not possible. One of the reasons is that the eigen-polarization states of the output of a nonlinear Fabry-Perot cavity cannot be switched independently. Although it is not possible to switch a single nonlinear Fabry-Perot cavity with positive pulses we were able to use the coupling of the eigen-polarization states to implement other kinds of optical switches which were demonstrated experimentally. The cross-talk effect in a metallic Fabry-Perot cavity was also studied.

Next, a steady state model of a system of two coupled nonlinear Fabry-Perot cavities was developed and it was found that positive pulse switching is possible in such a system. The output can be turned on and off either by pulses sent into different cavities or by pulses of different magnitudes sent into one cavity.

Finally, the dynamic behavior of the coupled cavities system was modeled by extending Goldstone and Garmire's model of a single cavity with one input to a system of two coupled cavities with two inputs. We verified by numerical calculations that positive pulse switching is also possible in the dynamic regime.

ACKNOWLEDGEMENTS

It is with deep gratitude that I wish to take this space to thank all the people who have been instrumental in helping me directly and indirectly with the research and the write up of this dissertation. I am indebted to them for all the help they provided in making this dissertation possible.

I would like first to thank my mentor and advisor Prof. Guy Indebetouw for the years of support and encouragement that make up the background of this writing. His knowledge is only surpassed by his willingness to share it and his devotion to his students. His wide knowledge has greatly influenced the substance of these pages. His patience and diligence in the labor of correcting earlier and later drafts have been much appreciated.

I would also like to thank Prof. Ting-chung Poon for being a supportive friend to me and serve in my committe, Prof. Dave Roper and Prof. Dick Arndt in the early phase of the learning of numerical computation and Prof. Dick Zallen for the sharp and constructive criticisms.

I am also thankful to Prof. Jerome Long and Prof. Larry Burton for letting me use their vacuum deposition facility. During my stay at Virginia Tech many fine people in the machine shop and in the electronic shop helped me made my equipment and the electronics that was needed.

My appreciation also goes to Peter Lo my colleage and my brother in Christ for his encouragment and his support in prayer.

I would like to thank my host parents Joseph and June Rieley, my spiritual parents Prof. Y.A.Liu and Dr. Hinghar Lo for their kindness and support.

I would like to express my sincere gratitude to my mom for her many years of support during my stay in Blacksburg. Her selfless love kept me going during difficult times. I would also like to thank my brother Patrick for his support in prayer and encouragment.

My deepest appreciation goes to my wife Sonya. She has not failed to shore up my sagging spirits time and again over these long months. It is to her that I dedicate this work.

Finally, I would first like to thank Christ my Lord and Savior for coming to this world to die on the cross for all mankind. He has sustained me ever since I came to know Him. He has provided all my needs and loved me with His unfailing love. Thank you Father!

TABLE OF CONTENTS

LIST OF FIGURES

Chapter 1

Introduction

Since the first demonstration of optical bistability in sodium vapor by McCall in 1974 [1], optical bistability has become a rapidly expanding field of research. A large amount of work has been done to study this phenomenon because of its potential application to all-optical logics. The intrinsic capability of parallel processing and the ultra fast switching speed it may offer attracts much attention [2]. Together with the present state of development of solid state lasers, fiber optics communication and integrated optics technology, an optical computer using millions of optical bistable elements with a speed ten thousand times faster than our present super computers is not inconceivable.

In addition to the vast amount of work that has been done in searching for the 'ideal' nonlinear material, there are many other aspects of such an optical computer that need to be investigated.

Several different tiny optical bistable elements using a variety of nonlinear effects in different materials have been demonstrated [3, 4, 5, 6]. It is difficult at this stage to determine which material could become the 'Silicon' of the future optical computer. Using a Fabry-Perot etalon filled with a nonlinear medium is one of the possible ways to construct an optical logic element. It has been shown that this device can perform different logic operations, transistor operation as well as limiter operation [3]. A

bistable nonlinear Fabry-Perot cavity can also be used as a memory element in an optical circuit.

In this dissertation, the possibility of utilizing bistable nonlinear Fabry-Perot cavities to implement memory elements in an optical circuit that is compatible with the present logic operation schemes is analyzed.

1.1 Types of Optical Bistability

A system is said to be optically bistable if it has two stable output states I_t for the same value of the input I_i over some range of input values. A characteristic curve for an optical bistable system is shown in Fig.1.1. There are two output states for one input intensity between I_d and I_u. The system is said to be bistable within this region. The output not only depends on the magnitude of the input but also depends on the history of the input. It is obvious that to be bistable the system must be nonlinear but this is not sufficient for bistability. The necessary condition for bistability is that the system has to be nonlinear with some feedback. It is the feedback that permits a multi-valued output.

Optical bistability can be classified as absorptive or dispersive depending on whether the feedback occurs by way of an intensity-dependent absorption or by way of an intensity-dependent refractive index.

1.1.1 Absorptive Optical Bistability

A simple system exhibiting optical bistability can be made of a Fabry-Perot etalon filled with a saturable absorber. This etalon is initially tuned to a maximum transmission. For a weak input intensity, the intra-cavity absorption spoils the finesse of the cavity even though the frequency of the radiation coincides with the cavity resonance frequency. This results in a low value of the transmitted intensity as long as the intra-cavity intensity is smaller than the saturation intensity of the medium. As the

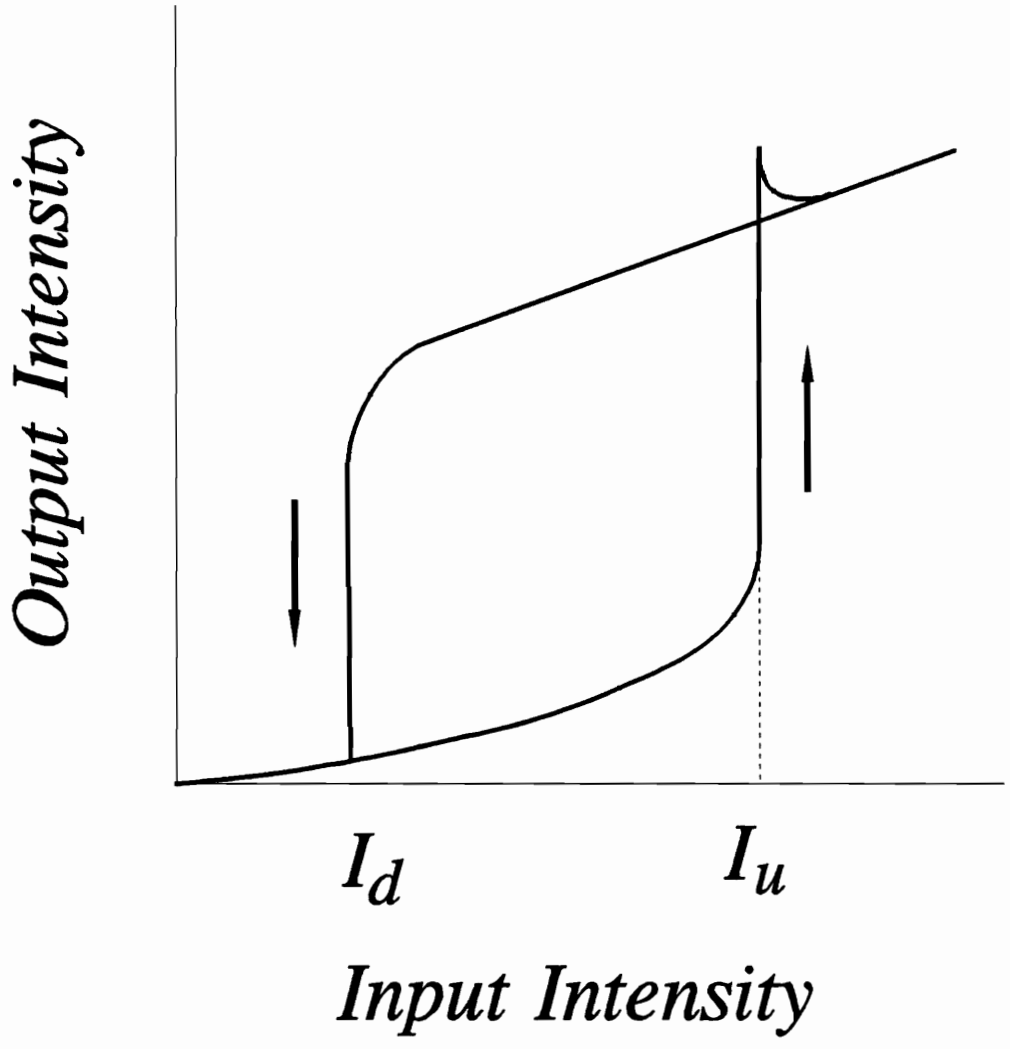

Figure 1.1: Characteristic response of an optical bistable system. There are two stable output states for one input value between I_d and I_u. The system is said to be bistable within this region

input intensity increases and becomes close to the value of the saturation intensity, the medium starts to bleach. The population of the lower level of the transition involved is depleted and the upper level population saturates, thus reducing the absorption coefficient at the resonance frequency. This leads to an increase in the finesse of the cavity resulting in an increase in the transmitted intensity. This transmitted intensity is then fed back by the end mirrors into the medium which further promotes the bleaching of the medium. Again this increases the transmitted intensity and bleaches the medium some more. The end result of this runaway effect is a sudden increase in the transmitted intensity via the rapid restoration of the finesse of the etalon. The mirrors act as a positive feedback for the medium.

A typical response curve of absorptive bistability in a GaAs etalon is shown in Fig.1.2 [7]. As the input power approaches 90mW, the absorption of the medium is close to saturation. Thus, increasing the input intensity further results in a rapid increase in the output intensity. This also increases the intensity fed back into the cavity by the mirrors of the etalon, bringing the medium even closer to saturation. Eventually a runaway effect occurs, as indicated by the rapid change in the output intensity. Decreasing the input power does not cause the output to drop immediately. As the power starts to decrease, the medium is still bleached which means that the cavity is still in a high transmission state. At some point where the intensity inside the cavity is not able to sustain the bleaching of the medium, the output power switches rapidly to a low value.

Different materials have been used as the nonlinear medium in the etalon. The choice of semiconductors for practical bistable optical materials is becoming more common because semiconductors provide good absorption ($\alpha_0 L \simeq 1$) in very short ($\simeq 1\mu$m) lengths in the infra-red region (a wavelength range compatible with efficient semiconductor lasers). A short length means a short round-trip time so that the cavity-lifetime can be very short. A short length also permits tighter focusing before beam walk-off losses become significant, so that input powers and switching energies are reduced. Switching times can then be very short ($\lesssim$ps) if a fast nonlinear mech-

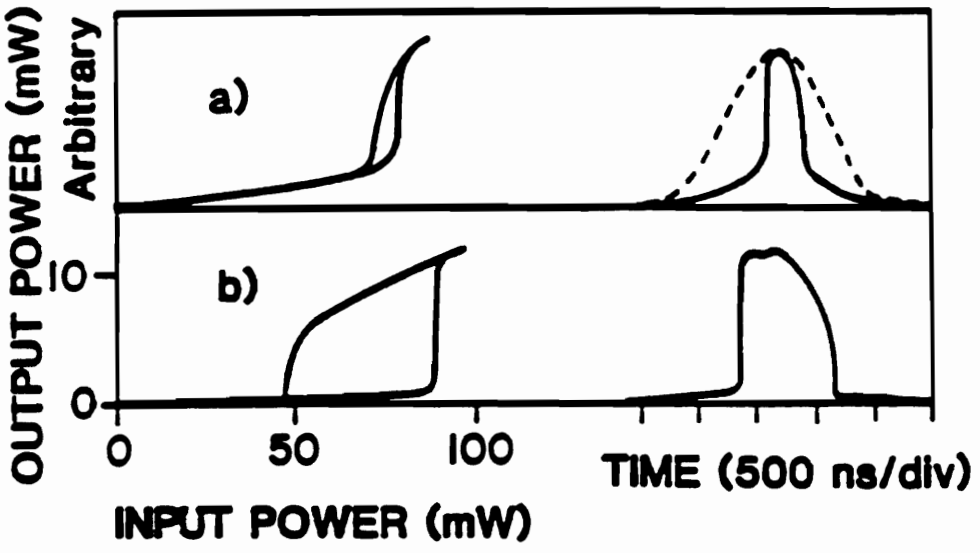

Figure 1.2: Optical bistability in GaAs etalons at 22°C with a triangularly shaped input, after Gibbs *et al* [7]. (a) Bulk GaAs, 879.9 nm. (b) multiple quantum well, 880.7 nm. The dashed line is the input, normalized to the output. The left half is the output power against the input power. Bulk GaAs shows a narrow bistable region while the multiple quantum well shows a wider bistable region. The switching time in both cases is of the order of tens of nanoseconds. The power of the curve in (b) was recorded but that of (a) was not registered.

anism is used. For example, in semiconductors the mechanism for the nonlinearity involves the narrowing of the optical band gap with increasing temperature [8]. The photon energy is chosen below the band-gap energy so that the increased temperature resulting from the absorbed power shrinks the band gap and increases the absorption and hence establishes a positive feedback mechanism [9].

Early in 1975 Gibbs *et al* had already suggest the use of GaAs as the nonlinear material of choice for optical bistable devices [1]. The first observation of bistability in GaAs was made by Gibbs [10] in 1979. Later on, from 1983 to 1985, many different semiconductor materials including CuCl [11], CdS [12], ZnS [13] and CdHgTe [14], have been used to demonstrate optical bistability.

1.1.2 Dispersive Optical Bistability

A second kind of bistability arises from the dispersive nonlinearity of a medium. Although optical bistability is classified as either absorptive or dispersive according to whether the feedback occurs by way of an intensity-dependent absorption or by way of an intensity-dependent refractive index, this distinction is clearly not sharp, since both absorptive and refractive mechanisms may be significant simultaneously. More fundamentally, they are always related [1] although the nonlinear effect caused by one of them may be much greater than the other.

As for its absorptive counterpart, a dispersive bistable system consists of a Fabry-Perot etalon filled with a medium whose refractive index varies with the intensity of the radiation. Initially the cavity can be tuned to a low transmission state near a resonance. The index of refraction of the medium depends on the total intensity inside the cavity which is proportional to the transmitted intensity. Therefore, as the radiation incident on the cavity increases, the refractive index changes. This shifts the frequency of the cavity. As the cavity resonance gets closer to the radiation

[1]The real part of the dielectric permittivity determines the index of refraction and the imaginary part determines the absorptivity of a dielectric material, one cannot change the real part of the dielectric permittivity without affecting the imaginary part. This would violate causality.

frequency, a small increase in the input intensity will result in a large change in the transmitted intensity as well as in the intensity inside the cavity. This in turn changes the refractive index of the medium by a larger amount, bringing the cavity closer yet to resonance. Eventually a runaway effect occurs. The output will then suddenly switch to a high value and will settle down at a transmitted intensity which is consistent with the change in the index of refraction of the medium.

1.2 Optical Computing

1.2.1 Present Computer Technology

The technology of computers has advanced tremendously in the past thirty years; from a giant calculator that can only do simple arithmetic to a laptop computer that can perform complicated computations in a shorter amount of time. All this was made possible because of the discovery of single-crystal silicon. As our society has become more and more dependent upon digital electronics, the demand for faster computers has become more acute. Digital signal processing has become essential in many areas. In automated processes which involve robots and machine vision, an enormous amount of information has to be processed in a very short time. The image processing speed is the limiting element of the decision making process. In dealing with digital signal processing we always have to face the high data rate requirement. It means that a huge amount of information has to be processed in a minimum amount of time. Also, there are many scientific inquire which require so much computation that it is only now with the fastest machines that we can contemplate the possibility of their investigation, e.g. nonlinear dynamical system of high dimensions.

Our present computer technology relies almost entirely on silicon-based electronics but how far can we go with electronics? Can we keep on increasing the speed of computers without limit? What is the upper limit of electronics? What is the biggest hindrance of our present electronic computer technology?

There are two factors that hold back the speed of our present electronic computers. One is the speed of electronic logic elements [15] and the other is the bottleneck in data transfer between logical units [16]. The former is due to the intrinsic response of semiconductor elements. The later is due to the architecture of our present computers.

The most common response to the demand for higher processing rate is to increase the speed of the electronics and to further miniaturize the components. Increasing the speed of the logical elements obviously increases the processing speed. Semiconductor electronic devices now can switch at a speed of 10^{-10}s and Josephson devices can switch at a higher speed of 10^{-11}s. One may be greedy enough to ask what comes next.

It is obvious that reducing the size of the components reduces the time taken for the information to be transported from one logical unit to another. The VLSI (very large scale integration) technology has gone very far in achieving this goal. However, Huang [17] has pointed out that VLSI does not solve the RC time constant problem. As the length of a wire shrinks by a factor α and the cross-sectional area of the wire is reduced by a factor of α^2, the capacitance of the wire is decreased by a factor of α while the resistance increases by the same amount. Thus the time constant remains the same, and the input charging time remains unaltered. It is independent of scaling. This delay time together with the power dissipation and surface area required by existing interconnection technology limits the performance of current VLSI systems.

1.2.2 Optical Interconnections

The standard method of computer communication in use today was suggested by John von Neumann. In this scheme, the logic unit is connected to the memory through an address device. This ingenious architecture reduces the number of interconnections between memory and logic elements thus drastically reduces the number of connections required between the logical element and the memory. The logic element can address one storage element at a time. The main goal was to miniaturize the computer unit. However, as the demand for computational speed drastically increases,

the architecture suggested by von Neumann becomes one of the biggest hindrances in the communication between the logical unit and the memory elements. This is commonly called the von Neumann bottleneck [16]. Fig.1.3 depicts this bottleneck of the communication scheme of von Neumann.

One way to solve this bottleneck problem is to address and process data in parallel. Of course this architecture requires a much larger number of interconnections between the logic units and the memory units. The ability to process information in parallel depends on the nature of the task. If the amount of information that needs to be processed in parallel is large, the increase in capacity of the system can be greatly improved. Signal processing of a two dimensional image is a good example to demonstrate the power of parallel processing. In general a task can be divided into different subtasks which are processed sequentially. Each subtask is further divided into smaller tasks which can be executed simultaneously. For example, edge enhancement of a picture can be done by first Fourier transforming the picture, then removing the low frequencies and finally performing an inverse Fourier transform. The above task can be split into three substasks, 1) Fourier transform, 2) low frequencies removal, 3) inverse Fourier transform. These tasks are done sequentially. Each subtask can however be processed separately, in parallel, i.e. the whole picture is processed at the same time instead of processing the picture pixel by pixel sequentially.

As the amount of information in each subtask increases, the requirement imposed on the processor becomes more demanding. For this reason, large vector processors and super computers are built to meet this need. All these computer facilities make use of a pipeline design in their data communication between processors. The size of the pipeline determines the amount of information that can be handled at one time. Normally, a set of data which is processed in parallel is called a vector. Different connection schemes can be used to perform different operations. For example, perfect shuffle connection scheme can perform different signal processing algorithms such as Fourier transformation, polynomial evaluation, and sorting [18]. Employing this connection scheme enables one to perform many operations without having to install

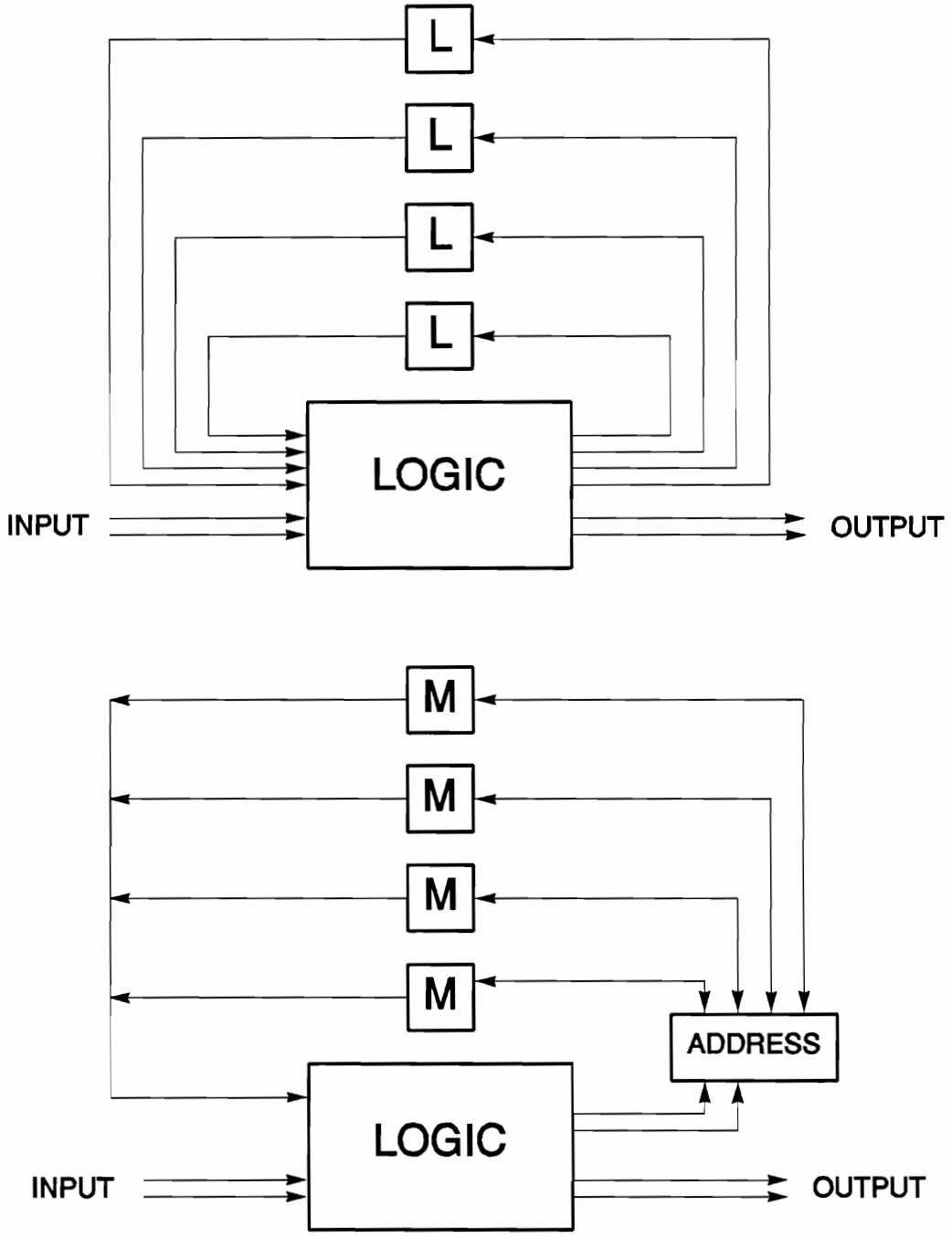

Figure 1.3: (a) Classical finite state machine not suffering from the von Neumann bottleneck, since it can update all its memory in parallel without the need for addresses. (b) Modified finite state machine suffering from the von Neumann bottleneck since it can only update one memory element at a time and consequently needs an address to do so. Note that the number of interconnections required in (a) is much higher than in (b)

extra logic units. For example, performing a Fast Fourier Transform (FFT) operation can be done entirely with hardware interconnections at a speed orders of magnitude faster than that achieved by a sequential logical processor. Of course, we cannot increase the size of the pipeline indefinitely.

The intrinsic parallelism characteristic of optics suggests a good way to increase the capacity of a computer system. Unlike electrons, photons can travel in free space without readily interacting with each other. This means that it is not necessary to guide photons with wires as it is with electrons. This reduces the number of interconnections necessary to transport photons from places to places. This intrinsic ability to address memory elements in parallel frees us from the drawback of the von Neumann addressing scheme. Because of its high bandwidth[2] , fiber optics has been widely used in communication for the past five years. Perhaps the first role for optics will be in chip-to-chip optical interconnection [15]. Goodman *et al.* [19] and Marhic [20] proposed the use of optical fibers or optical waveguides for optical connection systems. However, for large data arrays, large bundles of fibers are needed [21]. Much attention has recently been placed on free-space optics [22]. That is, each memory element is connected by light beams propagating in free-space.

1.2.3 Optical Logic Elements

Our present fiber optics communication technology has reached a mature stage and many fiber optics communication systems have been installed and are widely used, even down to the local area network (LAN) level. The data rate that an optical fiber can transmit approaches 1 THz. This rate is far beyond the capability of any presently known electronic light detector. In order to utilize this information-handling capacity, some optical signal processing will have to be performed before the light signals are converted to electronic ones.

The observation of optical bistablility has opened a new window of opportunity

[2]Bandwidth in digital communication measures the maximum data rate that a communication line/port can handle.

for optics. Namely, the exciting possibility exists of developing optical logic elements and to conceive an all optical computer. The nonlinear Fabry-Perot etalon, a Fabry-Perot etalon filled with an optically nonlinear medium, was the first proposed optical logic element. Later, different materials were used to increase the performance of the switching element. The main concerns in optimizing the elements are maximum speed and minimum switching energy. Among the media used, InSb and GaAs are the two most promising materials. The origin of their nonlinearity comes from the narrowing of the band gap due to the absorption of radiation of a suitable wavelength and subsequent heating of the material. The optical properties of the material thus change according to the amount of radiation incident on the material. The response time of such a mechanism can be very short.

Other types of media include liquid crystals, which have a nonlinear index of refraction orders of magnitude higher than that of semiconductors such as InSb and GaAs. However, since the mechanism governing the change of index of refraction is thermal or orientational, the response time of liquid crystals is orders of magnitude longer than that of the semiconductors.

Recently, a hybrid optically bistable switch which consists of a multiple quantum well structure with no mirror [23] was developed at the AT&T Bell Laboratories. This differs from the 'conventional' feedback method using mirrors in that the feedback is internal and positive. The device has a fast switching time as well as a very low switching power (30 ns with a switching energy density of 6.1 $fJ/\mu m^2$). For a $100\mu m$ sample, the switching power was 1.6mW. Another type of optical switching element was demonstrated recently, namely bistability at nonlinear interfaces [24, 25]. This also has the advantage of eliminating the mirrors required by the conventional nonlinear Fabry-Perot etalon. However, the switching power is still very high.

One certainly will ask: can we make use of the two advantages that optics can offer, namely the speed and the intrinsic ability to process data in parallel, to make a general purpose optical computer? Midwinter has compared the advantages and disadvantages of optics over electronics and concluded that it is almost inconceivable

that optics will displace electronics [15]. Also Smith has made a thorough investigation of optical switching elements [16]. He showed that optical switching could reach very high speed ($10^{-12} - 10^{-14}$s). This is much faster than present Josephson technology. This is a very exciting aspect of optical switching. However, he added, due to 'thermal transfer' and the high packaging density required for rapid operations, optical switching elements are unlikely to be used as building blocks for a general purpose computer. But this does not mean that optical switching is useless. For certain specific applications, such as the integrated-optical spectrum analyzer, and specific purpose optical computers for image processing and pattern recognition, it has been demonstrated that optics does have some advantages over general purpose digital computers [26, 27].

Much work has been done in studying different phenomena in nonlinear optical systems with feedback and in ways of implementing optical interconnections. The 'optical silicon' is yet to be found however. Research in the area of digital optical computing can be roughly divided into four areas: 1) searching for materials that can be switched with less energy, 2) finding out different ways to implement different optical interconnections, 3) putting existing elements into systems and searching for better system architectures, 4) exploring novel switching methods.

The focus of this dissertation is on the aspect of implementing optical memory elements that are compatible with present digital logic schemes.

1.3 Outline of The Dissertation

The dissertation is divided in two parts. The first part deals with the capabilities and limitations of a single optical cavity and the second part deals with a system of coupled nonlinear optical cavities.

In chapter 2, the theory of dispersive optical bistability in a nonlinear dielectric Fabry-Perot is reviewed. The normal operation of a nonlinear Fabry-Perot as an optical element is also discussed. Emphasis is put on the incompatibility of the normal

operation scheme with present digital circuitry. The need for an optical switching element that is compatible with the present digital switching schemes becomes apparent. Namely, one needs an optical switching element which can be switched on and off by positive pulses (positive pulse switchable). Positive pulse switching is necessary because present digital circuitry uses only two logical states, on and off, and not three levels ,on, zero and off, as required by a standard Fabry-Perot.

The search for such an optical switching element begins with Korpel and Lohmann's proposal of using the switching of the polarization states in a nonlinear birefringent cavity to implement an optical memory. Their scheme is described in chapter 3. The theory of optical polarization bistability in a nonlinear birefringent dielectric Fabry-Perot is developed from the model of chapter 1. A crucial result of this work was to disprove the claim that polarization bistability in a single birefringent nonlinear Fabry-Perot can be used to implement an optical memory that can be switched on and off with positive pulses. After reconciliation with the authors of the proposal, the Korpel and Lohmann's idea was abandoned.

In chapter 4, a model for optical polarization bistability in a Fabry-Perot with metallic mirrors is derived. This model was developed in order to explain the experimental results which could only be performed with metallic mirrors because of the technological and financial constraints.

The experimental part of the work is discussed in chapter 5. The details of the experiments and all the procedures for the preparation of the samples are documented. The results of the experiments are compared with the predictions of chapter 4. The results show good agreement with the theoretical predictions. It may be noted that we fell closely to but short of being first in demonstrating experimentally polarization bistability in a nonlinear Fabry-Perot [28, 29].

We demonstrate in chapter 3 that positive pulse switching is not possible in a single nonlinear cavity. In chapter 6, we develop the steady state theory for a two coupled nonlinear Fabry-Perot cavities system. We prove that it is possible to switch this coupled cavities system on and off with positive pulses. Two different switching

schemes are described in details in this chapter.

In chapter 7, the dynamic model of a single nonlinear Fabry-Perot cavity is reviewed and some of the main features of the dynamic response of the nonlinear Fabry-Perot are discussed. The dynamic model is then extended to a system of two coupled cavities and studied numerically. The main result of this study is the demonstration that switching with positive pulse only is also achievable in the dynamic regime and not only in the steady state or quasi steady state regime, as demonstrated in chapter 6.

Chapter 8 summarize all the results obtained in our search for an optical memory device which is compatible with the digital switching scheme.

Chapter 2

Optical Bistability in Dielectric Nonlinear Fabry-Perots

2.1 Nonlinear Fabry-Perot Cavities

In this chapter, we will focus on one type of optical nonlinear element, namely the nonlinear Fabry-Perot cavity (NLFP). We analyze the steady state solution of the model and discuss its potential applications.

A NLFP consists of a Fabry-Perot etalon of length d, filled with an optically nonlinear medium. This nonlinear medium could be either absorptive or dispersive, or more generally a mixture of both.

Fig.2.1 is a generic configuration of a NLFP. M_1 and M_2 are dielectric mirrors of intensity reflectivity R. This cavity is filled with a dispersive nonlinear medium of the Kerr type, the index of refraction of which can be written, to first order in intensity, as:

$$n(I) = n_0 + n_2 I, \tag{2.1}$$

where n_0 and n_2 are the linear and nonlinear indices of refraction, respectively and I is the average intensity inside the cavity. The nonlinearity could come from the nonlin-

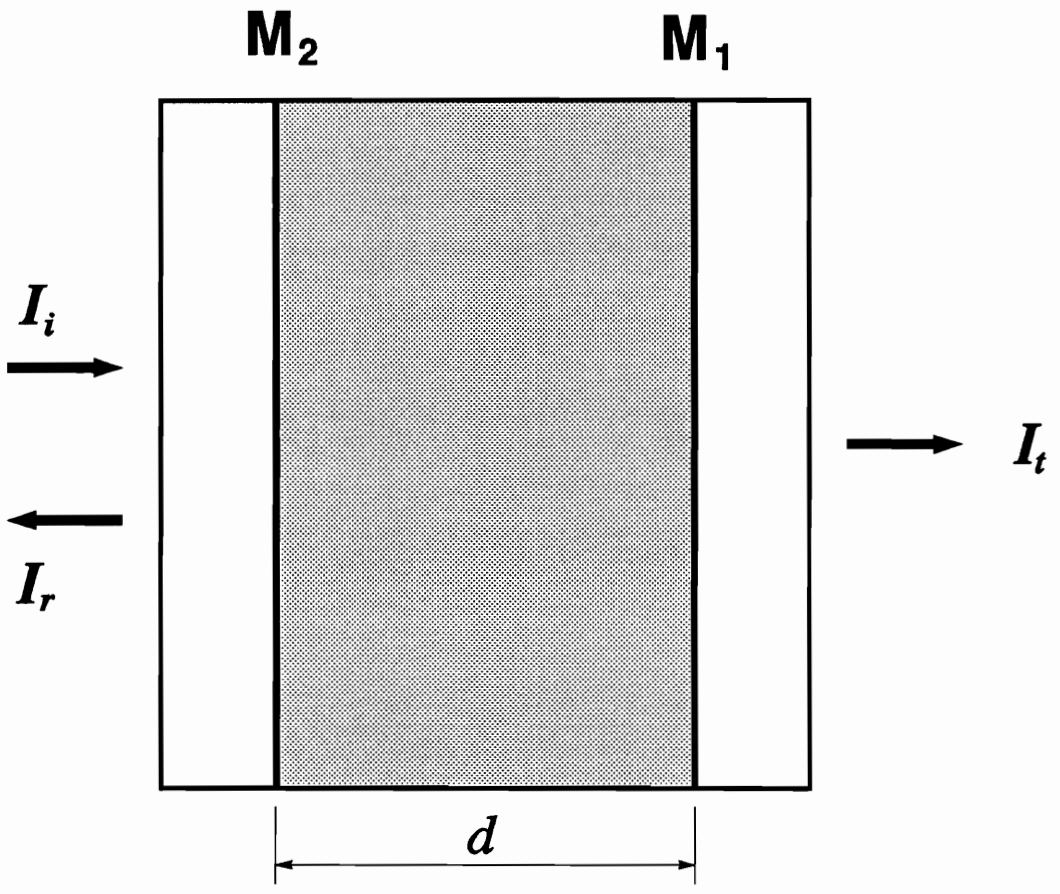

Figure 2.1: Fabry-Perot etalon of length d with mirrors M_1 and M_2 of reflectivity R, filled with a dispersive nonlinear medium. I_i is the incident intensity, I_t is the intensity transmitted and I_r is the intensity reflected.

ear electronic response of the material, from thermal nonlinearity, from orientational effects of long molecules or from the photorefractive effect due to charge redistribution in a photorefractive material, to name a few examples. The magnitude of the nonlinearity and the time scale of the response are different for each mechanism. The round trip phase change inside the cavity can be expressed as

$$\phi = 2kd(n_0 + n_2 I) \,, \tag{2.2}$$

where k is the wavenumber of the incident radiation in vacuum and d is the length of the cavity. Presently, the nonlinearity of the medium may be assumed to come from a direct absorption of the radiation in the bulk medium. In later chapters, we will see that this nonlinearity can also come from indirect absorption through the metallic mirrors when a thermo-optic material is used as a nonlinear medium.

The response of the cavity can be derived as follow. Consider a plane wave E_i incident on the cavity which is made up of two dielectric mirrors and a nonlinear absorbing material between the mirrors. The electric fields transmitted and reflected after multiple passes through the cavity are shown in Fig.2.2. Carrying through the infinite sum shown in Fig.2.2, the resultant transmitted amplitude is found to be

$$E_t = E_i e^{i\phi/2} \left[\frac{T e^{-\alpha d/2}}{1 - R e^{-\alpha d} e^{i\phi}} \right] \tag{2.3}$$

and the reflected field is obtained as

$$E_r = \sqrt{R} E_i \left[1 + \frac{T e^{-\alpha d} e^{i\phi}}{1 - R e^{-\alpha d} e^{i\phi}} \right] \,, \tag{2.4}$$

where $R = |r|^2$ and $T = |t|^2$ are the reflectivity and transmissivity of the mirrors and α is the intensity absorption coefficient of the medium. Here, we have assumed that the nonlinear medium has a long diffusion length so that any local effect is averaged out and the plane wave approach is valid. Defining E_+ and E_- to be the forward and backward propagating fields inside the cavity, we have:

$$E_+ = \frac{t E_i}{1 - R e^{-\alpha d} e^{i\phi}} \exp(-\frac{\alpha}{2} z + ikz) \tag{2.5}$$

$$E_- = \frac{r t E_i}{1 - R e^{-\alpha d} e^{i\phi}} \exp[-\frac{\alpha}{2}(2d - z) - ikz]. \tag{2.6}$$

The total intensity inside the cavity can be obtained from squaring the sum of the forward and backward fields:

$$\begin{aligned} & I_{tot}(z) \\ = \; & |E_+ + E_-|^2 \\ = \; & \frac{T|E_i|^2}{1 + R^2 e^{-2\alpha d} - 2Re^{-\alpha d}\cos\phi} \left\{ e^{-\alpha z} + Re^{-\alpha(2d-z)} + 2\sqrt{R}e^{-\alpha d}\cos(2kz) \right\} \end{aligned} \quad (2.7)$$

The average intensity inside the cavity is then found to be

$$\begin{aligned} & I \\ = \; & \frac{1}{d}\int_0^d I_{tot}(z)dz \\ = \; & \frac{TI_i}{1 + R^2 e^{-2\alpha d} - 2Re^{-\alpha d}\cos\phi} \frac{1}{d}\int_0^d \left[e^{-\alpha z} + Re^{-\alpha(2d-z)} + 2\sqrt{R}e^{-\alpha d}\cos(2kz) \right] dz \\ = \; & \frac{T(1-e^{-\alpha d})(1+Re^{-\alpha d})}{\alpha d(1-Re^{-\alpha d})^2} \frac{1}{1 + F\sin^2\phi/2} I_i \\ = \; & \frac{A}{\alpha d}\frac{(1-R)(1+R_\alpha)}{(1-R_\alpha)^2} \frac{1}{1 + F\sin^2\phi/2} I_i \,, \end{aligned} \quad (2.8)$$

where $A = 1 - e^{-\alpha d}$.In performing the integration, it was assumed that $d \gg \lambda$ so that all spatial variations are averaged out.

Squaring Eq.(2.3) gives the transmissivity of the cavity:

$$\mathcal{T} \equiv \frac{I_t}{I_i} = \frac{T^2 e^{-\alpha d}}{(1-R_\alpha)^2} \frac{1}{1 + F\sin^2\phi/2} \,, \quad (2.9)$$

where

$$\begin{aligned} R_\alpha &\equiv Re^{-\alpha d} \\ \text{and} \qquad F &\equiv \frac{4R_\alpha}{(1-R_\alpha)^2}. \end{aligned} \quad (2.10)$$

Since the round trip phase shift ϕ inside the cavity depends on the average intensity inside the cavity, we can write the transmitted intensity as

$$I_t = \frac{(1-R)^2 e^{-\alpha d}}{(1-R_\alpha)^2} \frac{1}{1 + F\sin^2\phi(I)/2} I_i \,. \quad (2.11)$$

We have assumed that the mirrors are lossless i.e. $T + R = 1$.

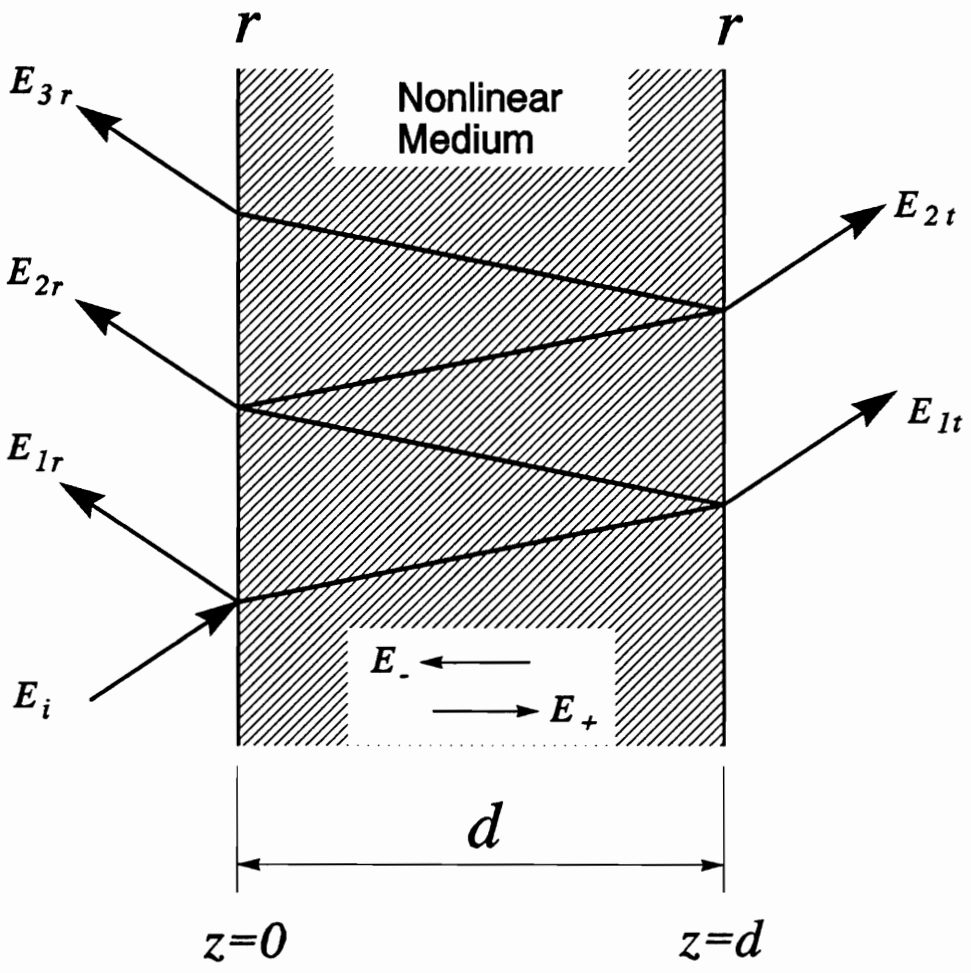

The amplitudes of the reflected waves (at z=0) are :

$$\begin{aligned} E_{1r} &= E_i r \\ E_{2r} &= E_i t^2 r e^{-\alpha d} e^{i\phi} \\ E_{3r} &= E_i t^2 r^3 e^{-2\alpha d} e^{i2\phi} \\ &\vdots \end{aligned}$$

The amplitudes of the transmitted waves (at z=d) are:

$$\begin{aligned} E_{1t} &= E_i t^2 e^{-\alpha d/2} e^{i\phi/2} \\ E_{2t} &= E_i t^2 r^2 e^{-3\alpha d/2} e^{i3\phi/2} \\ E_{3t} &= E_i t^2 r^4 e^{-5\alpha d/2} e^{i5\phi/2} \\ &\vdots \end{aligned}$$

Figure 2.2: Electric field inside a dielectric FP cavity. $R \equiv |r|^2$; $T \equiv |t|^2$ are the mirror reflectivity and transmissivity, respectively. ϕ is the roundtrip phase shift and α is the intensity absorption coefficient.

The average total intensity inside the cavity can then be expressed in terms of the transmitted intensity as

$$I = \frac{A(1+R_\alpha)}{\alpha d(1-R)(1-A)} I_t \,, \tag{2.12}$$

and the incident intensity can be written as a function of the transmitted intensity as

$$I_i = \frac{(1-R_\alpha)^2}{(1-R)^2(1-A)}[1 + F\sin^2\phi(I)/2]I_t. \tag{2.13}$$

A plot of the function I_i versusI_t is shown in Fig.2.3(a). It is clear from the graph that there are three values of I_t corresponding to the same value of I_i between $I_i = I_u$ and $I_i = I_d$. Fig.2.3(b) shows the plot of I_t versus I_i which is the same as Fig.2.3(a) rotated 90°. Stability analysis shows that the part of the curve with negative slope, between I_u and I_d, is an unstable branch. Therefore, the only possible value for I_t are on the upper or the lower branch of the hysteretic curve. a and c are the stable points for the incident intensity I.

Clearly, as the incident intensity increases from zero, the transmitted intensity is single valued as long as $I_i < I_d$. When the incident intensity is between I_u and I_d, the intensity transmitted not only depends on the incident intensity but also on the history. As the incident intensity increases from zero to some value larger than I_u, the transmitted intensity will first follow the lower branch of the hysteretic curve. At $I_i = I_d$, the transmitted intensity jumps up to the upper branch. As I_i decreases, the transmitted intensity follows the upper branch and jumps down to the lower branch at $I_i = I_d$. This hysteresis defines a bistable region between I_u and I_d. The overall response is the same as that shown in Fig.1.1.

The response of the cavity depends on the value of the finesse of the cavity ($\mathcal{F} = \pi^2 F/4$). For a low finesse cavity, the response is shown in Fig.2.4(a). The response is simply nonlinear but shows no hysteresis. When the cavity is biased with an intensity I_b, a small variation in the input intensity will result in a larger variation in the output intensity. The cavity can thus be used as an optical transistor. With a higher finesse, the cavity can be used as an optical limiter or a thresholder as shown in Fig.2.4(b). With an even higher finesse, the response of the cavity is hysteretic and the cavity

can be used as an optical memory element (Fig.2.4(c)).

These examples illustrate some of the possible uses of a single nonlinear Fabry-Perot cavity. It can perform many logical operations and can serve as an essential building block in an optical computer. A single nonlinear Fabry-Perot cavity can also be used as a memory element in an optical circuit. Conventionally, when a bistable Fabry-Perot cavity is operated as a memory element, it is biased by a constant beam which has an intensity between the switch-up value and the switch-down value. Initially the cavity is ,for example, in a low state (point a in Fig.2.5). The cavity can be turned on by adding a pulse to the cavity (a - b - c). To reset the cavity, one must interrupt the bias beam (c - d - a).

However, the above scheme of operation cannot be used directly in a digital circuitry because all the elements in a digital circuit must be activated by positive pulses. An interruption of the bias requires the removal of energy from the bias beam and is equivalent to a negative input pulse. In order to use this cavity as a memory element in a digital circuit, modifications have to be made so that it can be switched by positive pulses. Our goal is to search for systems of nonlinear Fabry-Perots that can be switched by positive pulses.

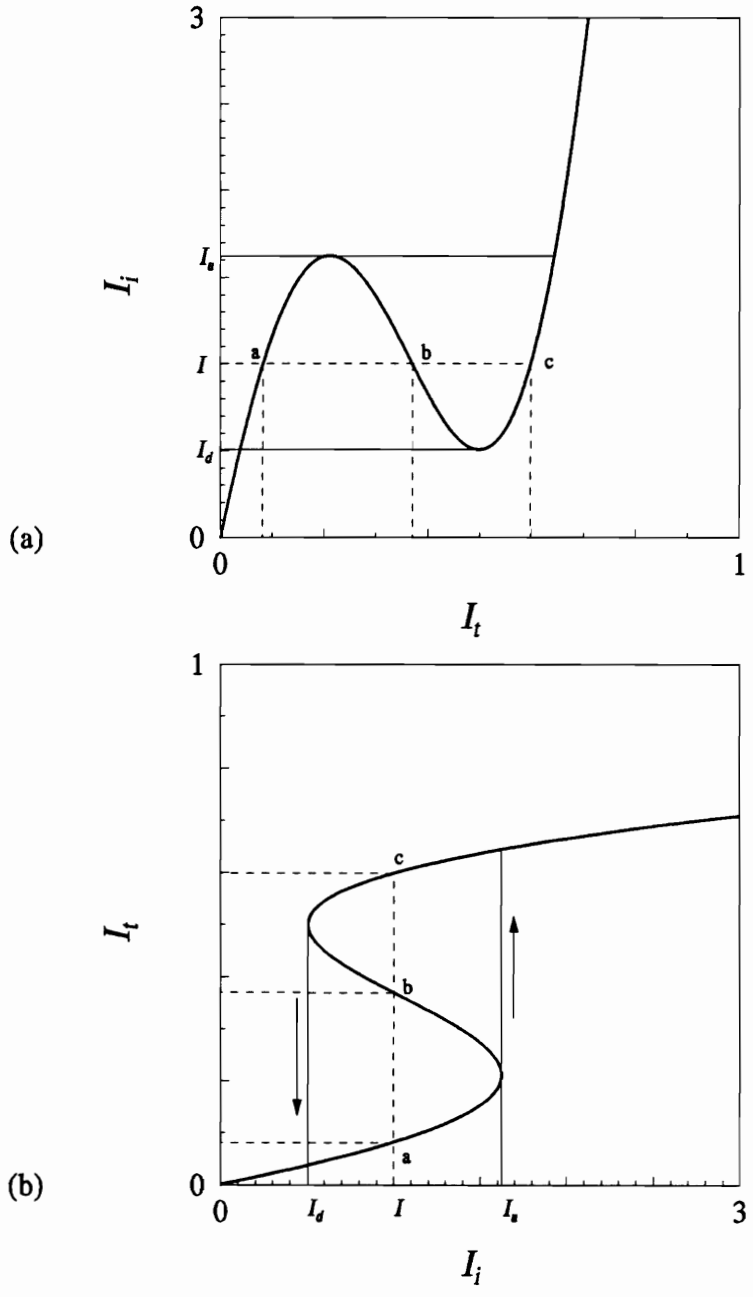

Figure 2.3: (a)Function I_i versus I_t. a, b, c are the three different values of I_t corresponding to one value of I_i. (b)Plotting the output I_t versus the input I_i reveal bistability and hysteresis – one value of input I results in two possible values of the output a and c (the middle point b is unstable).

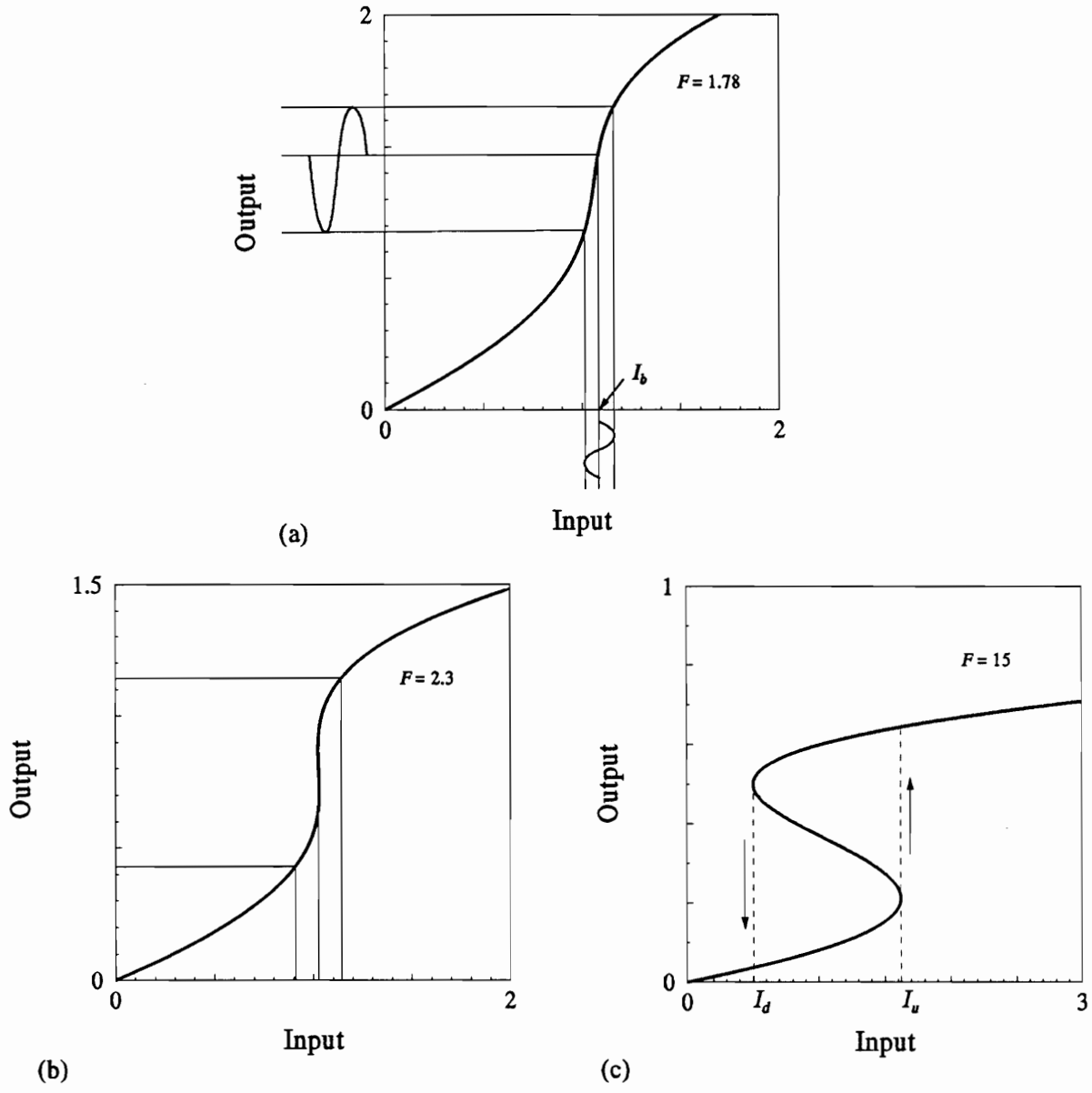

Figure 2.4: Three uses of a NLFP. (a) optical transistor (b) thresholder (c) optical memory element

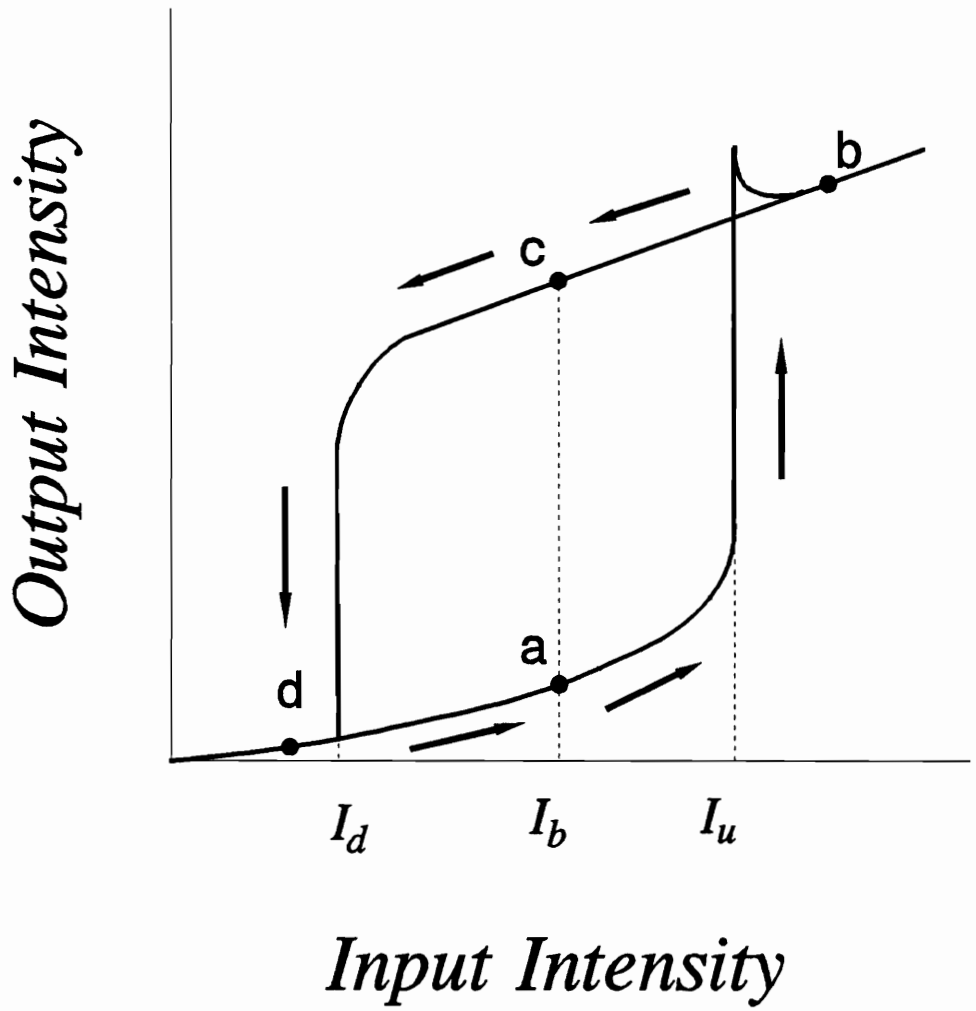

Figure 2.5: Single NLFP operating as a memory element. The cavity is biased with an intensity I_b. The output is turned on by adding a pulse to the cavity (a - b - c). In order to reset the cavity, the bias must be interrupted (c - d - a).

Chapter 3

Polarization Bistability

The conventional way of using a bistable Fabry-Perot cavity as a memory element was described in chapter 2. The Fabry-Perot cavity is biased within its bistable region at all times during the operation. The biasing beam 'holds' the information in the cavity. To set the memory, one needs to bring the incident intensity above its bistable region. As the incident intensity returns to the biasing level, the cavity will be left in a high state. If the cavity is in a high transmission state, in order to reset the cavity, the bias has to be temporarily interrupted or reduced. However, this interruption scheme is not compatible with conventional binary logic operations. In order to control the output of the cavity, three levels of input are necessary, namely, the OFF level which is the same as the biasing level, the ON level and a negative level for turning the device off. To turn the cavity on, one needs a positive pulse. To turn the cavity off, one needs a negative pulse. To be able to use the bistable Fabry-Perot cavity as a memory element in a digital optical circuit, modifications of the operation scheme have to be made.

In this chapter, a method proposed by Korpel and Lohmann [30] in which the output of a optically bistable element can be turned on and off by positive pulses is reviewed. The authors proposed to use the two orthogonal polarization states of a birefringent Fabry-Perot as an additional design parameter to achieve the goal. We

will show, however, that this device can only be turned on and off once with positive pulses.

3.1 Korpel and Lohmann's proposal

So far, the two output states of a bistable device have been identified by the magnitude of the output intensity. Korpel and Lohmann proposed a way to modify a normal bistable Fabry-Perot cavity into a device in which the two states of the output are identified by their state of polarization. This device has an important advantage over the conventional optical bistable device in that its total output power will always remain constant for both states. In an ideal device of this kind, there is no energy loss in switching except for the necessary inherent absorption. All the energy entering the device will be transmitted and the state of polarization determines the state of the device. This scheme has important advantages. For example, because the total output states have the same energy, cascadability[1] is easily achieved. Another advantage is that complementary logic signals are obtained simultaneously (when one polarization state is high the other must be low).

Fig.3.1(a) shows the setup proposed by Korpel and Lohmann. NLFP is an isotropic optically bistable cavity. It is illuminated by x-polarized light. The x-polarization state of the reflected light is changed into a y-polarization state by a halfwave plate H. Both transmitted and reflected beams are combined at the polarization beam splitter PBS. Therefore, when the cavity is in a high transmission state, the output is x-polarized and when the cavity is in a low transmission state, the output is y-polarized. The intensities transmitted and reflected, I_{t_x} and I_{r_x}, of the Fabry-Perot cavity for the x-polarization input are shown in Fig.3.1(b).

Korpel and Lohmann further proposed that this kind of polarization bistable device could be used to implement optical flip-flops. Consider now a layer of anisotropic

[1]Cascadability describes the ability to use the output of one device as an input to switch another device of the same kind.

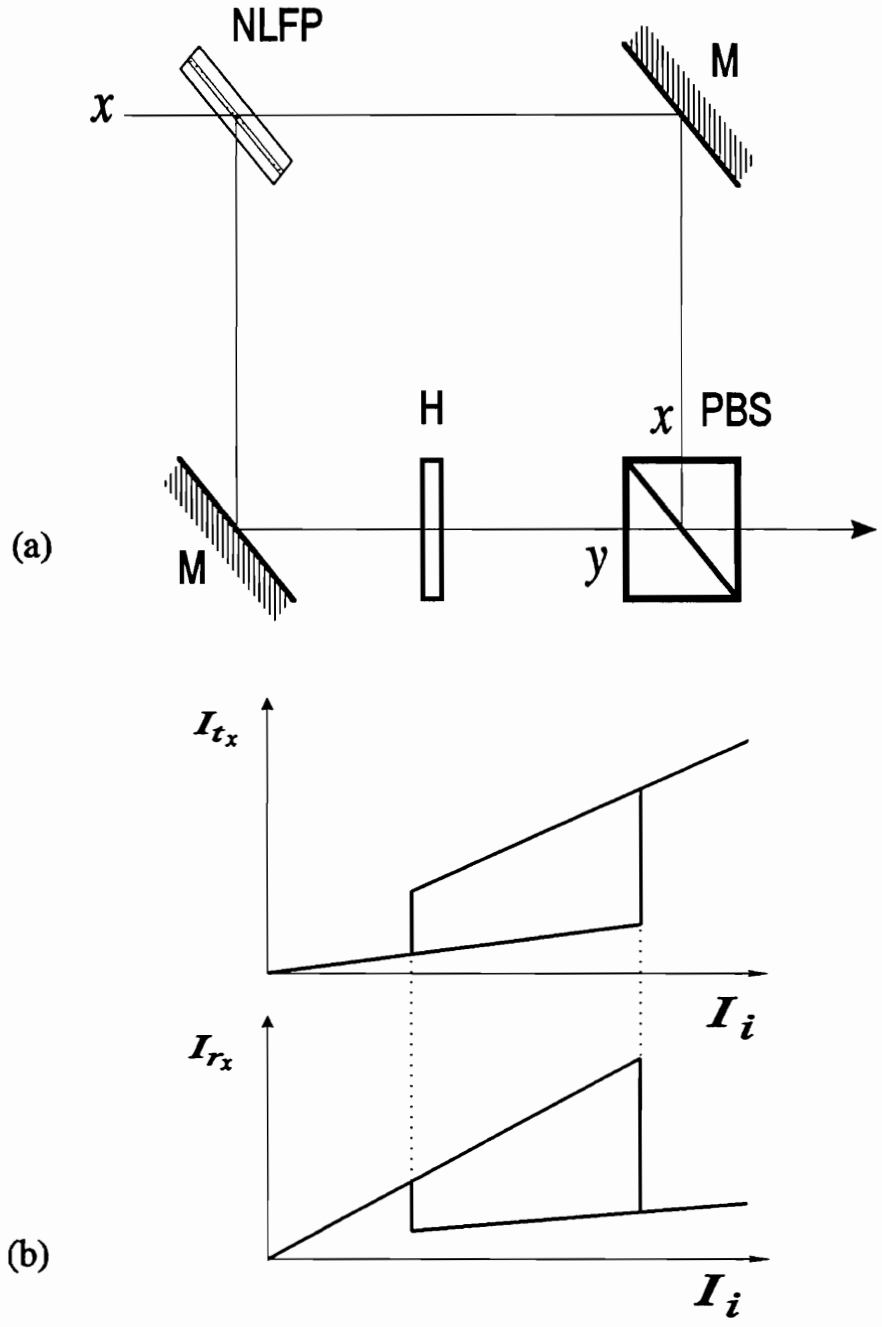

Figure 3.1: Output combining two orthogonal states of polarization. (a) NLFP bistable Fabry-Perot cavity; H halfwave plate; PBS polarization beam splitter. (b) hysteresis curves for the output of the Fabry-Perot in the x-polarization.

material inserted into the cavity. Light of different polarizations entering the cavity will experience different indices of refraction. Thus, the round-trip phase shifts for the polarization parallel and perpendicular to the axis of anisotropy of the medium will be different. The relative phase difference due to the anisotropic medium can be small, just enough to shift the transmission peak of the Airy curve by about a half peak width (see Fig.3.2(a)). This results in a shift of the hysteresis for both polarizations (see Fig.3.2(b)). This shift should be such that the hysteresis loops of both polarizations overlap appreciably but not entirely, as indicated by the shaded region in Fig.3.2(b).

Based on these concepts, we invented the setup of Fig.3.3 to implement the optical flip-flop proposed by Korpel and Lohmann. There are two outputs: I_{o_1} and I_{o_2}, which are derived from the two orthogonally polarized input I_{i_x} and I_{i_y} incident at disjointed areas on the cavity. I_{i_x} is x-polarized and I_{i_y} is y-polarized. The four polarization beam splitters PBS1 to PBS4 reflect y-polarized radiation and transmit x-polarized radiation. The transmitted and reflected beams of both polarizations are separated according to their state of polarization by the beam splitters PBS1 and PBS2. The transmitted beam in the x-polarization T_x, is combined with the reflected beam in the y-polarization R_y by PBS4 and the transmitted beam of the y-polarization T_y is combined with the reflected beam of the x-polarization R_x by the beam splitter PBS3, to form the two outputs $I_{o_1} = R_x + T_y$, and $I_{o_2} = T_x + R_y$.

The optical flip-flop proposed by Korpel and Lohmann is operated as follow: two inputs I_{i_x} and I_{i_y} of equal magnitude enter the nonlinear birefringent Fabry-Perot cavity NLFP, at two different locations. The individual hysteresis curves for the reflected and transmitted radiation for both polarizations are shown schematically in Fig.3.4(a). Notice that the hysteresis curves of both polarizations are shifted with respect to each other by an appreciable amount. They both overlap in region C which is the region where the device is biased. The outputs can be turned on or off, depending upon the magnitude of the input. For the purpose of illustration, only I_{o_1} is considered here ($I_{o_1} = R_x + T_y$). Initially, $R_x + T_y$ is at a + a, a high

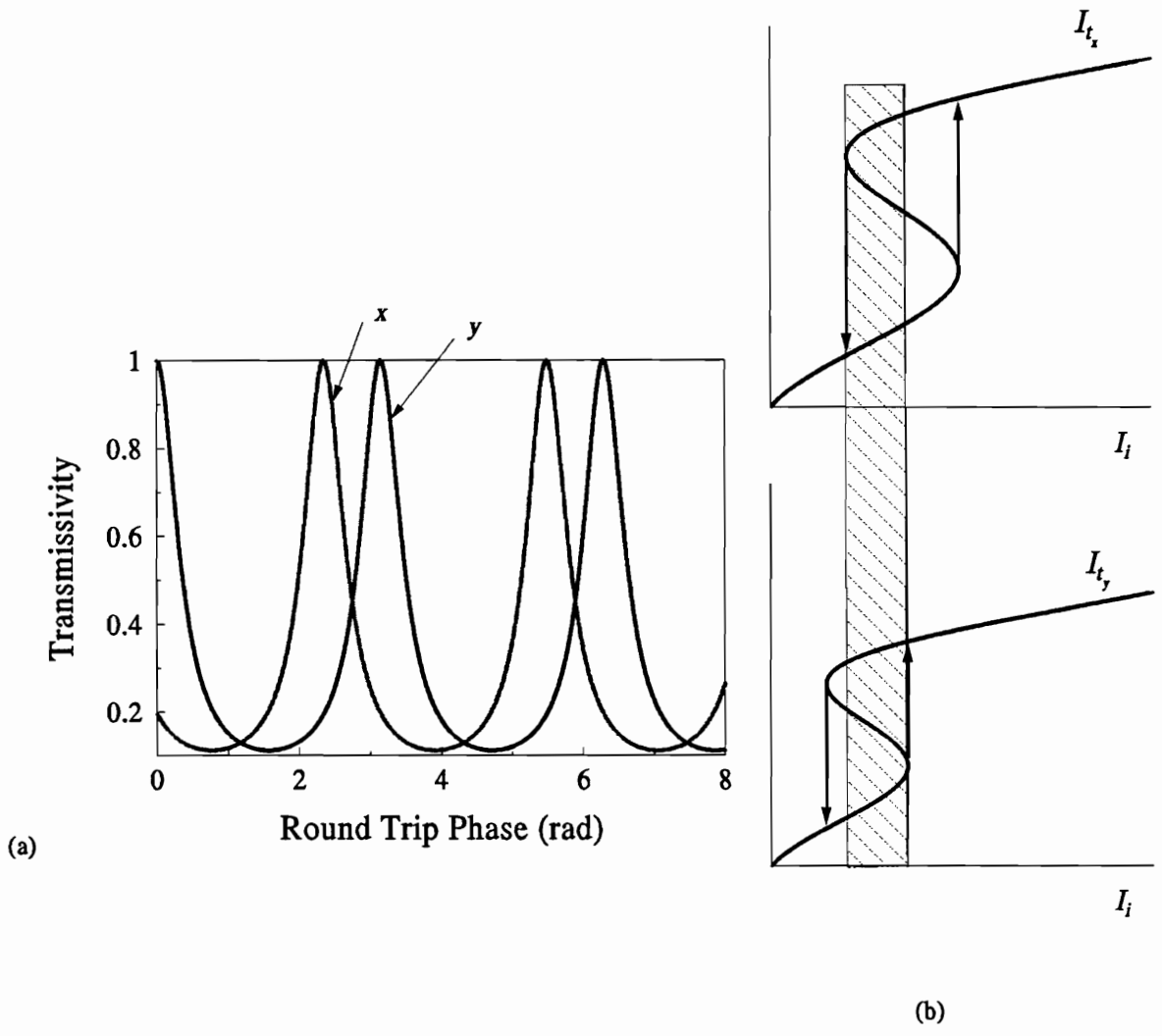

Figure 3.2: (a) When a layer of anisotropic material is inserted into the Fabry-Perot cavity, the round-trip phase is different for the polarization state parallel and perpendicular to the axis of anisotropy of the medium. Thus, the transmissivity curves versus the round-trip phase for the two polarization states are shifted with respect to one another. (b) As a consequence, the hystereses of the transmitted intensity I_{t_x} and I_{t_y} in each polarization are also shifted with respect to one another.

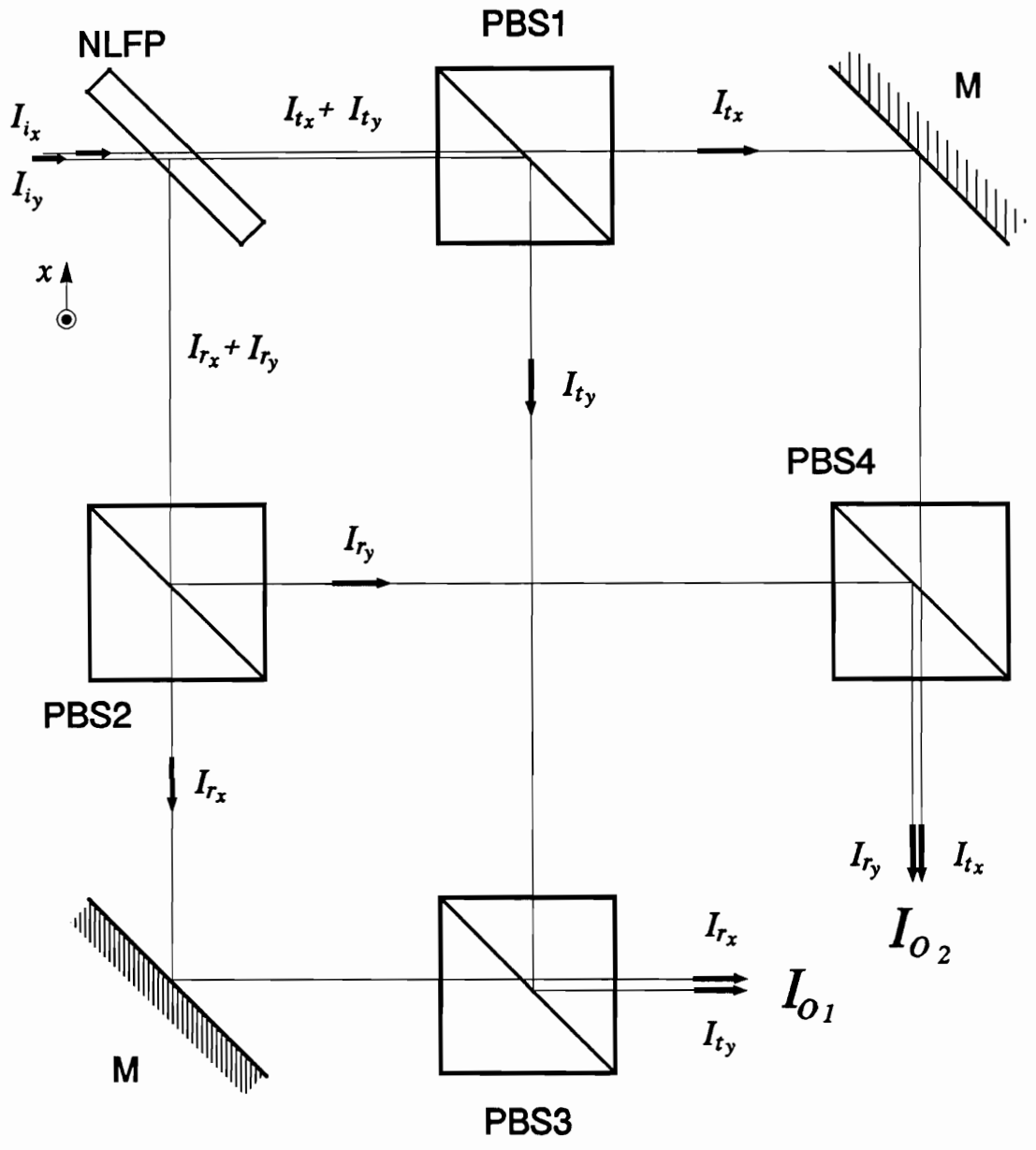

Figure 3.3: Implementation of the Korpel Lohmann optical flip-flop. Two inputs of orthogonal polarizations I_{i_x} and I_{i_y} are incident on the anisotropic bistable Fabry-Perot cavity at disjointed areas. The transmitted and reflected beam of orthogonal polarizations are split according to their state of polarization by the polarization beam splitter PBS1 and PBS2 and recombined by the polarization beam splitters PBS3 and PBS4 to form the outputs I_{o_1} and I_{o_2}.

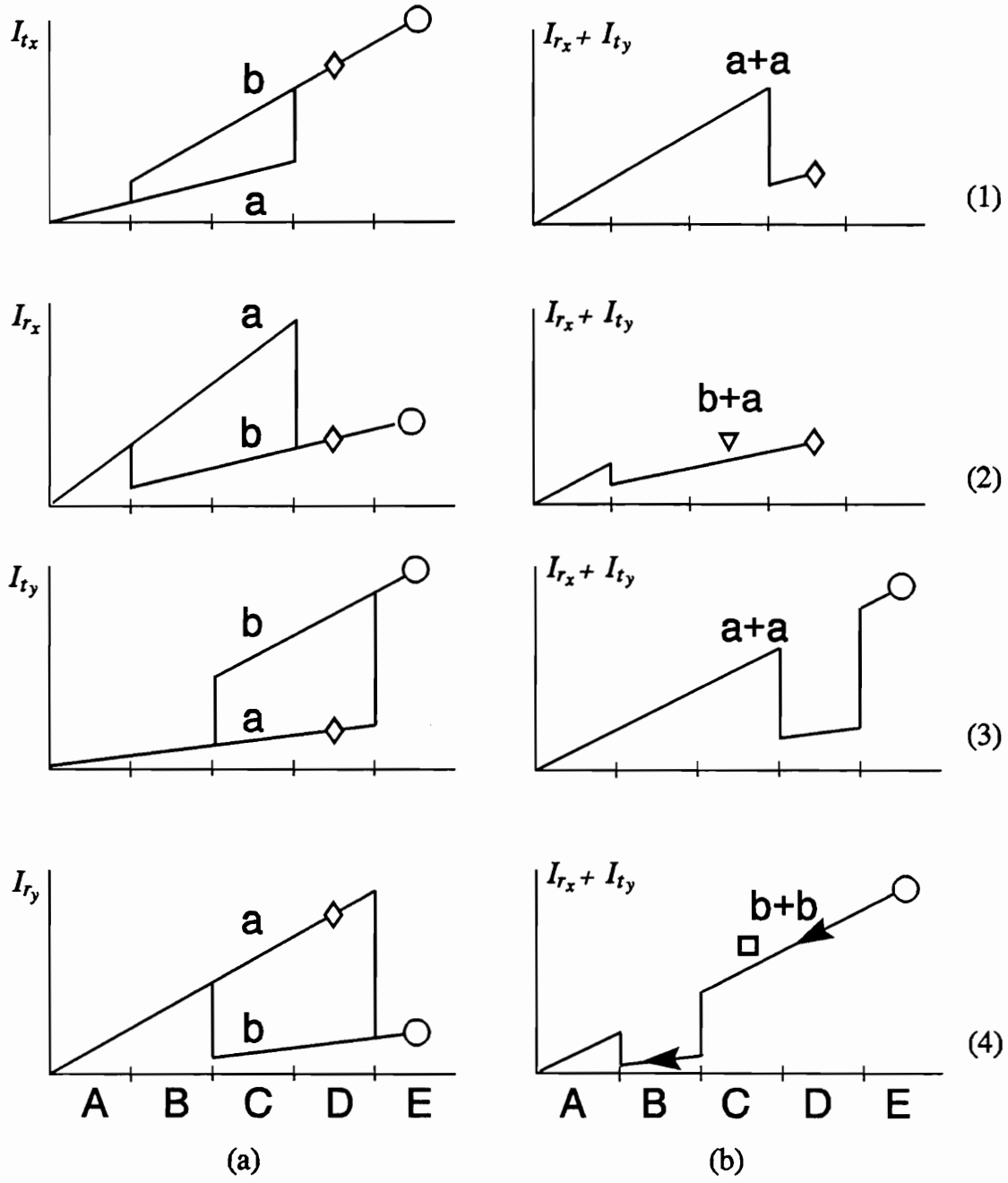

Figure 3.4: (a) Hysteresis curves for an anisotropic bistable Fabry-Perot cavity. Due to the anisotropy, the transmission peaks of the cavity for each polarization are shifted, resulting in a shift of the switching points. (b) The output $R_x + T_y$ implements an optical flip-flop operation. The end state depends only on the magnitude of the pulse received and not on the previous state.

state (Fig.3.4(b-1)). This corresponds to a high state in R_x (Fig.3.4(a-2)) and a low state in T_y (Fig.3.4(a-3)). If a short pulse shifts the input temporarily to region D (indicated by the diamond), R_x will be switched to a low state (Fig.3.4(a-2)) and T_y will remain in a low state a (Fig.3.4(a-3)). Therefore, the output $R_x + T_y$ will switch to a low state indicated by the diamond in Fig.3.4(b-1). As the pulse is removed the output $R_x + T_y$ stays in the low state in region C (indicated by the inverted triangle in Fig.3.4(b-2)).

Assuming the same initial condition, i.e. R_x in a high state a and T_y in a low state a, a somewhat larger pulse will temporarily bring the input to the region E (indicated by the circle). R_x will be switched to a low state (Fig.3.4(a-2)) and T_y will be switched to a high state (Fig.3.4(a-3)). The resultant output $R_x + T_y$ will first go through a low state in region D when R_x switches down then will switch back to a high state in region E when T_y switches up (Fig.3.4(b-3)). After the pulse is removed, $R_x + T_y$ will stay in the high state in region C (indicated by the square) as the pulse is removed (Fig.3.4(b-4)).

From the above example, it can be seen that the end state of the output depends only on the magnitude of the pulse. Namely, a small pulse turns the output on and a large pulse turns the output off. This summarizes the idea proposed by Korpel and Lohmann for implementing an optical flip-flop using a polarization bistable device. It turns out that the authors had overlooked a slight detail. The possibility of polarization switching will be investigated in more detail in section 3.3.

3.2 Steady State Model of Polarization Bistability

Let us consider a linearly polarized plane wave incident on a lossless Fabry-Perot cavity with mirror reflectivity R and containing a nonlinear birefringent material. With slight modification, the method described in chapter 2 can be used to derive the steady-state solution of this nonlinear birefringent cavity. To first order dependence in intensity, the index of refraction of the medium, for each polarization, can be written

as

$$n_x(I) = n_{0_x} + n_{2_x} I, \tag{3.1}$$

$$n_y(I) = n_{0_y} + n_{2_y} I, \tag{3.2}$$

where x and y denote the two eigen-polarization states parallel and normal to the fast axis of the medium, respectively. $n_{0_{x,y}}$ and $n_{2_{x,y}}$ are the linear and nonlinear indices of refraction of the medium for the two polarization states, respectively. I is the average intensity trapped inside the cavity. I_x and I_y are the total average intensities inside the cavity for the two orthogonal polarizations of the radiation. Since the polarization components are orthogonal, we can write the average intensity inside the cavity as the sum of the intensity of the individual polarizations:

$$I = I_x + I_y. \tag{3.3}$$

In general, not only the linear indices of refraction but also their nonlinear counterparts can be different for both polarization states. Therefore, the two orthogonal polarizations of the radiation 'see' two different cavities. The round trip phase change for each polarization can be expressed as

$$\phi_x = 2kd\left(n_{0_x} + n_{2_x} I\right), \tag{3.4}$$

$$\phi_y = 2kd\left(n_{0_y} + n_{2_y} I\right), \tag{3.5}$$

where k is the wavenumber of the incident radiation in vacuum and d is the intracavity spacing, which is also the thickness of the nonlinear medium.

It is assumed that the incident light is linearly polarized at 45° from the x-axis, i.e.: $E_{i_x} = E_{i_y} \equiv E_i$ (an angular factor can be added to deal with an input having unequal polarization components). Using the results of chapter 2, the resultant transmitted amplitudes for the two orthogonal polarization components are given by:

$$E_{t_{x,y}} = E_i \left[\frac{T e^{-\alpha d/2}}{1 - R e^{-2\alpha d} e^{i\phi_{x,y}}}\right]. \tag{3.6}$$

Similarly, the reflected fields are obtained as

$$E_{r_{x,y}} = \sqrt{R} E_i \left[1 + \frac{T e^{-\alpha d} e^{i\phi_{x,y}}}{1 - R e^{-\alpha d} e^{i\phi_{x,y}}}\right]. \tag{3.7}$$

Squaring Eq.(3.6) gives the transmitted intensity

$$I_{t_{x,y}} = \frac{T^2 e^{-\alpha d}}{(1-R_\alpha)^2} \frac{1}{1+F\sin^2(\phi_{x,y}/2)} I_i \ , \tag{3.8}$$

where

$$R_\alpha = Re^{-\alpha d}$$

and

$$F = \frac{4R_\alpha}{(1-R_\alpha)^2} \ .$$

Since the the round-trip phase shifts $\phi_{x,y}$ depend on the average intensity inside the cavity, the transmitted intensities for both polarizations take the from

$$I_{t_x} = \frac{(1-R)^2 e^{-2\alpha d}}{(1-R_\alpha)^2} \frac{1}{1+F\sin^2\phi_x(I)/2} I_i \ , \tag{3.9}$$

$$I_{t_y} = \frac{(1-R)^2 e^{-2\alpha d}}{(1-R_\alpha)^2} \frac{1}{1+F\sin^2\phi_y(I)/2} I_i \ . \tag{3.10}$$

The average intensity of each polarization component inside the cavity is obtained by integrating the square of the sum of the forward and backward propagating fields for that polarization component over the cavity length. This leads to

$$I_x = \frac{T(1-e^{-\alpha d})(1+Re^{-\alpha d})}{\alpha d(1-Re^{-\alpha d})^2} \frac{1}{1+F\sin^2\phi_x(I)/2} I_{i_x} \tag{3.11}$$

$$I_y = \frac{T(1-e^{-\alpha d})(1+Re^{-\alpha d})}{\alpha d(1-Re^{-\alpha d})^2} \frac{1}{1+F\sin^2\phi_y(I)/2} I_{i_y} \ , \tag{3.12}$$

where α is the absorption coefficient which is assumed be the same for both polarizations.

Rewriting Eq.(3.12) and Eq.(3.12) gives

$$I_x = \frac{A}{\alpha d} \frac{(1-R)(1+R_\alpha)}{(1-R_\alpha)^2} \frac{1}{1+F\sin^2\phi_x(I_x+I_y)/2} I_i \ , \tag{3.13}$$

$$I_y = \frac{A}{\alpha d} \frac{(1-R)(1+R_\alpha)}{(1-R_\alpha)^2} \frac{1}{1+F\sin^2\phi_y(I_x+I_y)/2} I_i \ , \tag{3.14}$$

where $A \equiv 1 - e^{-\alpha d}$ is the medium absorption.

The response of the cavity is governed by Eq.(3.10), (3.10), (3.13) and (3.14). However, these equations cannot be solved analytically. The response was then computed numerically.

First, Eq.(3.13) and (3.14) are added together to give the average total intensity inside the cavity.

$$I = \frac{A}{\alpha d}\frac{(1-R)(1+R_\alpha)}{(1-R_\alpha)^2}\left[\frac{1}{1+F\sin^2\phi_x(I)/2}+\frac{1}{1+F\sin^2\phi_y(I)/2}\right]I_i\,. \qquad (3.15)$$

Solving for the incident intensity gives

$$I_i = \frac{\alpha d}{A}\frac{(1-R_\alpha)^2}{(1-R)(1+R_\alpha)}\left[\frac{1}{1+F\sin^2\phi_x(I)/2}+\frac{1}{1+F\sin^2\phi_y(I)/2}\right]^{-1} I. \qquad (3.16)$$

The incident intensity can now be found knowing the average total intensity inside the cavity. Using the average total intensity inside the cavity as a running parameter, the incident intensity is found from Eq.(3.16). The transmitted intensity for each individual polarization state is then determined by substituting the running parameter I and the incident intensity found from Eq.(3.16) into Eq.(3.10) and (3.10).

A typical result of polarization switching is shown in Fig.3.5. The plotted curves show that as the incident intensity I_i increases, the two polarization components of the transmitted intensity switch alternatively into a high transmission state (first T_x switches to a high state and then T_y). As one polarization component switches up, the orthogonal polarization component switches down.

In this example, the cavity parameters were fixed in such a way that the cavity is closer to resonance for the x-polarization than for the y-polarization. As a result, the x-polarization component switches up first (at a),a further increase of the input I_i is needed for the orthogonal polarization component (y) to switch (at b).

An important implication of the equations governing the response of the cavity is that the two polarizations will always switch simultaneously if the two orthogonal polarizations are carried by the same beam. From (3.10) and (3.10), the transmitted intensity for each polarization is seen to be a single valued function of the average intensity inside the cavity. From (3.10) to (3.14), it is seen that the intensity I_x and

I_y are related to the transmitted intensity by a proportionality factor. Therefore, the average total intensity inside the cavity can be expressed in terms of the transmitted intensity as:

$$\begin{aligned} I_{x,y} &= \frac{A(1+R_\alpha)}{\alpha d(1-R)(1-A)} I_{t_{x,y}} \\ &= bI_{t_{x,y}} \ . \end{aligned} \tag{3.17}$$

An equation of the following form can thus be written for the average intensity:

$$\begin{aligned} f(I) &= I_x + I_y - I \\ &= b\mathcal{T}_x I_{i_x} + b\mathcal{T}_y I_{i_y} - I. \end{aligned} \tag{3.18}$$

The roots of this equation determine the possible values of I for a given input. Fig.3.6 is a graphic representation of Eq.(3.18), using $I_{i_x} = I_{i_y} = I_i$ and the parameter values pertaining to a cavity filled with a nematic liquid crystal (e.g. : MBBA): $n_{0_x} = 1.56, n_{0_y} = 1.80, n_{2_x} = 2n_{2_y} = 10^{-3}$ for thermo-optic effects, $d = 50\mu$m, mirror reflectivity $R = 0.85$, and medium absorption coefficient $\alpha = 7.5\text{cm}^{-1}$. For a small input intensity ($I_i = 1$) there is only one root. Above a critical value of I_i there are three roots for I ($I_i = 2$); two are stable and one is unstable. This is the bistable region. For higher input intensities other roots appear as the successive peaks of the Airy function cross the axis ($I_i = 4$). Clearly if I has two stable solutions for a particular input I_i, $\mathcal{T}_{x,y}(I)$ also has two stable solutions. As a consequence, *the two polarization states always switch for the same critical value of* I_i. The only way to avoid this coupling is to spatially separate the two orthogonally polarized beams in the cavity.

3.3 Is Polarization Switching a Solution to Positive Pulse Switching?

From section 3.2 we have learned that polarization bistability can be realized in a nonlinear birefringent Fabry-Perot cavity. The nonlinear material can itself

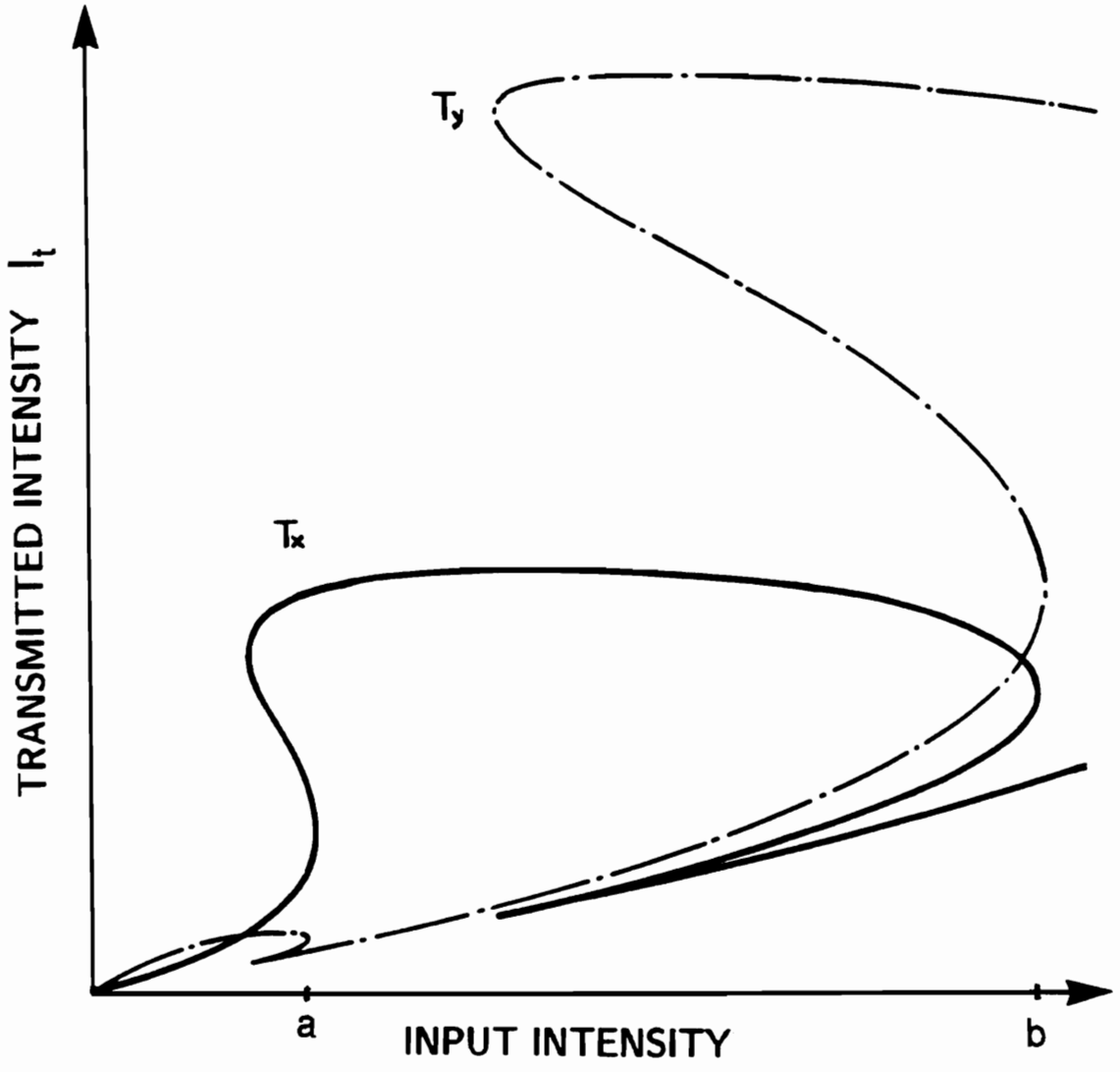

Figure 3.5: Example of hysteresis curve for polarization bistability. The two polarization components switch in opposite ways into a high and a low transmission state.

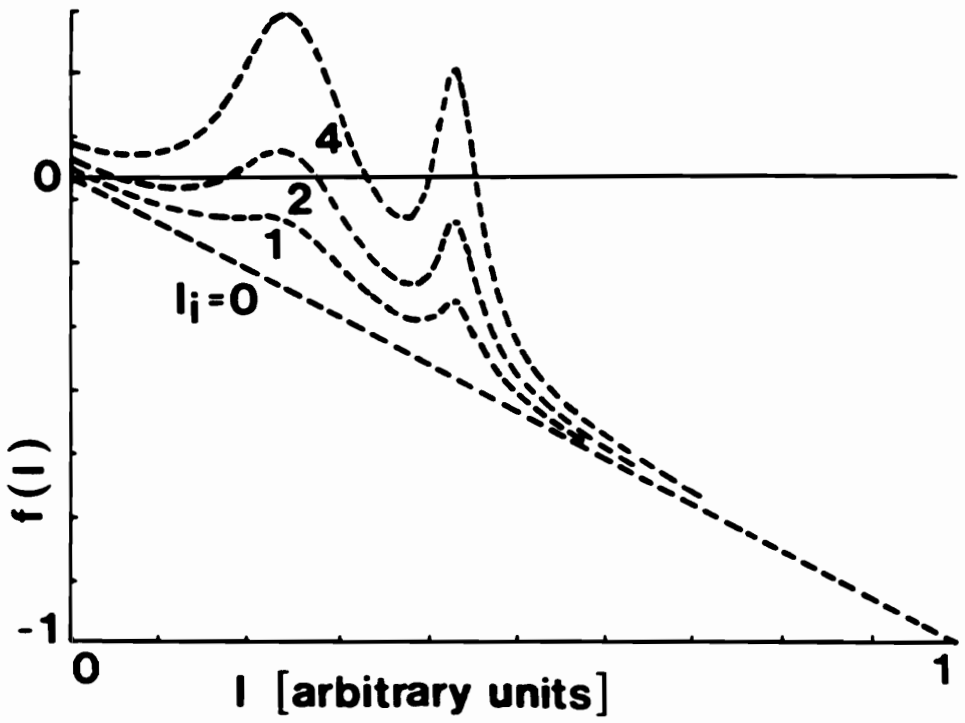

Figure 3.6: Graphical representation of Eq.(3.18). The roots of the equation $f(I) = 0$ determine the possible values of the irradiance I in the cavity for a given input irradiance I_i

be birefringent, or a fixed birefringent plate can be used in series with a nonlinear isotropic cell. These cavities have two eigenpolarization states along the fast and the slow axis of the birefringent material. In the frame-work of a plane wave theory, we have found from (3.10) and (3.10) that the transmissivity of the cavity is proportional to an Airy function:

$$\mathcal{T}_{x,y} = a_{x,y}\frac{1}{1 + F_{x,y}\sin^2\phi_{x,y}/2}, \tag{3.19}$$

where $a_{x,y}$ is a function of the mirror reflectivity and of the absorption of the medium and $F_{x,y}$ is the coefficient of finesse of the cavity. Notice that in section 3.2, $F_{x,y}$ was assumed to be the same for the two eigen-polarizations. In general, this assumption can be relaxed to include any anisotropic scattering or absorption due to the medium or the mirrors. The resonance peaks of the cavity occur at different values of the round-trip phase for the two polarizations, and the rates at which these peaks shift as a function of I are also in general different. As a result, the two polarizations will switch independently for different values of the input and will have different hysteresis loops.

The idea proposed by Korpel and Lohmann which consists in combining the reflected x-polarized beam with the transmitted y-polarized beam to operate the device as a flip-flop will however fail. If we look closely at Fig.3.4, we discover that the output can switch up and down only once. It will then be 'locked' in a state from which it cannot be displaced by a positive pulse. This fact had been overlooked by the authors.

Starting at state a in Fig.3.4(a), one needs to add a small pulse to displace momentarily the input to D in order to change the output $R_x + T_y$ to a low state. T_x and R_x will switch to b while T_y and R_y will remain in a. To change the output $R_x + T_y$ back to a high state, one needs to add a larger pulse to bring the input momentarily to E. This 'locks' R_x, T_x, R_y and T_y in state b from which it can never be brought back to state a without having to reduce the bias below B. This conflicts with the original goal of positive pulse switching. The key point is that the final high state is not the same as the original high state. This can be seen easily in the overall

hysteresis curve in Fig.3.7. There are two high states A and G and one low state D. Initially the output is at A, a high state. The output can be brought to a low state by a small pulse following the path A-B-C-D. It can then be turned on again by a bigger pulse following the path D-E-F-G. It is clear from Fig.3.7 that the output can never be displaced from state G by positive pulses of any magnitude. This reduces the attractiveness of polarization switching but nevertheless does not abolish its other advantages, such as the fact that the total output intensity remains constant and that complementary logic states are accesible simultaneously. Another advantage comes from the fact that both polarization states in the cavity are coupled together. In chapter 5 it will be shown that the coupling between the polarization states can be used to implement optical switches in which one polarization is controlled by a beam of orthogonal polarization.

An interesting way of resetting the device was suggested by Lohmann in a private discussion about the flaws of his first scheme [31]. It consists in rotating the polarization of the source to align it with one of the axes of the birefringent cavity. This can be achieved with a fast Pockels cell. If the polarization state is momentarily aligned with for example the x-polarization, T_y is reset to a low state a (Fig.3.4) and the device is turned off to a low state. This is equivalent to interrupting the y-beam, with the important difference that the total power incident on the device remains constant.

There are other ways of achieving positive pulse only switching. One way is to use two physically different mechanisms for the up and down switching. The previous example using a Pockels cell falls into this category. Tarng *at al* have proposed a brute-force method to switch the output from a high state to a low state. They used a small pulse to turn a GaAs etalon ON and used a very large pulse to heat up the cavity so that the hysteresis loop moves to a high switching energy thus forcing the output to switch down [32]. Another way of achieving positive pulse switching, which will be described in latter chapters, makes use of two coupled cavities.

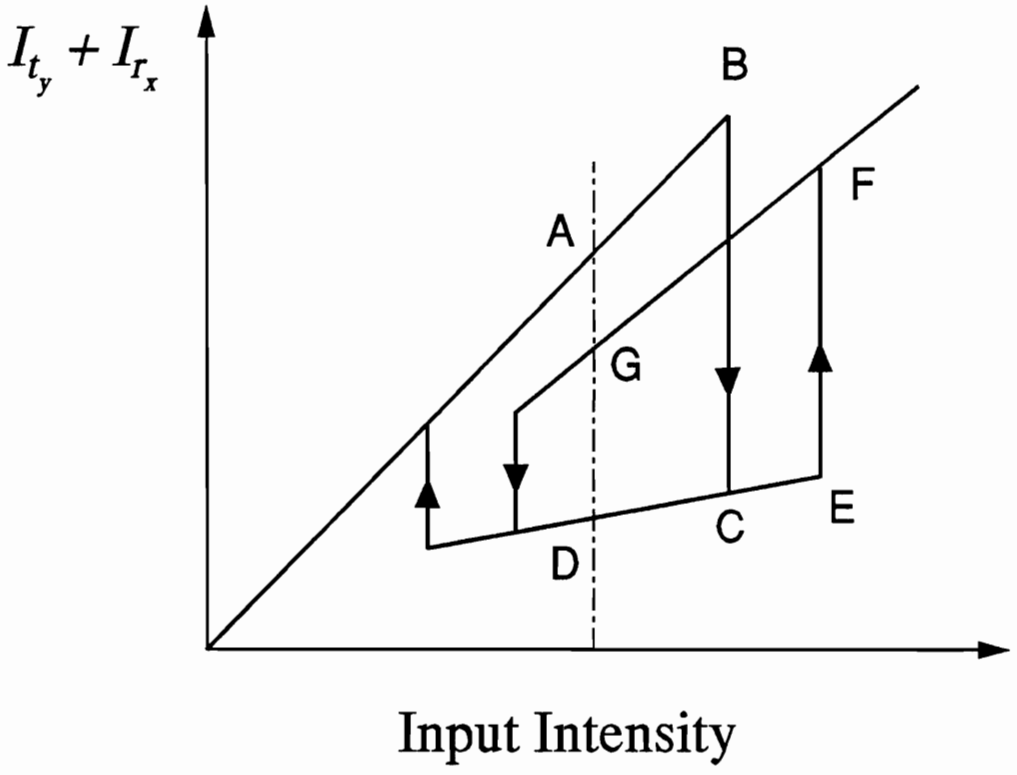

Figure 3.7: Overall hysteresis curve for Lohmann's positive pulse switching scheme. The device eventually locks in state G from which it cannot be dislodged by a positive pulse.

Chapter 4

Nonlinear Fabry-Perot Cavity with Metallic Mirrors

In a dielectric Fabry-Perot cavity filled with a thermo-optic [1] medium, the change in refractive index is caused by a change of the temperature of the medium induced by the incident radiation. In general, this comes from the intrinsic absorption of the medium. The temperature change in thermo-optic materials having low absorption coefficients will thus be very small. This is not desirable for practical devices. Among some of the known thermo-optic materials, liquid crystals and ZnSe have very high thermo-optic coefficients but have quite low absorption coefficients. To be able to utilize their large thermo-optic nonlinearity, it is essential to induce a large change in the temperature of the medium. One way of doing this is to add a dye as an absorbing agent into the nonlinear medium. The temperature of the medium will then increase due to the radiation absorbed by the dye. Dyes can be easily introduced in liquid media. For solid media, it is more difficult especially if the nonlinear medium is crystalline. In addition, adding an absorbing agent to the nonlinear medium will reduce the finesse of the cavity. The coefficient of finesse of an absorptive cavity is

[1] A thermo-optic medium has an temperature dependent index of refraction

given by $F = 4R_\alpha/(1-R_\alpha)^2$. This may become a disadvantage when a high finesse cavity is required, as for example to achieve high contrast switching.

Another way of introducing a thermal excitation to a nonabsorbing nonlinear medium is to use a Fabry-Perot with metallic mirrors. Energy from the incident radiation is absorbed by the metallic mirrors which changes the temperature of the medium locally and alters its index of refraction. There is a fundamental difference between a Fabry-Perot with metallic mirrors and the Fabry-Perot with dielectric mirrors considered so far. As a result of the absorption losses in the mirrors, the transmission peaks and the reflection minima of the cavity do not coincide. Consequently, the shape of the hysteresis curve is in general very different from the usual S-shape.

The experimental results reported in chapter 5 were obtained with metallic Fabry-Perots, the only kind that could be manufactured in house. A theoretical model of a nonlinear Fabry-Perot with metallic mirrors must thus be developed in order to correctly interpret these experimental results. This chapter is organized as follows: First, a steady state model of an isotropic nonlinear metallic Fabry-Perot cavity is developed. The general behavior of this cavity is then described. Next, this model is extended to the case of a birefringent cavity and the behavior of this cavity is discussed.

4.1 Steady-State Theory of a Nonlinear Metallic Fabry-Perot

It is the imaginary part of the electric susceptibility of a material that brings about absorption. The reflectivity, and transmissivity of a thin metallic film between two dielectric media at normal incidence are given by [33]

$$R = \frac{{\rho_{12}}^2 e^{2v_2\eta} + {\rho_{23}}^2 e^{-2v_2\eta} + 2\rho_{12}\rho_{23}\cos[\phi_{23} - \phi_{12} + 2u_2\eta]}{e^{2v_2\eta} + {\rho_{12}}^2\rho_{23}^2 e^{-2v_2\eta} + 2\rho_{12}\rho_{23}\cos[\phi_{12} + \phi_{23} + 2u_2\eta]}, \tag{4.1}$$

$$T = \frac{n_3}{n_1} \frac{{\tau_{12}}^2 {\tau_{23}}^2 e^{-2v_2\eta}}{1 + {\rho_{12}}^2 \rho_{23}^2 e^{-4v_2\eta} + 2\rho_{12}\rho_{23} e^{-2v_2\eta} \cos[\phi_{12} + \phi_{23} + 2u_2\eta]} . \quad (4.2)$$

where n_1 and n_3 are the indices of refraction of the dielectric media on either sides of the metallic film. ρ_{ij} , $\tau_{i,j}$ $(i,j = 1,2,3)$ are the magnitude of the reflection and transmission coefficients of the metal-dielectric interfaces for the radiation going from medium i to medium j. $\phi_{i,j}$, $\chi_{i,j}$ are the phase changes upon reflection and transmission at the metal-dielectric interfaces, respectively. u_2 is the index of refraction and v_2 is the extinction coefficient of the metallic film. $\eta = 2\pi h/\lambda$ is the normalized thickness of the metallic film (thickness h) for the incident wavelength λ. These equations include all the contributions due to multiple reflections between the boundary surfaces of the metallic film. The reflection and transmission coefficients of the metal-dielectric boundaries are:

$$\begin{aligned} r_{12} &= \rho_{12} e^{i\phi_{12}} \\ t_{12} &= \tau_{12} e^{i\chi_{12}} \\ r_{23} &= \rho_{12} e^{i\phi_{23}} \\ r_{23} &= \tau_{12} e^{i\phi_{23}}. \end{aligned} \quad (4.3)$$

The quantities above depend on the indices of refraction on both sides of the interface.

The absorptivity A of the metallic film is defined as the ratio of absorbed intensity to incident intensity. From conservation of energy, $A = 1 - T - R$. The phase of the incident wave will also be changed after reflection or transmission by the metallic film. The phase shifts due to reflection (δ_r) and transmission (δ_t) are given by:

$$\tan \delta_r = \frac{\rho_{23}(1 - {\rho_{12}}^2)\sin(2u_2\eta + \phi_{23}) + \rho_{12}[e^{2v_2\eta} - {\rho_{23}}^2 e^{-2v_2\eta}] \sin \phi_{12}}{\rho_{23}(1 + {\rho_{12}}^2)\cos(2u_2\eta + \phi_{23}) + \rho_{12}[e^{2v_2\eta} + {\rho_{23}}^2 e^{-2v_2\eta}] \cos \phi_{12}} , \quad (4.4)$$

$$\tan[\delta_t + \chi_{12} + \chi_{23} + u_2\eta] = \frac{e^{-2v_2\eta} \sin 2u_2\eta - \rho_{12}\rho_{23} \sin(\phi_{12}\phi 23)}{e^{-2v_2\eta} \cos 2u_2\eta + \rho_{12}\rho_{23} \cos(\phi_{12}\phi 23)}. \quad (4.5)$$

In general, the phase shift due to reflection and the phase shift due to transmission are not identical. As the thickness of the film approaches zero, δ_t approaches zero and δ_r approaches to $-\pi/2$ which are the phase shifts of a dielectric-dielectric interface. A plot of the theoretical optical properties of an Aluminum film is shown in Fig.4.1.

The refractive index and the extinction coefficient are taken from the CRC handbook of physics and chemistry (1965).

The transmissivity decreases as the thickness of the film increases while the reflectivity increases and the absorptivity increases at first and then levels off. The slope of the transmission and reflection curve versus the thickness of the film depend on the extinction coefficient $v_2 = n_2\kappa_2$ of the metallic film. This coefficient is directly related to the absorption coefficient of the bulk metal by $\alpha = 4\pi\kappa_2 n_2/\lambda_0$ where λ_0 is the wavelength of the radiation in vacuum. The phase changes due to reflection and transmission are different in the entire range of thicknesses shown.

Let us consider now a Fabry-Perot cavity made of two metallic mirrors of reflectivity R, filled with a nonabsorbing medium. Summing up all the contributions to the transmitted field, keeping in mind that there is an additional phase change δ_r after each reflection and a phase change δ_t after each transmission, the amplitude of the transmitted field is found to be:

$$E_t = \frac{E_i t^2 e^{i(\varphi+2\delta_t)}}{1 - r^2 e^{2i(\varphi+\delta_r)}} , \tag{4.6}$$

where E_i is the amplitude of the incident field, and $\varphi = nkd$ is half of the round trip phase shift. The transmissivity of the metallic Fabry-Perot is then given by

$$\mathcal{T} \equiv \left|\frac{E_t}{E_i}\right|^2 = \frac{T^2}{(1-R)^2}\frac{1}{1 + F\sin^2(\varphi + \delta_r)} , \tag{4.7}$$

where $F \equiv 4R/(1-R)^2$. Notice that the phase change due to transmission does not come into play in the above equation.

Summing up all the contributions to the reflected field, we find

$$E_r = E_i r e^{i\delta_r} + \frac{E_i r t^2 e^{i(\delta_r+2\delta_t+2\varphi)}}{1 - r^2 e^{2i(\varphi+\delta_r)}} . \tag{4.8}$$

The reflectivity of the cavity is then

$$\begin{aligned} \mathcal{R} &= \left|\frac{E_r}{E_i}\right|^2 \\ &= \left\{(1-R+T)^2 - 4\left[T\sin^2(\varphi+\delta_t) - R\sin^2(\varphi+\delta_r) - RT\sin^2(\delta_r-\delta_t)\right]\right\} \\ &\quad \frac{R}{(1-R)^2}\frac{1}{1+F\sin^2(\varphi+\delta_r)}. \end{aligned} \tag{4.9}$$

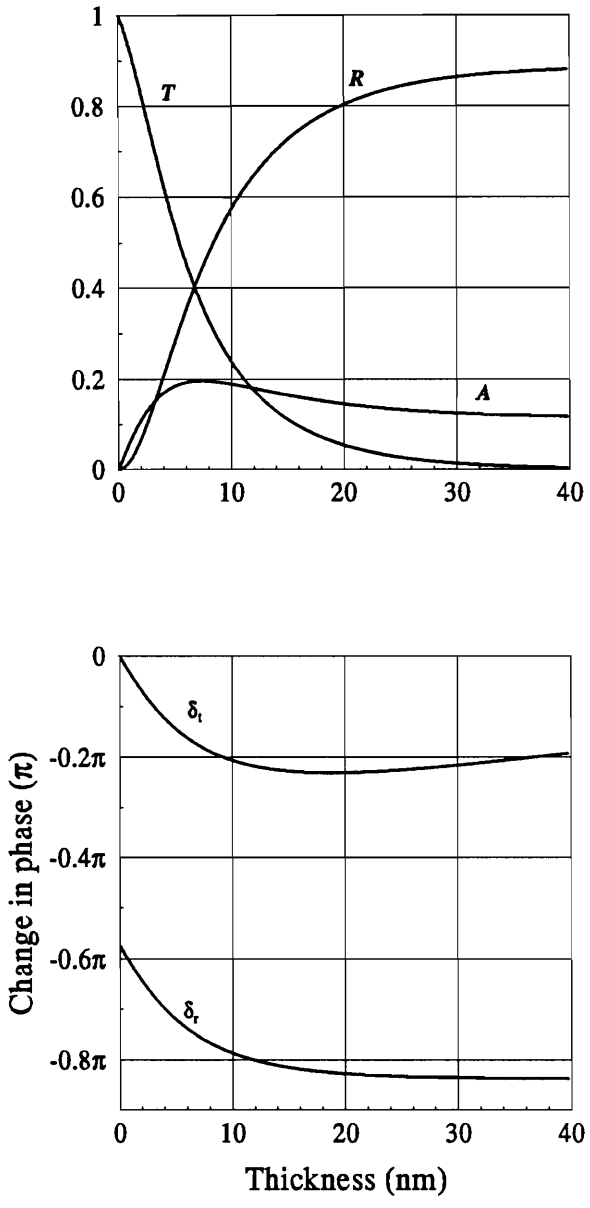

Figure 4.1: Theoretical optical properties of an aluminum film. (a) Reflectivity R, transmissivity T and absorptivity A versus the thickness of the metallic film. (b) The phase change upon reflection δ_r and transmission δ_t versus the thickness of the metallic film. The index of refraction and the extinction coefficient are $n = 0.713$ and $k = 8.00$ at a wavelength $\lambda = 514$nm. The index of refraction of the media on both sides of the film is assumed to be 1. Data is taken from the CRC handbook of physics and chemistry (1965).

From conservation of energy, the absorptivity of the metallic Fabry-Perot is

$$\mathcal{A} = 1 - \mathcal{T} - \mathcal{R}. \tag{4.10}$$

The transmissivity $\mathcal{T}$ against the round trip phase shift is an Airy function (see Eq.(4.7)). However, Eq.(4.9) indicates an additional shift in the peak of the reflectivity curve. In the case of dielectric Fabry-Perot cavities, the extrema of $\mathcal{T}$ and $\mathcal{R}$ occur for the same phase. The shift in the peaks of the transmissivity, reflectivity and absorptivity curves for a metallic Fabry-Perot are shown in Fig.4.2. The maxima of transmissivity, minima of reflectivity and the maxima of absorptivity occur for different values of the induced phase change $\Delta\phi = \varphi - n_0 kd = n_2 Ikd$.

The shift between the transmission maxima and the corresponding reflection minima is due to the fact that when the transmission is in resonance there is a phase shift of $2(\delta_t - \delta_r)$ between the directly reflected incident field and the field inside the cavity propagating in the backward direction. This phase shift is no longer either 0 or π, as it is in the case of non-absorbing mirrors.

The absorption within the metallic film causes a rise in temperature in the film, thus increasing the temperature of the substrates and of the thermo-optic material. The change in temperature inside the cavity comes from two sources, one is the absorption due to the front metallic mirror and the other is the absorption from the back mirror. Referring to Fig.4.3, the front mirror is heated by the incident beam and by the backward propagating beam inside the cavity while the back mirror is heated by the forward propagating beam only. We can write the average temperature change inside the cavity as:

$$\Delta T \simeq \frac{\partial T}{\partial I_A}\mathcal{A}(I_i + I_f + I_b) \tag{4.11}$$

where I_i is the incident intensity, I_f and I_b are the intensities of the forward and backward propagating beam inside the cavity. $\frac{\partial T}{\partial I_A}$ is the temperature rise per unit intensity absorbed which depends on the cavity's construction, on the beam spot size and on the thermal conductivities of the substrates, of the metallic film and of

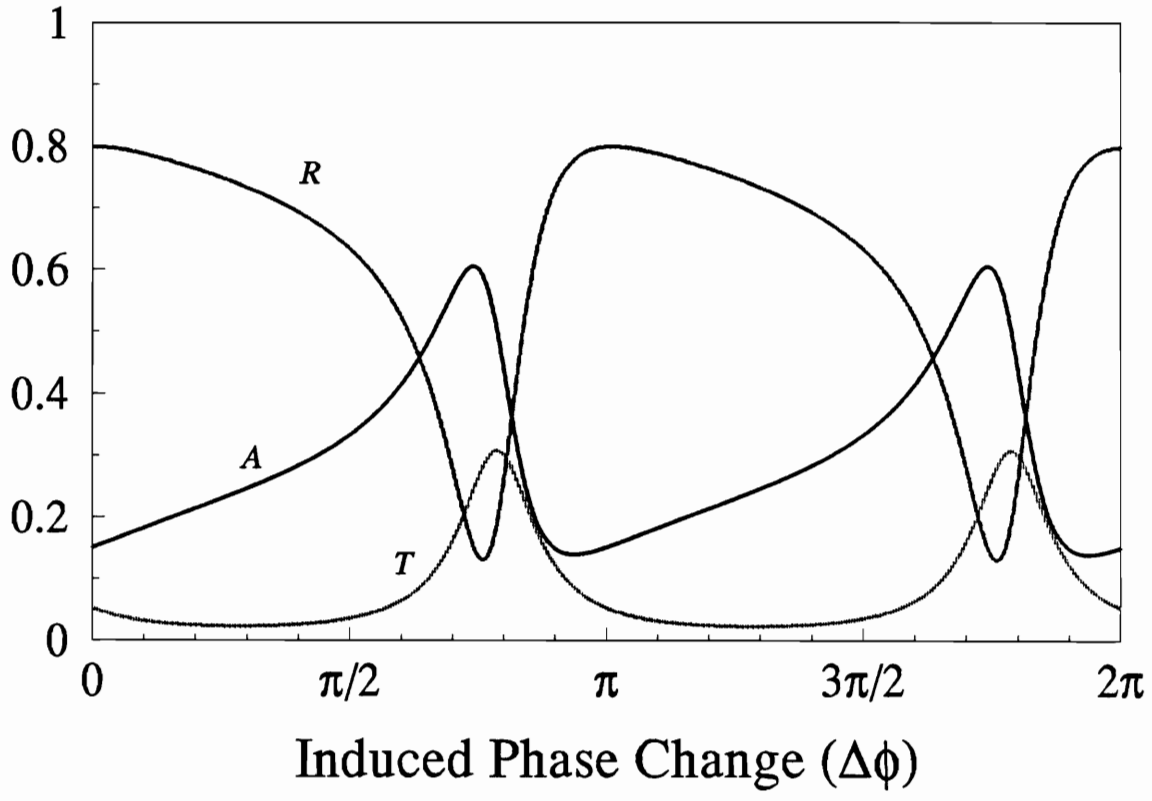

Figure 4.2: Transmissivity T, reflectivity R and absorptivity A versus the induced phase change in a metallic nonlinear Fabry-Perot cavity. Due to the different phase changes upon reflection and transmission on a metallic film, the transmission maxima and reflection minima are shifted occur for different induced phase changes.

the thermo-optic medium. The phase change inside the cavity which is filled with a thermo-optic medium is given by

$$\begin{aligned} \Delta\phi &= kd\Delta n \\ &\simeq \frac{\phi_o}{n_0}\left(\frac{\partial n}{\partial T}\frac{\partial T}{\partial I_A}\right)\mathcal{A}(\varphi)(I_i + I_f + I_b) \end{aligned} \tag{4.12}$$

where $\partial n/\partial T$ is the thermo-optic coefficient of the medium. The quantity $\Delta\phi/\phi_o$ is proportional to the absorbed intensity $A(\varphi)(I_i + I_f + I_b)$.

The intensities of the forward traveling and backward traveling waves I_f and I_b are related to the transmitted and reflected intensities by the mirror transmissivity T:

$$I_f = \frac{I_t}{T} = \frac{1}{T}\mathcal{T}I_i\ , \tag{4.13}$$

$$I_b = \frac{I_r}{T} = \frac{1}{T}\mathcal{R}I_i. \tag{4.14}$$

Therefore we can write

$$\Delta\phi \simeq \frac{\phi_o}{n_0}\left(\frac{\partial n}{\partial T}\frac{\partial T}{\partial I_A}\right)\mathcal{A}(\varphi)I_i\left[1 + \frac{1}{T}(\mathcal{T} + \mathcal{R})\right]. \tag{4.15}$$

The response of the cavity can then be determined numerically using the change in phase as a running parameter. First, the initial detuning ($\phi_o = 2kdn_o$) is chosen by fixing all the cavity parameters such as mirror reflectivity, length of cavity and index of refraction of the medium. Then the transmissivity of the cavity $\mathcal{T}$ and the reflectivity of the cavity $\mathcal{R}$ are determined from Eq.(4.7) and Eq.(4.9) by stepping through the phase of the cavity ($\phi_o + \Delta\phi$). For each phase step, the incident intensity I_i can be calculated from (4.15). The intensity transmitted and reflected are then found by using

$$I_t = \mathcal{T}I_i \tag{4.16}$$

$$I_r = \mathcal{R}I_i. \tag{4.17}$$

The response of the cavity can also be determined graphically as follow (This method is similar to that used by Marburger for the case of a dielectric Fabry-Perot [34]).

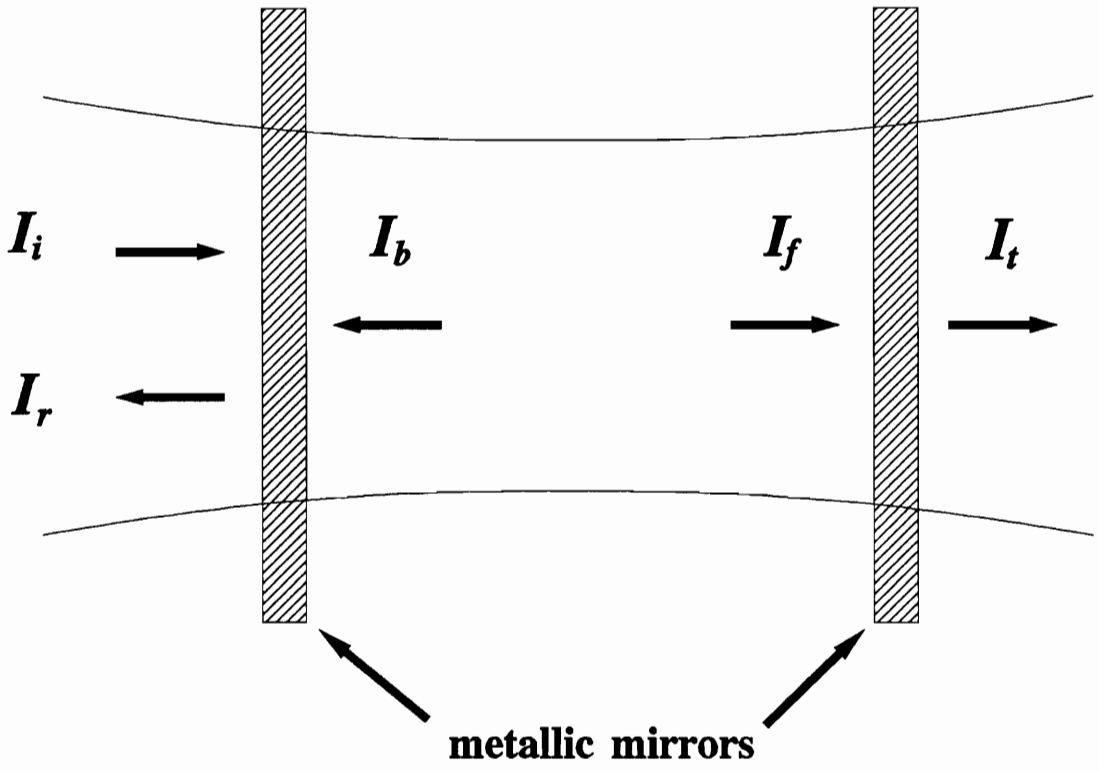

Figure 4.3: The front and back metallic mirrors in a Fabry-Perot are heated by the incident and the backward propagating waves and by the forward wave, respectively.

Neglecting the heating effect which comes from the forward and backward propagating wave inside the cavity, and keeping only the heating effect due to the incident wave, Eq.(4.12) can be written as

$$\mathcal{A} = \frac{\Delta\phi}{\phi_o}\left(\frac{1}{n}\frac{\partial n}{\partial T}\frac{\partial T}{\partial I_A}\right)^{-1}\frac{1}{I_i}. \tag{4.18}$$

This is a reasonable approximation when the absorptivity and the reflectivity of the mirrors are high. The plot of the absorptivity $\mathcal{A}$ versus the induced phase change $\Delta\phi$ is a straight line. The slope of this line is determined by the thermo-optic coefficient $\partial n/\partial T$, the index of refraction of the medium n, the temperature rise per unit absorbed intensity $\partial T/\partial I_A$ and the incident intensity I_i. All these quantities are constants for a particular cavity configuration, except for the incident intensity. Changing the incident intensity changes the slope of the straight line.

Fig.4.4(a) shows the absorptivity curve versus the induced phase change for a 10nm aluminum film evaporated on glass substrate having a refractive index equals to 1.56. This absorptivity curve is different for different metallic films. The absorptivity for a certain value of the incident intensity is given by the intersection of the straight line representing Eq.(4.18) and the absorptivity curve. Varying the incident intensity will change the slope of the straight line which intersects the absorptivity curve at different places. The sign of the slope of the straight line is determined by the sign of the thermo-optic coefficient.

Starting from zero intensity which corresponds to a straight line of infinite slope, up to line a, the absorptivity is single valued. As the incident intensity increases beyond this point, the straight line intersects the absorptivity curve at three different places which gives three different values of $\mathcal{A}$. This can be seen in Fig.4.4(b), the graphical solution of Fig.4.4(a). The range a-c defines the bistable region. The middle branch of $\mathcal{A}$ in Fig.4.4(b) is unstable. As the incident intensity increases, the absorptivity follows the lower branch up to line c as seen in Fig.4.4(a). Beyond line c the absorptivity will jump from point S_1 to the upper branch of $\mathcal{A}$. The absorptivity will then follow the upper branch of $\mathcal{A}$. As the incident intensity decreases from line

d until it reaches line a. At S_2, the absorptivity switches back down to the lower branch.

The transmissivity of the cavity is shown in dotted lines in Fig.4.4(b). Notice that the transmissivity curve makes a loop. The upper portion of the loop is unstable. This type of transmissivity curve is generally known as "butterfly" hysteresis.

Another feature making the metallic cavity different from the dielectric cavity is that the cavity switches between a high and a low level of absorptivity. This is not necessarily correlated to a high and a low level of transmittance because of the shift between the transmission peaks and the absorption peaks. The shape of the butterfly hysteresis depends not only on the characteristics of the metallic film but also on the sign of the thermo-optic coefficient.

Fig.4.5(b) and (c) show two different butterfly hysteresis curves obtained with two identical metallic Fabry-Perots filled with thermo-optic materials having thermo-optic coefficients of opposite signs. The magnitude of the thermo-optic coefficients of both media are equal. Fig.4.5(a) shows the absorptivity of the cavity versus the induced phase change. Since the cavities have identical parameters except for the sign of the thermo-optic coefficients, the initial detuning ϕ_0 are the same. Therefore, the two cavities have the same absorptivity when the incident intensity is zero. The sign of the thermo-optic coefficient determines the sign of the slope of the straight line (Eq.4.18). The absorptivity curve in Fig.4.5(a) consists of two parts. The curve on the left of ϕ_0 corresponds to the absorptivity curve of the medium having a negative thermo-optic coefficient. The curve on the right of ϕ_0 corresponds to the absorptive curve of the medium having a positive thermo-optic coefficient. Notice that the absorptivity curve is not symmetric about any ϕ_0 value. Therefore, unlike dielectric Fabry-Perots, the features of the hysteresis curves for metallic Fabry-Perots filled with materials having thermo-optic coefficient of opposite signs are different. It can be seen from Fig.4.5(a) that the cavity with a positive thermo-optic coefficient is bistable within the range between line a and line b. The corresponding hystersis curve is shown in Fig.4.5(c). In contrast, the cavity with a negative thermo-optic coefficient only undergoes a sharp

nonlinear change in absorptivity as the straight line reaches the position c.This sharp change in absorptivity shows up as a small kink for an incident intensity of about 0.5 unit in the butterfly hysteresis curve of Fig 4.5(b).

A metallic Fabry-Perot filled with a material having thermo-optic coefficients of opposite signs will result in normal and inverted butterfly hysteresis, respectively. An inverted butterfly hysteresis (Fig.4.5(c)) appears when the product $n_2(|\delta_r|-|\delta_t|-\pi/2)$ is negative.

The difference between the phase shift upon transmission and reflection of the metallic mirrors is seen to greatly affect the shape of the hysteresis. Fig.4.6 shows how the shape of the hysteresis curve changes from a normal butterfly to an inverted butterfly hysteresis as the difference in the phase shifts changes. There are two major features affected by this phase difference. First, the butterfly hysteresis is inverted when the product $n_2(|\delta_r| - |\delta_t| - \pi/2) < 0$. Secondly, the width of the loop depends on the quantity $|\delta_r - \delta_t|$. A large difference between the phase changes upon reflection and transmission will result in a switching curve of lower contrast. This is indicated by the elongation of the hysteresis curves seen in Fig.4.6(b) and (d). The hysteresis curves for a phase difference $|\delta_r - \delta_t| - \pi/2 = \pm 0.03\pi$ show a higher contrast switching (Fig.4.6 (a),(c)) than the ones with a phase shift $|\delta_r - \delta_t| - \pi/2 = \pm 0.14\pi$ (Fig.4.6 (b),(d)) As the quantity $|\delta_r - \delta_t|$ approaches $\pi/2$, the contrast increases. The butterfly hysteresis curve changes to normal hysteresis when $|\delta_r - \delta_t| = \pi/2$ (Fig.4.7) which is the case of a dielectric Fabry-Perot for which the phase change upon reflection is $\pi/2$.

4.2 Birefringent Metallic Fabry-Perot Cavity

In section 4.1 the nonlinear medium in the cavity was isotropic. In this section we extend the analysis to the case of a birefringent medium. The response of the cavity can easily be found by adapting the equations of the last section and generalizing them to include the two eigen-polarizations of the medium. Rewriting Eq.(4.7), Eq.(4.9) and Eq.(4.10) for the transmissivity, reflectivity and the absorptivity of the two eigen-

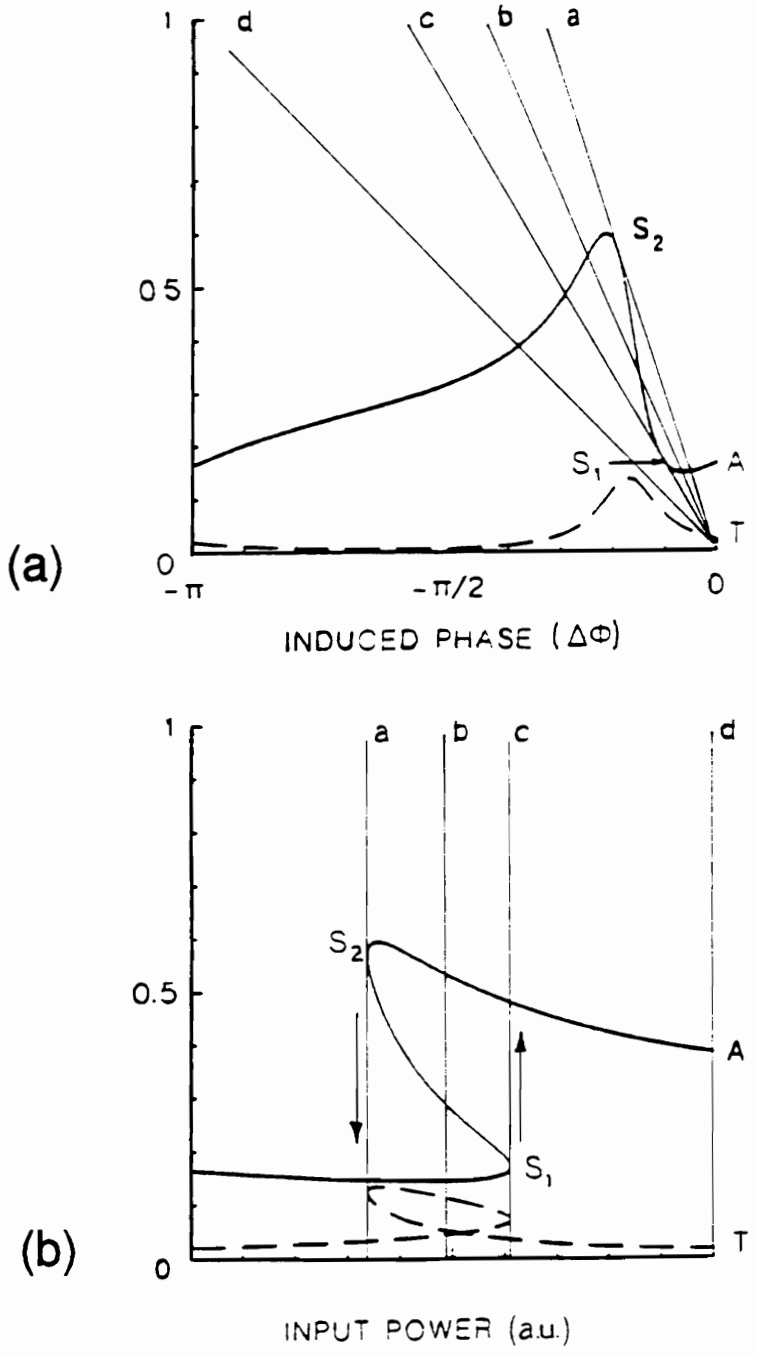

Figure 4.4: Graphical solution of the response of a metallic Fabry-Perot. (a) Absorptivity A against the induced phase $\Delta\phi$. The solutions are the intersections of this curve with the line of Eq.(18). The transmissivity is plotted in dashed line. (b) Absorptivity A versus input power. The corresponding transmissivity is shown in dashed line.

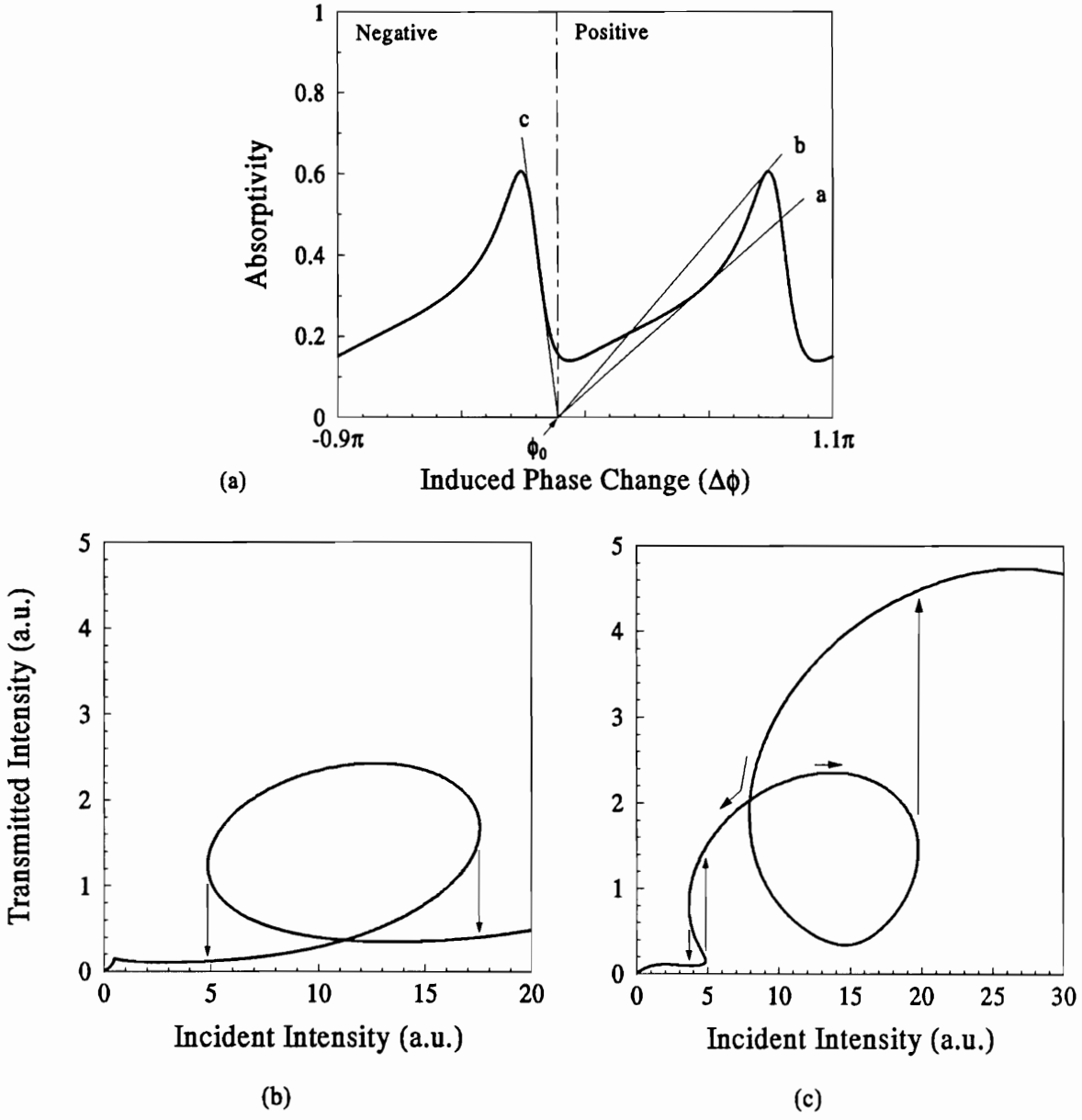

Figure 4.5: Identical cavities filled with materials having thermo-optic coefficients of opposite signs result in normal and inverted butterfly hysteretic response depending on the product $(|\delta_r - \delta_t| - \pi/2)n_2$. (a) Absorptivity of a metallic Fabry-Perot etalon. The thickness of the aluminum film is 10nm. Intra-cavity spacing is 49.99μm. The cavity is filled with a thermo-optic medium with $n_0 = 1.56$ and $n_2 = \pm 10^{-3}$. (b) The cavity with a negative thermo-optic coefficient results in a normal butterfly hysteresis. (c) The one with a positive thermo-optic coefficient results in an inverted butterfly hysteresis.

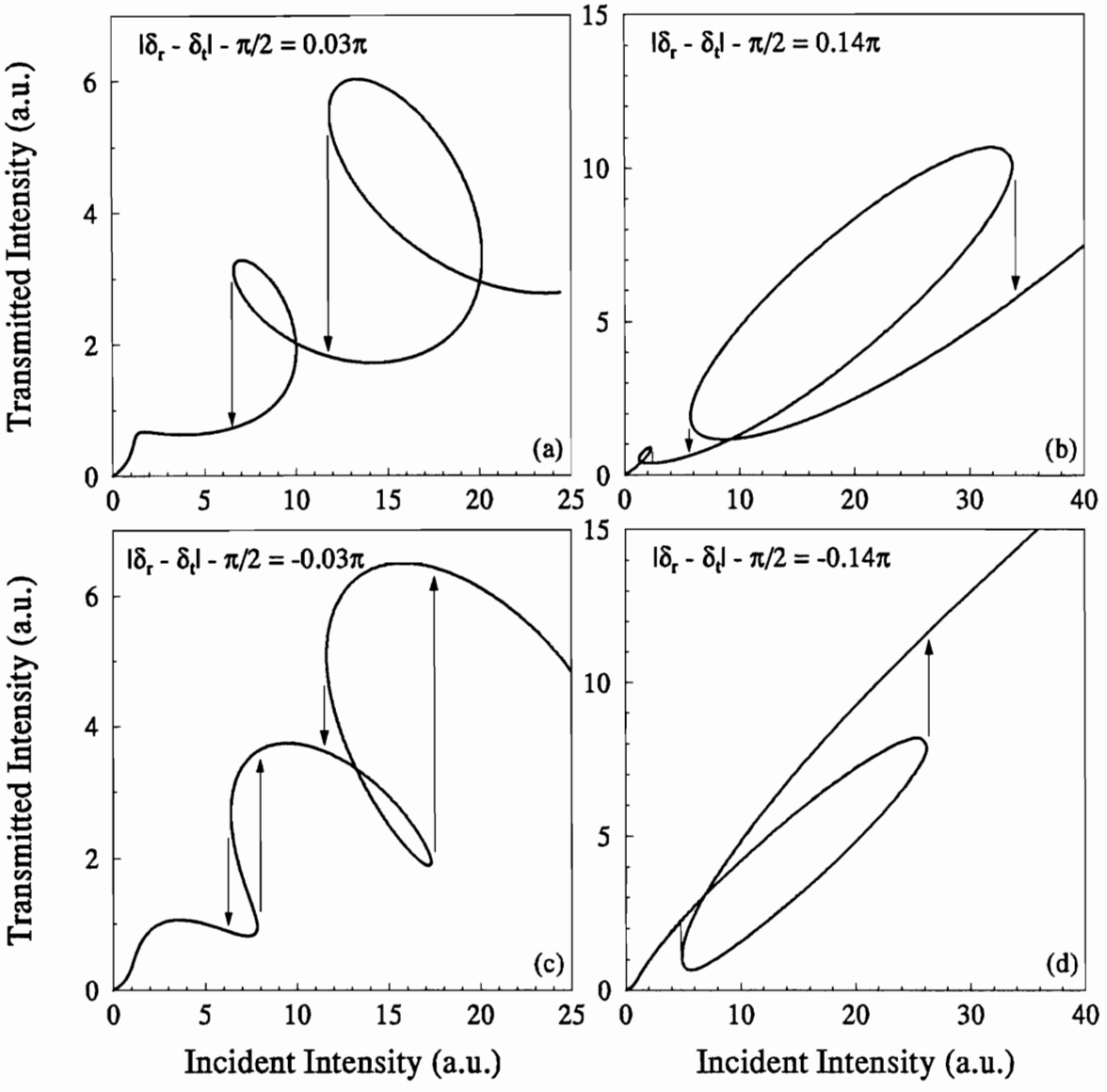

Figure 4.6: Hysteresis curves for various nonlinear metallic Fabry-Perots. The cavity parameters are $R = 0.354$, $T = 0.449$, $n_0 = 1.56$, $|n_2| = 10^{-3}$ for all four curves. The shape of the hysteresis curve depends on two factors: $|\delta_r - \delta_t|$ and the sign of the thermo-optic coefficient. The width of the loops depends on the difference $|\delta_r - \delta_t|$. The larger this value is the longer the loop. The cavity switches with a normal butterfly hysteresis when the product $(|\delta_r - \delta_t| - \pi/2)n_2 > 0$ ((a) and (c)) and switches with an inverted butterfly hysteresis when $(|\delta_r - \delta_t| - \pi/2)n_2 < 0$ ((b) and (d)).

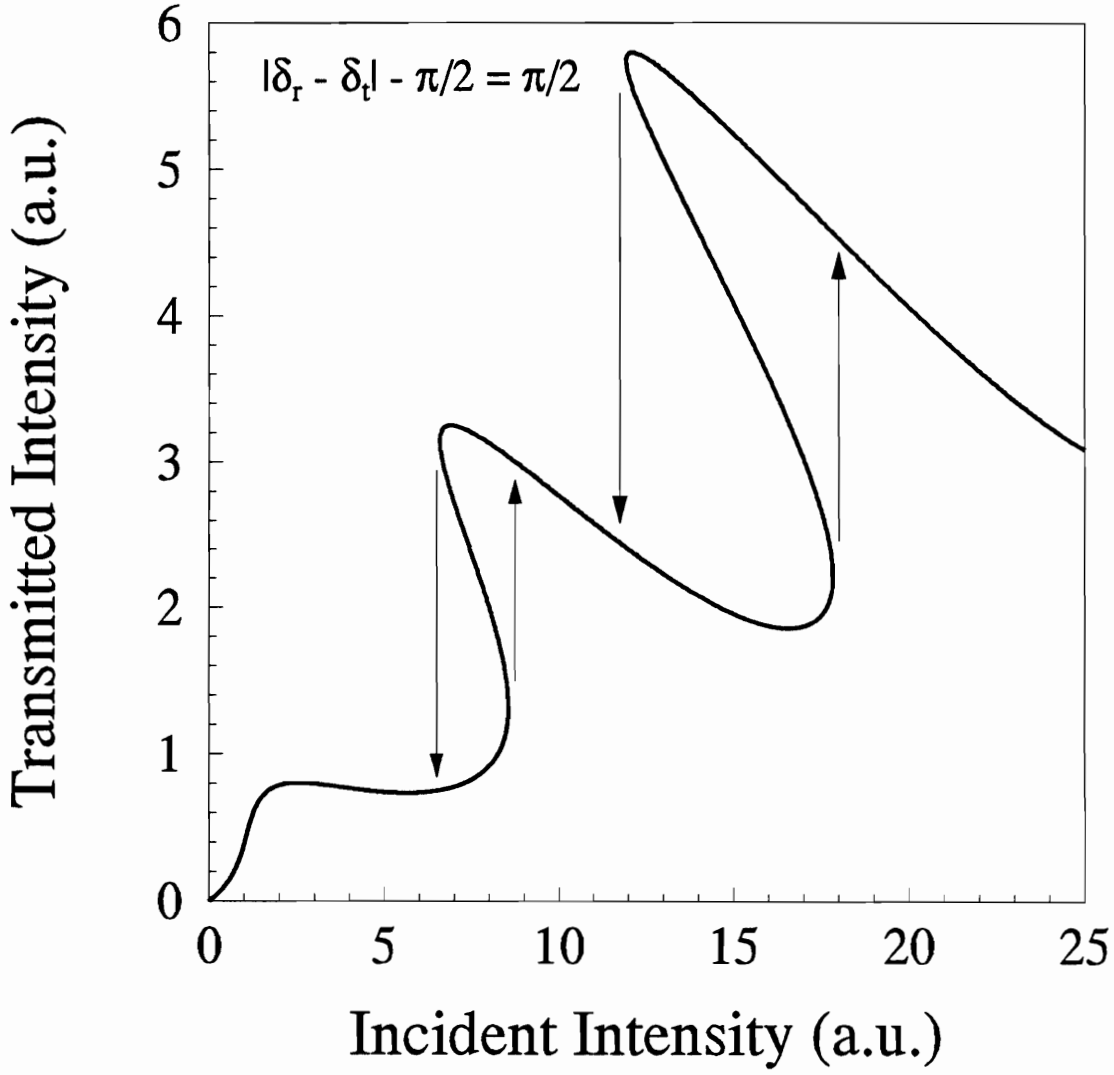

Figure 4.7: When $|\delta_r - \delta_t| = \pi/2$, the cavity switches with a normal S-shape hystersis curve.

polarizations, we have

$$\mathcal{T}_{x,y} \equiv \left|\frac{E_{t_{x,y}}}{E_i}\right|^2 = \frac{T^2}{(1-R)^2}\frac{1}{1+F\sin^2(\varphi_{x,y}+\delta_r)} \tag{4.19}$$

$$\begin{aligned}\mathcal{R}_{x,y} \;=\; & \frac{R}{(1-R)^2}\frac{1}{1+F\sin^2(\varphi_{x,y}+\delta_r)}\Big\{(1-R+T)^2 \\ & -4\Big[T\sin^2(\varphi_{x,y}+\delta_t) \\ & -R\sin^2(\varphi_{x,y}+\delta_r) - RT\sin^2(\delta_r-\delta_t)\Big]\Big\}\end{aligned} \tag{4.20}$$

$$\mathcal{A}_{x,y} = 1 - \mathcal{T}_{x,y} - \mathcal{R}_{x,y}\ , \tag{4.21}$$

where the subscripts x and y stands for the two eigen-polarizations of the birefringent material. R and T are the reflectivity and transmissivity of the metallic mirrors. δ_t and δ_r are the phase changes upon transmission and reflection respectively. R, T, δ_r and δ_t are assumed to be the same for both polarizations. This is generally true for most birefringent materials. A plot of the above quantities for an aluminum film on a glass substrate in contact with a nematic liquid crystal (MBBA) aligned parallel to the substrates is shown in Fig.4.8. For thicknesses greater than 10nm, the above quantities are approximately the same for both polarizations.

In Eq.(4.9), (4.19)-(4.20), it was also assumed that the incident wave is linearly polarized at 45° with respect to the fast axis of the birefringent medium. The induced temperature change depends only on the total radiation incident on each metallic mirrors and not on the polarization. The induced phase changes for the two polarizations are

$$\Delta\phi_{x,y} \simeq \frac{\phi_{o_{x,y}}}{n_{0_{x,y}}}\left(\frac{\partial n_{x,y}}{\partial T}\frac{\partial T}{\partial I_A}\right)\mathcal{A}(\varphi)(I_i + I_{f_x} + I_{f_y} + I_{b_x} + I_{b_y})\ , \tag{4.22}$$

where ϕ_{0_j} is the initial detunings of the cavity for the eigen-polarizations j, n_{0_j} is the linear index of refraction, I_{f_j} and I_{b_j} are the forward and backward propagating wave intensities inside the cavity for the eigen-polarization state ($j = x$ or y). The nonlinear indices of refraction of the medium for the eigen-polarizations are defined as $n_{2_{x,y}} \equiv \frac{\partial n_{x,y}}{\partial T}\frac{\partial T}{\partial I_A}$. Keeping in mind that the transmitted intensity and the intensity

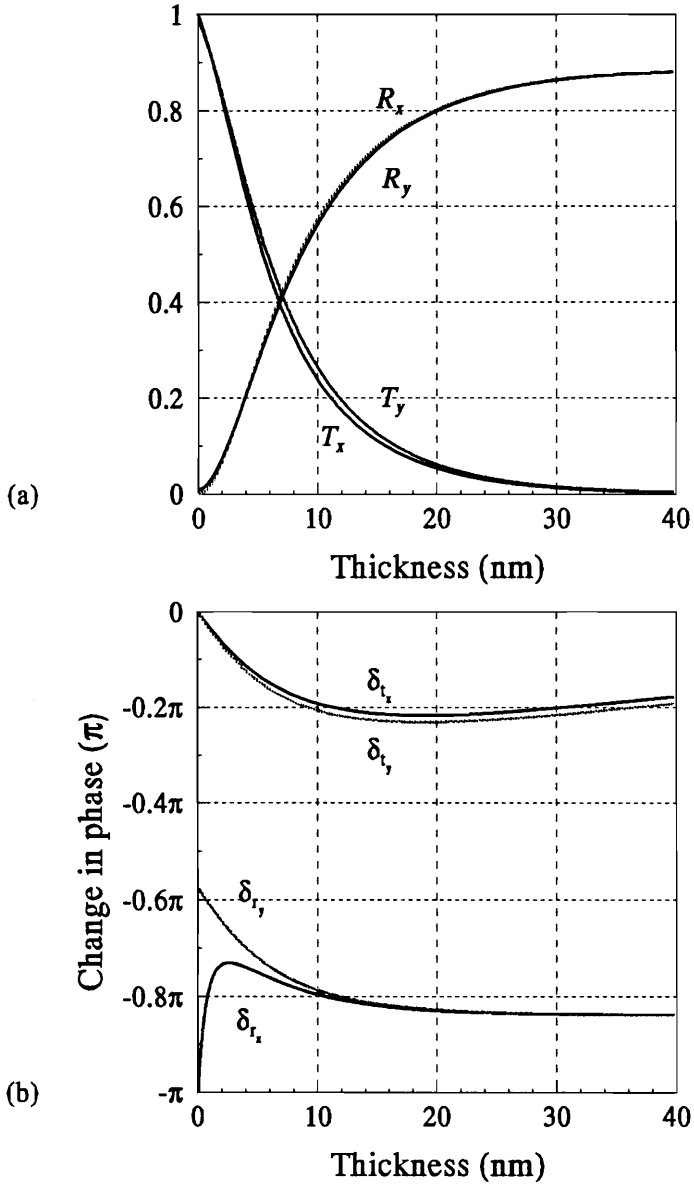

Figure 4.8: (a) Transmissivity T, reflectivity R, (b) phase change upon reflection and transmission of an aluminum film on a glass substrate and in contact with a liquid crystal (MBBA) in planar orientation. The subscripts x and y refer to the polarization parallel and perpendicular to the director of the liquid crystal, respectively.

inside the cavity differ only by the proportionality constant T, the induced phase shifts can then be written as

$$\Delta\phi_x = \frac{\Delta\phi_x}{n_{0_x}} n_{2_x} \left[1 + \frac{1}{T}(\mathcal{T}_x + \mathcal{T}_y + \mathcal{R}_x + \mathcal{R}_y)\right](1 - \mathcal{T}_x - \mathcal{R}_x) I_i \qquad (4.23)$$

$$\Delta\phi_y = \frac{\Delta\phi_y}{n_{0_y}} n_{2_y} \left[1 + \frac{1}{T}(\mathcal{T}_x + \mathcal{T}_y + \mathcal{R}_x + \mathcal{R}_y)\right](1 - \mathcal{T}_y - \mathcal{R}_y) I_i \,. \qquad (4.24)$$

Eq.(4.23) and (4.24) can be solved numerically by searching for consistent solutions of the induced phase changes $\Delta\phi_x$ and $\Delta\phi_y$ for a given incident intensity. Once the induced phase changes are found, the transmissivities and reflectivities can then be calculated from Eq.(4.19) and Eq.(4.20).

The response of the birefringent cavity is much more complicated than that of its isotropic counterpart. The shape of the transmitted intensity curve is determined by the reflectivity, the phase changes upon reflection and transmission at the mirror surfaces as well as on the sign of the thermo-optic coefficients of the medium for each polarization. The transmitted versus incident intensity curves are further complicated by the fact that the two polarizations are coupled by the temperature change in the medium. This coupling depends on the detuning of the cavity. The coupling is more noticeable when the detuning is closer to an absorption resonance. In the neighborhood of an absorption resonance a slight change in the cavity phase will result in a large change of absorption and the coupling is enhanced.

The change in coupling of the eigen-polarizations can be seen in Fig.4.9 and Fig.4.10. Fig.4.9 and Fig.4.10 are hysteresis curves for the switching of two identical metallic Fabry-Perot cavities filled with the same nonlinear medium but having different initial detunings. The cavity in Fig.4.9 is tuned[2] to a value of 0.66π for the x-polarization state and 0.58π for the y-polarization state. The cavity in Fig.4.10 is tuned to 0.48π and 0.38π for the x and y-polarization states respectively. Fig.4.9(a) shows the switching curve of the x-polarization state and Fig.4.9(b) shows the switching curve of the y-polarization state. Since the detuning of the cavity

[2]The detunings are defined by $\phi_0 = 2kdn_0$ as usual.

for the y-polarization is smaller, the y-polarization state switches first at approximately 0.18 units. The switching of the y-polarization does not show much effect on the x-polarization. The x-polarization then switches at 0.3 unit. This switching causes a change in the temperature inside the cavity which affects the detuning of the y-polarization as well. The end result is a change in the transmitted intensity in the y-polarization. As the incident intensity decreases, both polarizations switch simultaneously at about 0.156 unit.

Fig.4.10 shows a silimar switching curve for a larger difference in the initial detuning of the eigen-polarizations. As seen, the first switching of the y-polarization has very little effect on the x-polarization.

We have derived in this chapter the steady state model of both isotropic and birefringent nonlinear Fabry-Perot cavities. The cavities responds with a butterfly shaped hysteresis curves. It will be seen in chapter 5 that the experimental results agree very well with this prediction.

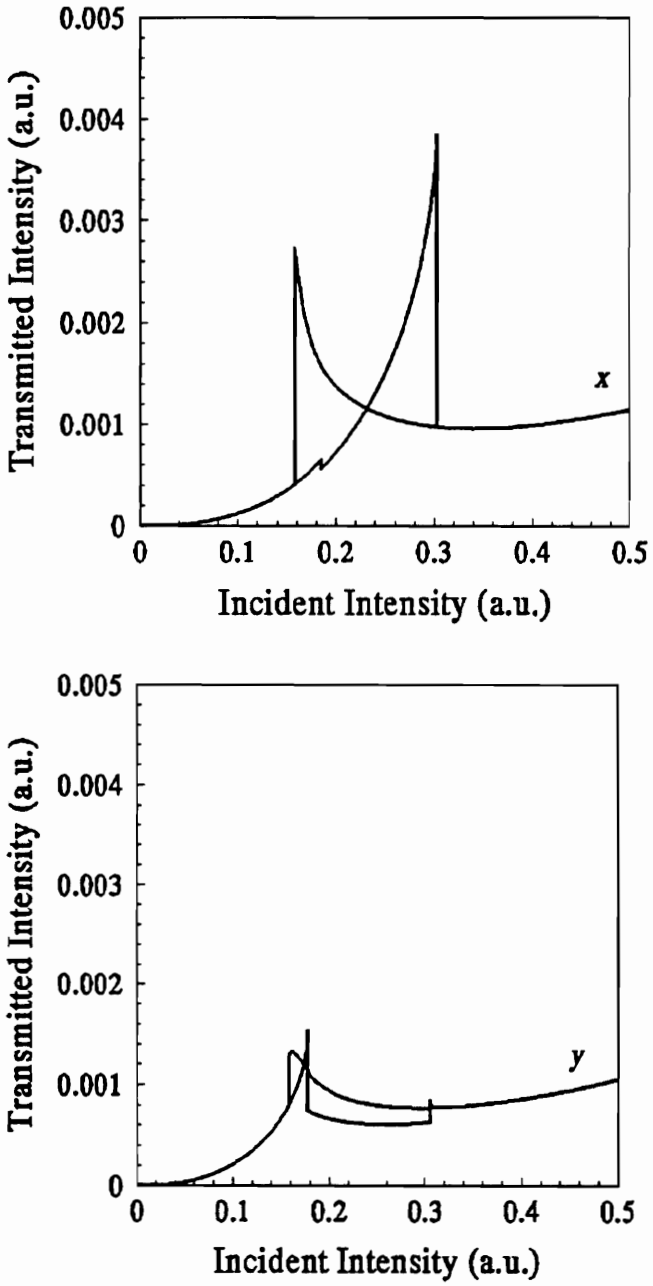

Figure 4.9: Hysteresis curves of a nonlinear birefringent metallic Fabry-Perot cavity. The cavity parameters are as follow: $R = 0.686$, $T = 0.126$, $n_{0_x} = 1.562$, $n_{0_y} = 1.806$, $n_{2_x} = n_{2_y} = 10^{-3}$ and $d = 49.97\mu$m. This corresponds to detunings $\phi_{0_x} = 0.66$ (mod π) and $\phi_{0_y} = 0.58$ (mod π) for each polarization. The phase changes upon reflection and transmission at the metallic mirrors are $\delta_r = -0.41$ (mod 2π) and $\delta_t = -0.011$ (mod 2π). The switchings show some coupling between the polarization states.

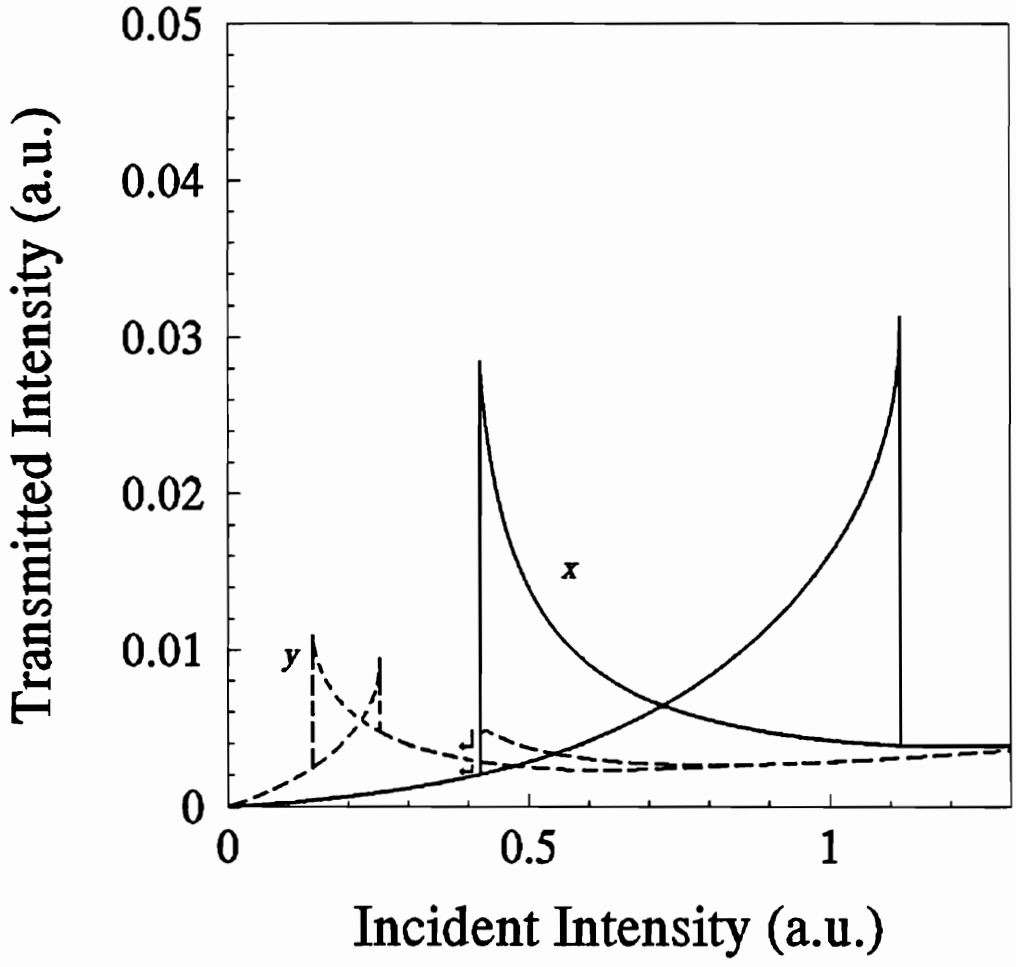

Figure 4.10: Hysteresis curves of the same nonlinear birefringent metallic Fabry-Perot cavity as in Fig.4.9 but for a different initial detuning. With $d = 49.975\mu$m, the detunings are of $\phi_{0_x} = 0.48 \pmod{\pi}$ and $\phi_{0_y} = 0.38 \pmod{\pi}$ for each polarization. The switchings show little coupling between the polarization states.

Chapter 5

Experimental Investigation of Optical Bistability in a Nonlinear Fabry-Perot with Metallic Mirrors

It was shown in chapter 4 that a dielectric Fabry-Perot cavity has a normal hysteretic response while a metallic Fabry-Perot cavity has a "butterfly hysteresis" response. For most applications, a normal hysteresis is preferred because the output has, in this case, two distinct levels. However, due to the limitation of vacuum deposition/sputtering facility available, it was impossible for us to fabricate multicoated dielectric mirrors. Therefore, metallic Fabry-Perot cavities were used in the experiments. Nonetheless, since the principle of operation of both types of cavity is the same, these experiments offer both a valid test of the theory and a means to test experimentally the main features of the device. In the first part of this chapter, we describe the construction of the nonlinear birefringent cavities. In the second part, we discuss the experimental results.

5.1 Construction of The Nonlinear Fabry-Perot Cavity

In this section,the construction and testing of a nonlinear birefringent Fabry-Perot cavity are described. A nonlinear birefringent metallic Fabry-Perot cavity consists of a metallic Fabry-Perot filled with a nonlinear birefringent material. N-(*p*-methoxybenzylidene)-*p*-butylaniline (MBBA), a nematic liquid crystal, was used as the nonlinear medium. Its very high thermo-optic coefficient ($\sim 10^{-3}/°C$) allows one to observe its nonlinear effects with modest laser power. Furthermore, MBBA is readily available and has well known properties.

The construction of a nonlinear birefringent cavity involves two main steps: the evaporation of the metallic mirrors and of a protective coating, and the alignment of the liquid crystal.

5.1.1 Evaporation of Aluminum Mirrors

Fig.5.1 shows a schematic setup of a vacuum evaporation system. Normally, deposition of aluminum is done in a moderate vacuum of about 10^{-5} torr. The presence of oxygen in the vacuum chamber will 'fog' the aluminum mirror. The reflectivity of aluminum film on glass decreases as the rate of evaporation is lowered. This rate can be monitored by a crystal oscillator O placed near the substrate S. The reflectivity will also decrease as the substrate temperature increases. It was discovered that metallic films deposited too slowly tend to develop an agglomerate structure. This agglomeration causes an increase in the electrical resistivity and in the optical absorption. All the mirrors used in the experiments were produced by 'fast evaporation' at a pressure $\simeq 10^{-5}$ torr. Some of the mirrors were evaporated in the Physics Department and others in the Electrical Engineering Department at Virginia Tech.

Substrate Cleaning

The adhesion of aluminum on glass is poor unless the substrate is adequately prepared. Surface cleanliness is the most critical factor for producing a high quality

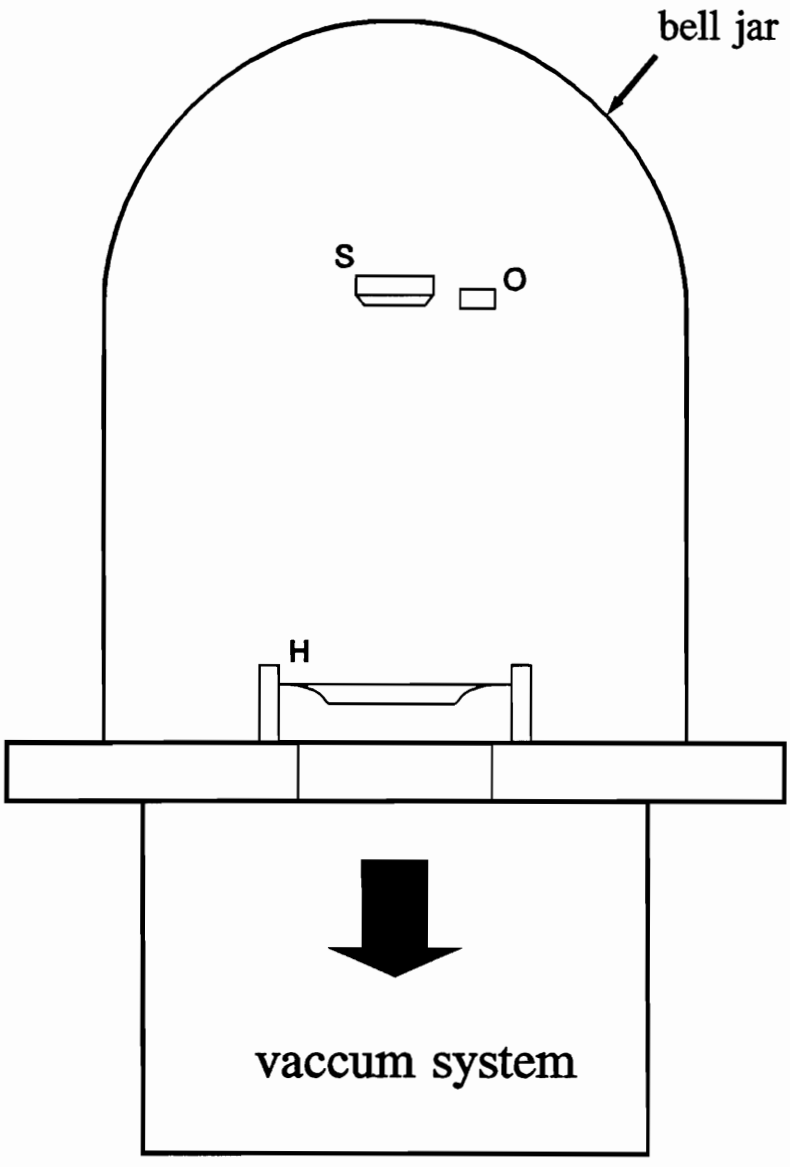

Figure 5.1: Vacuum evaporation setup. The substrate S is mounted upside down with the side to be coated facing the evaporation source. Heating element H, usually a tungsten boat or a tunsten coil, is used to evaporate pure aluminum wires. When the material reaches the melting point, the metal melts, evaporates then condenses and adhere on the target.

mirror. Stower and Patton [35] have compared different methods of preparing the surface of a substrate before evaporation. Among the methods investigated, high pressure (2500 psi) solvent spraying was found to be the most effective. They also found that acid and alkali cleaning, though very effective can have a mild etching effect which is not desirable for optics.

They pointed out that mechanical abrasion and scrubbing is also very effective towards removing stubborn contaminants. The recommended cleaning procedure is as follow. A clean wet tissue is wrapped around a common cotton ball. The combination is wetted with either acetone or ethanol (spectral grade) and the surface is scrubbed. After inspection with a high intensity light for any visible remaining contaminant, the surface is dragged or "wiped" with a solvent-saturated tissue. A fresh tissue is used for each wipe. If the part fails to pass the visual inspection, the process is repeated.

This technique was the only one available to us. Thus, before coating, the substrates were first cleaned in an ultrasonic bath and then cleaned using the method described.

Protective Coating

Alignment of the liquid crystal (LC) involves rubbing the mirror surface. It is thus necessary to harden or to protect the surface. Burnishing with a soft cloth under running water is an effective hardening process but may produce scratches and often results in low transmittance mirrors.

Our mirrors were protected by a silicon oxide layer deposited on the Aluminium. The refractive index of rapidly evaporated SiO film is about 1.97. The suggested thickness of SiO is 1500Å [36]. Note that this dielectric coating acts as a multiple interference thin film. Therefore, a uniform thickness of the layer is of great importance. Uniform coating thicknesses are difficult to achieve with large mirrors. However, the area of our substrates was small, (about 1 inch in diameter) thus, fast evaporation of SiO was used both for protection of the mirror and as a mean of aligning the liquid

crystal, as will be described later.

5.1.2 Nematic Liquid Crystal

Liquid crystals have properties of both liquid and crystal. Although they do not have a definite shape as solid crystals do, there exist a long range correlation in the arrangement of the molecules. Liquid crystals are less ordered than solid crystals but more ordered than a liquid. There are three main classes of liquid crystals: nematics, cholesterics and smectic. Only nematics are described here.

Fig.5.2 is a schematic representation of the order in a nematic phase. The main features are as follows:

1. The center of mass of the molecules have no long-range order, as in a conventional liquid.

2. There is some order however in the direction of the molecules. They tend to be oriented parallel to some common axis, called the director $\hat{\mathbf{n}}$. The molecules are allowed to rotate freely about their long axis. The anisotropy of the molecules and their arrangement is reflected in an anisotropy of the optical properties of the medium. The birefringence is usually large, typically 0.25 for MBBA. In all know cases, there appears to be a complete rotational symmetry around the axis $\hat{\mathbf{n}}$.

3. $\hat{\mathbf{n}}$ and $-\hat{\mathbf{n}}$ are indistinguishable.

4. Nematic phases occur only with materials which do not distinguish between right and left.

5. The direction of $\hat{\mathbf{n}}$ can be controlled by external forces either electrical, magnetic or mechanical.

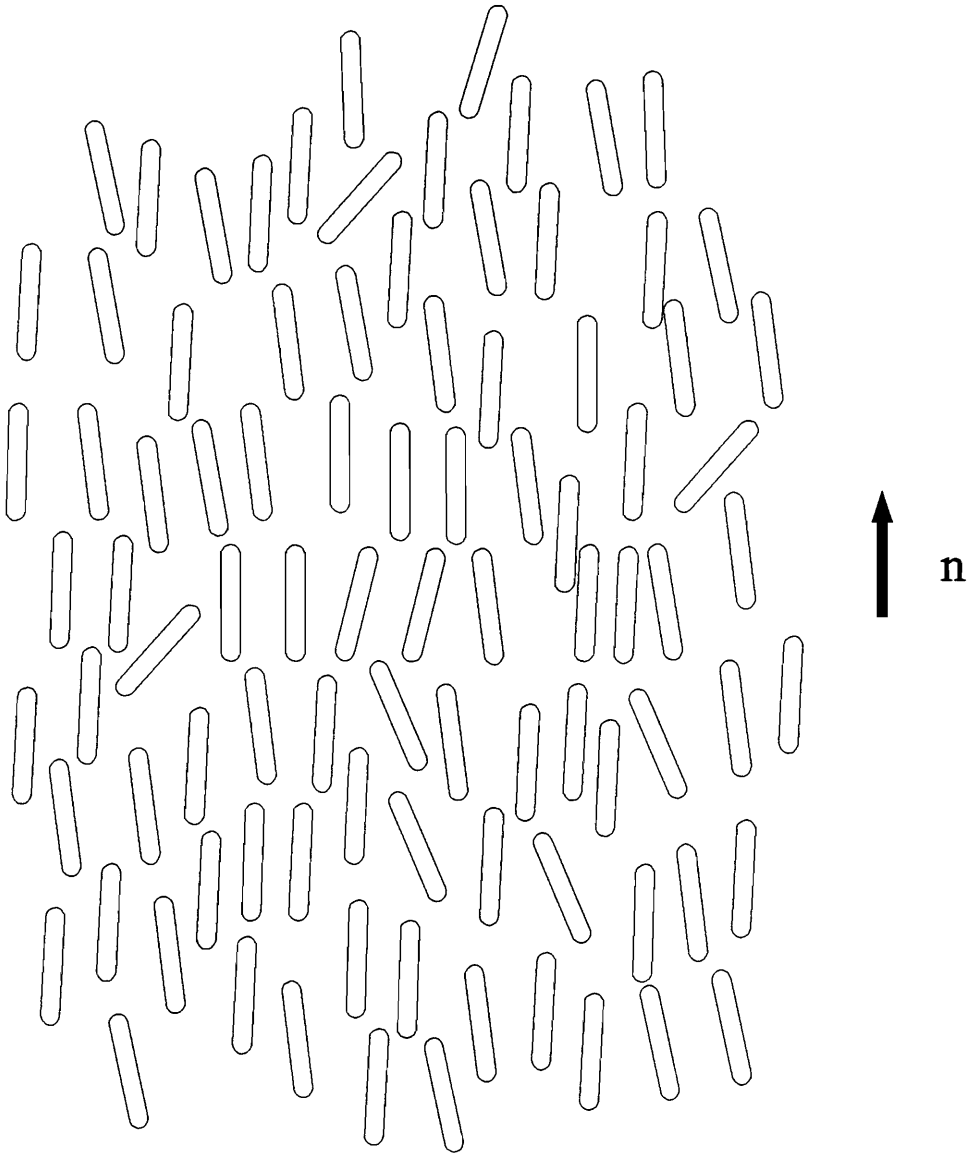

Figure 5.2: Arrangement of molecules in a nematic liquid crystal. : the center of mass have no long range order but the direction of the molecules tend to be parallel to some axis $\hat{\mathbf{n}}$.

Nematic MBBA was used as the nonlinear medium to fill the Fabry-Perot cavity. Its molecular structure is given by

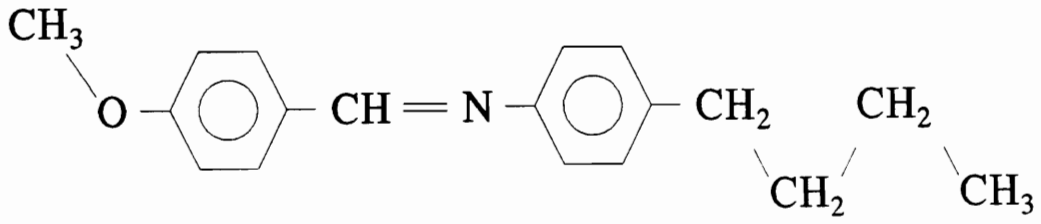

The molecule has the shape of a rod with a length of approximately 20Å and a width of 5Å. This gives rise to its strong anisotropy. It has refractive indices of 1.81 and 1.56 in directions parallel and perpendicular to its long axis, respectively. MBBA appears as a milky liquid when it is in a container at room temperature because the molecules are not aligned in any particular direction. When all the molecules are aligned in one direction, the liquid becomes transparent.

5.1.3 Aligning Nematic Liquid Crystals

There exist several methods for aligning nematic liquid crystals [36]. Nematics can be aligned in a direction normal to the surface (homeotropic orientation) or parallel to the surface (planar orientation). For example, MBBA molecules will align homeotropically on acid treated glasses but will align parallel to fired or detergent cleaned glasses. Four methods of alignment have been tested to construct our cavities: Magnetic field, thin SiO film and rubbing for planar alignments, and chemical surface treatment for homeotropic alignment.

Homeotropic alignment by surfactant treatment

Nematics will align perpendicularly to the substrate surface if it is treated with an hexadecyltrimetylammoniumbromide (HTAB) solution. To test the technique, two samples were used: two clear glass substrates and two aluminum coated glass substrates. With the clear glass substrates, each substrate was soaked in approximately

1% by weight of HTAB solution for half an hour, taken out and dried in hot air. The substrates were then put together as a Fabry-Perot with a mylar spacer of 50μm and the cell was filled with LC. The alignment was then tested by conoscopic method [37] which will be described in section 5.1.4. The glass cell showed very good alignment.

Aluminum coatings, however were found to be completely dissolved after a half hour in HTAB. Reducing the amount of time that the aluminum mirrors were soaked seemed to produce an acceptable result at first, but the quality of the aluminum mirror was still degraded by the HTAB solution. A suggestion to cure this problem may be to anodize the mirror before it is soaked in HTAB. However, Puang-ngern [38] has pointed out that HTAB coating does lead to a long term stable orientation of the LC molecules because it slowly dissolves in the LC. A well aligned sample lasts only about four weeks at room temperature.

Alignment by tangentially evaporated SiO

Evaporating a layer of SiO at an angle to the substrate leads to an efficient and reproducible alignment of the LC both on glass and on aluminum. The tilt angle between the director $\hat{\mathbf{n}}$ of the LC and the substrate surface varies with the angle of evaporation. It is reported in the literature that parallel alignment can be obtained with a 30° evaporation angle. Pure silicon monoxide from Balzers was evaporated at a pressure of 10^{-4} torr to a typical thicknesses of 200-300Å.

Homogeneous planar alignment by rubbed PVA

This is the method of alignment most commonly used in industry. A thin polymeric film such as Polyvinyl alcohol (PVA) is deposited on the substrate by spin coating or by dip coating. PVA was dissolved to form an aqueous solution (3%). The substrate was then dipped into this solution and drawn out at a constant rate. The substrate was then dried in hot air. The thin film of PVA was rubbed by a spinning (850rpm) cylinder two inches in diameter covered with Micro$-$cloth^{TM}. The rubbing produces many micro grooves in the PVA layer. The presence of these groves reduces

the elastic energy of the LC molecules aligned with the groves. The substrates were put together with a 50μm thick mylar spacer and filled with MBBA. To insure a homogeneous planar alignment, the cell was warmed up with hot air from a heat gun to a temperature exceeding the liquid crystal isotropic/nematic transition temperature. In the isotropic phase, the cell becomes transparent. As the cell cools slowly through its isotropic/nematic phase transition, all the molecules fall parallel to the groves in the PVA, producing a very efficient alignment of the LC.

5.1.4 Testing the Alignment

Each cell was tested by conoscopy, a method commonly used to confirm and to qualitatively examine the alignment of the LCs [37].

The experimental setup is shown in Fig.5.3. A strongly convergent linearly polarized beam illuminates the LC cell. The interference pattern can be observed through polarizer A on the screen S.

When the LC molecules are aligned perpendicularly to the substrates, the LC acts as a uniaxial crystal with its optic axis perpendicular to the substrates. The index ellipsoid thus has its axis of symmetry parallel to the optic axis of the crystal. When a linearly polarized beam enters the LC cell, it splits into the two eigen-polarization components. Rays of the same inclination with respect to the optic axis experience the same index of refraction. The interference pattern produced after passing through the analyser A is made of circular rings except for a dark cross due to the extinction of the vibrations perpendicular to the analyser's axis. If the polarizer P is aligned in the y direction, the vibrations in the $y-z$ and the $x-z$ plane are extinguished (Fig.5.3(b) and Fig.5.4(a)).

When the LC molecules are aligned parallel to the substrates, the index ellipsoid has its axis of symmetry parallel to the surface of the substrates. In this case, rays of the same inclination no longer experience the same index of refraction. Instead, the lines of equal index of refraction are hyperbolae. Therefore, the interference fringes

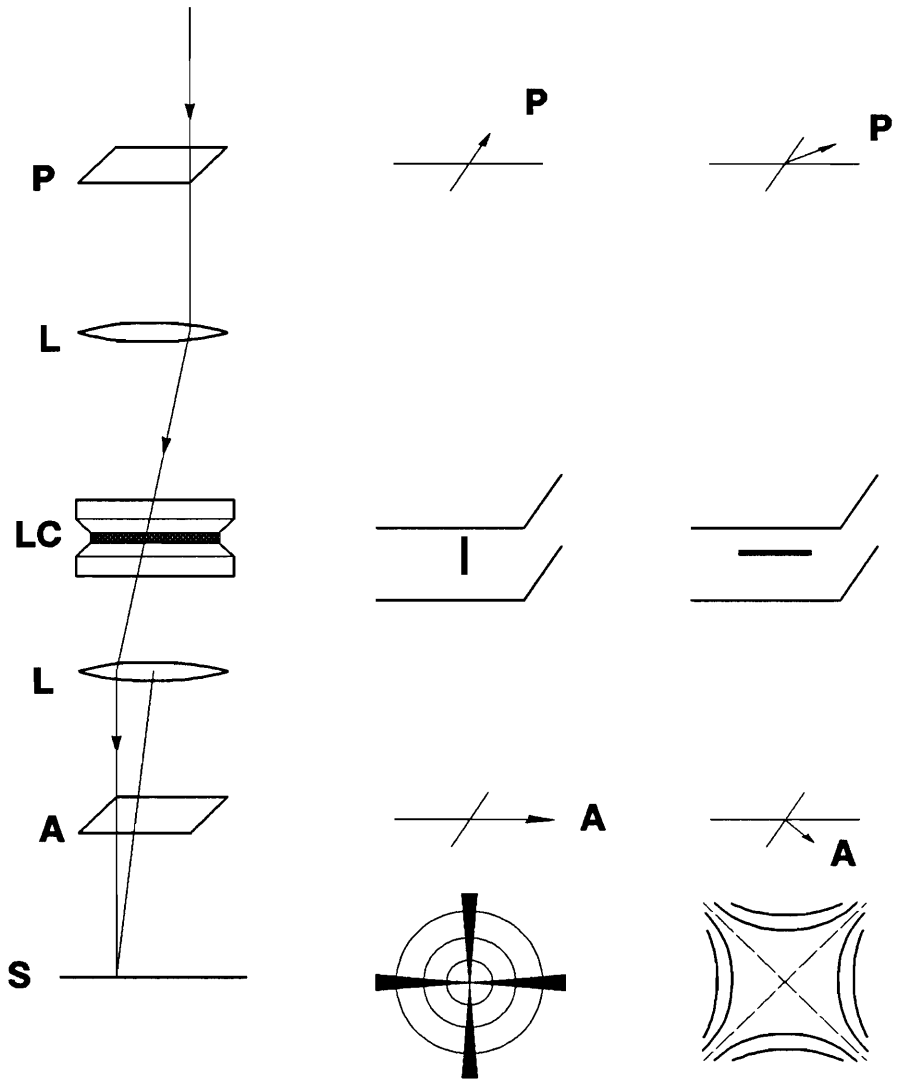

Figure 5.3: Conoscopic method for the examination of the alignment of liquid crystal. (a) Schematic set up for the conoscopic examination. P : polarizer; LC: liquid crystal cell under examination; L converging lens; A analyser; S screen for the observation of the interference pattern. (b) Homeotropic alignment give rise to concentric circles with a dark cross in the middle. (c) Homogeneous alignment results in hyperbolic interference pattern.

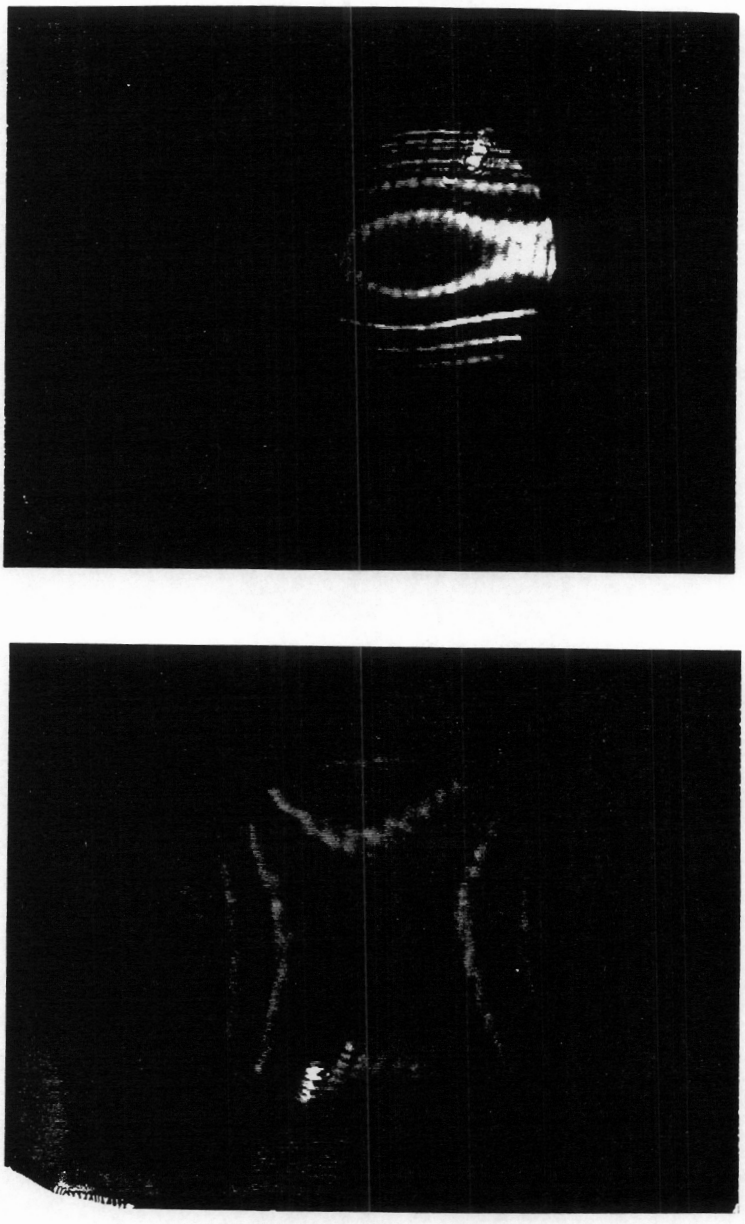

Figure 5.4: Pictures of the interference pattern (a) concentric ellipses for homeotropic alignment (b) hyperbolas for planar alignment. The interference pattern for perpendicular alignment is elliptical due to large astigmatism occur when a highly converging beam entering two thick glass substrates.

are hyperbolic (Fig.5.3(c) and Fig.5.4(b)).

The alignment of a LC cell can be easily checked by conoscopy. If the interference pattern is circular, the alignment is homeotropic. If the interference pattern is hyperbolic, the alignment is planar. The quality of the alignment will show up in the contrast and the broadening of the interference fringes. If the LC molecules are not well aligned, the finnesse of the cell will be reduced due to increased scattering losses. This scattering will then broaden the interference fringes and reduce the contrast of the fringes. A sample result of a conoscopic test is shown in Fig.5.4.

5.2 Polarization Switching in Nonlinear Birefringent Fabry-Perot Cavity

The setup of Fig.5.5 was used to demonstrate polarization switching in a nonlinear birefringent cavity. The incident beam was ellptically polarized after passing through the quarter-wave plate, $\lambda/4$. The polarization beam splitter PBS1 splits the elliptically polarized beam into two orthogonal components. The acousto-optic modulator AOM modulates one of the polarization components (y) which is called the signal beam. The other polarization (x), called the heating beam, is kept constant.

The intensity of the x-polarized beam was controlled by two polarizers P1 and P2. P1 transmits only x-polarized radiation and P2 is used to attenuate the beam intensity. The two beams with orthogonal polarization are then brought back together by PBS2 and PBS3 and are focused on the birefringent metallic cavity NLFP. The intensity of the modulating beam was measured indirectly by monitoring the leakage from the polarization beam splitter PBS2. The signal from detector Dx was then fed to the x-channel of a storage oscilloscope. The heating and the signal beams were focused at two different locations in the NLFP. The spacing between the two spots could be varied without changing the beams' orientation by rotating PBS3. The separation between the beams in the cavity was measured by the microscope MIC equipped with a calibrated moving cross-hair in the eyepiece. The microscope

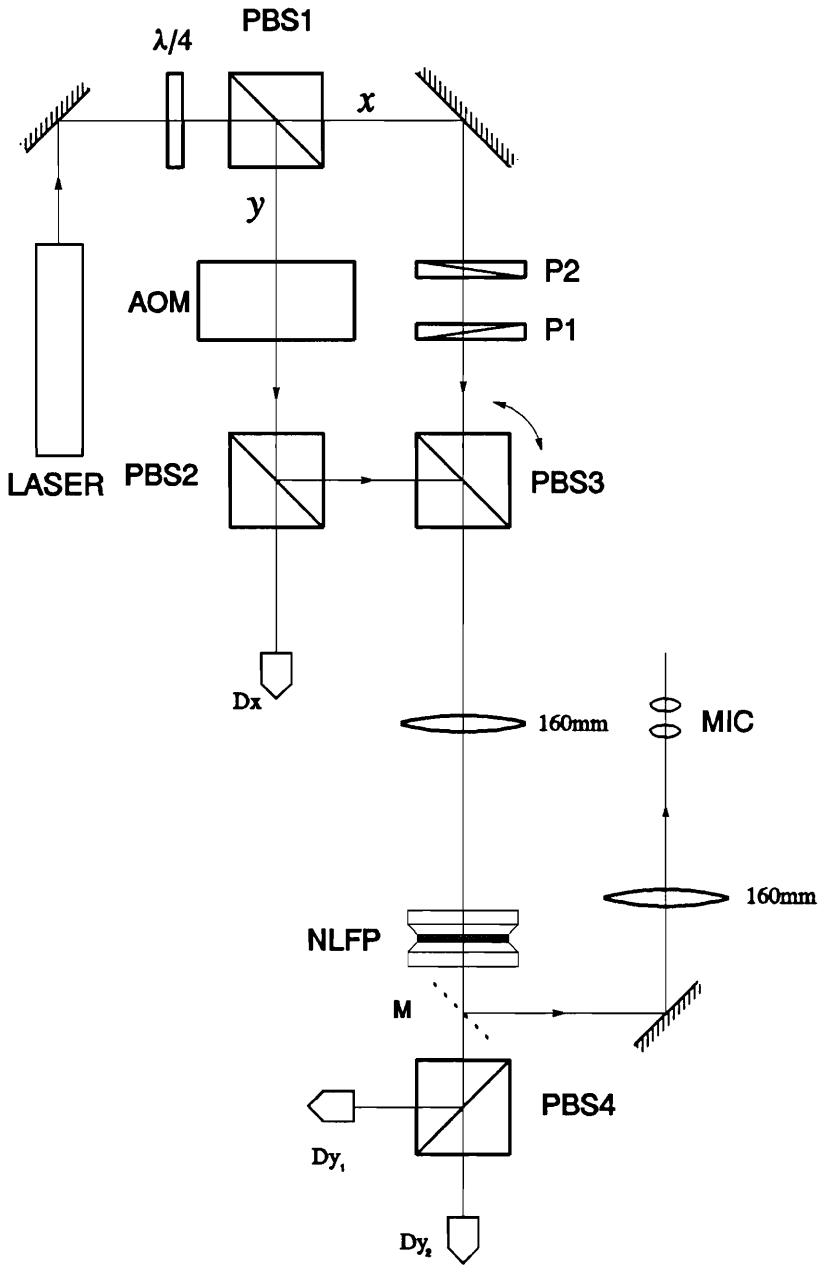

Figure 5.5: Experimental setup used for studying transverse cross-talks in a nonlinear metallic Fabry-Perot cavity.

was then calibrated using a known Ronchi grating (1000 lines/in) in place of the metallic Fabry-Perot. M is a sliding mirror used to measure the spot size and the beam separation. The transmitted beams were then separated by PBS4 and their intensities measured by two photomultiplier tubes. The two signals D_{y_1} (x-polarized) and D_{y_2} (y-polarized) were fed to the y-channels of the storage oscilloscope.

Fig.5.6 shows a typical polarization switching curve observed in a nonlinear metallic Fabry-Perot cavity when the heating beam and the signal beam are colinear and focused at the same spot in the NLFP. The upper curve is the intensity of the x-polarized beam and the bottom curve is that of the y-polarized beam. The x-polarized beam was modulated with a triangular waveform, while the y-polarized beam was kept constant at 16mW.

As the intensity of the x-beam increases, it undergoes a small switching (at approximately 5mW). This has little effect on the y-beam. Around 25mW, the x-beam switches up. The effect of this transition is strongly felt by the y-beam. When the intensity reaches 30mW, the y-beam switches up and the x-beam switches down simultaneously. As the intensity of the x-beam is reduced, both beams switch down at the same intensity ($\simeq$ 17mW). The result of this experimental demonstration is very similar to the polarization switching predicted by the model described in section 4.2.

5.3 Implementation of An Optical Switch with A Nonlinear Birefingent Fabry-Perot Cavity

A metallic Fabry-Perot can be used to implement optical switches or latches. An experimental demonstration is given in this section. Fig.5.7 shows the setup used to implement an optical switch. FP is a metallic Fabry-Perot filled with a nematic liquid crystal (MBBA). The orientation of the LC can be either planar or homeotropic. The signal beam and the control beam are orthogonally polarized. The polarization beamsplitter PBS is used to combine the signal and the control beam and to focus them onto the 50μm thick cavity. The polarizer P transmits only the signal beam.

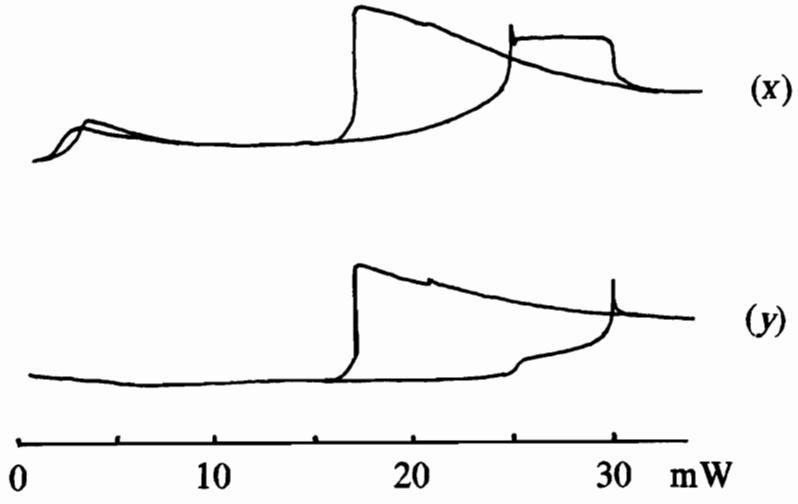

Figure 5.6: Typical switching curves for the polarization switching experiment. The upper trace is the x-polarized output and the lower trace is the y-polarized output. The y-polarized input was fixed at 16mW. The x-polarized input was varied linearly by the AOM. The x-polarized beam switches up at around 25mW and affects the y-polaried beam. When the y-polarized beam switches up near 30mW, the x-polarized beam switches down. On the return path, both beams switch down at the same intensity (around 17mW).

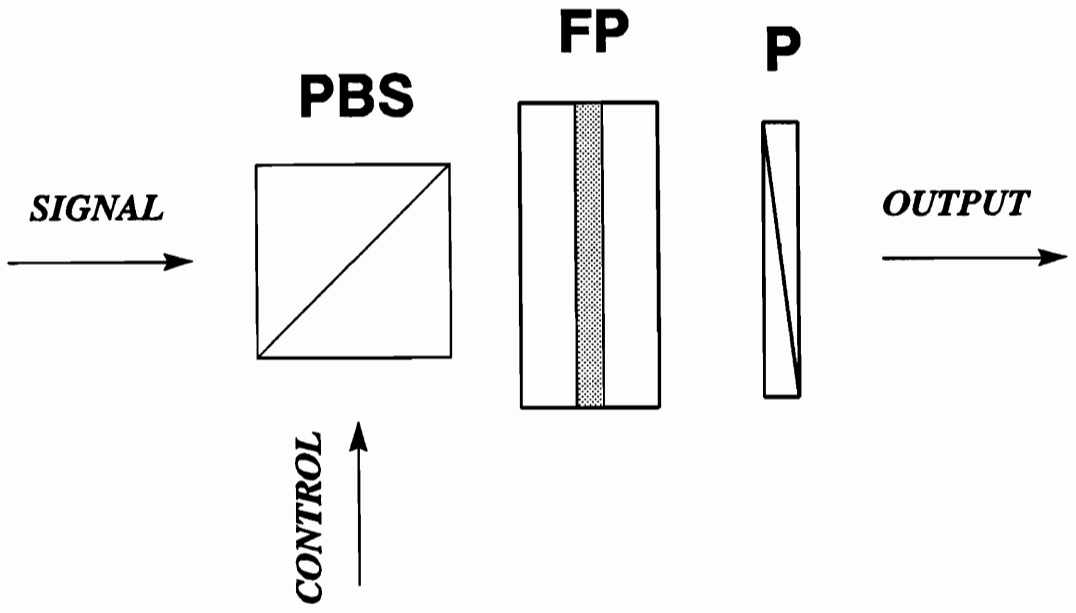

Figure 5.7: Setup implementing an optical latch with a nonlinear birefringent Fabry-Perot.

Fig.5.8(a) shows the response of an optical latch in which one polarization carries a clock signal C used to switch an orthogonally polarized signal beam S. The shape of the output can be explained by referring to the hysteresis curve in Fig.5.8(b). Initially, the device is biased in state 1. Turning the clock on translates the hysteresis curve to the left, shifting the transmitted signal beam from state 1 to state 2. Interrupting the clock returns the signal to state 3. To reset, the input signal is momentarily interrupted. This brings the output to state 4 and then immediately back to its original state 1 when the input signal is restored.

Reset can also be achieved by interrupting a constant background (holding beam) added to the clock signal C. This is shown in Fig.5.9. The clock signal C is used to switch the output on from state 1 to state 3 as in the previous case. Interrupting the holding beam H momentarily shifts the hysteresis curve to the right, and drives the output to state 4. When the holding signal is restored the output goes back to its original state 1.

5.4 Cross Talk in Nonlinear Metallic Fabry-Perots

Because of transverse heat diffusion in the metallic cavity, the response of the device is not local. If metallic cavities are to be put together to contruct a two dimensional array of switching elements, the cross talk between the different elements has to be minimized. It thus becomes important to estimate the amount of crosstalk in metallic Fabry-Perots.

The setup used to measure the crosstalk is the same as that used for the polarization switching experiment (Fig.5.5). The purpose of the experiment is to study the influence of a nearby heating beam on the switching characteristic of the cavity.

Fig.5.10 shows typical switching curves for the heating beam and the modulated signal beam when they are colinear and focused at the same spot. The modulated beam scans a range of 33mW and the power of the heating beam is fixed at 1mW. As the modulating beam switches, the temperature inside the cavity changed suddenly

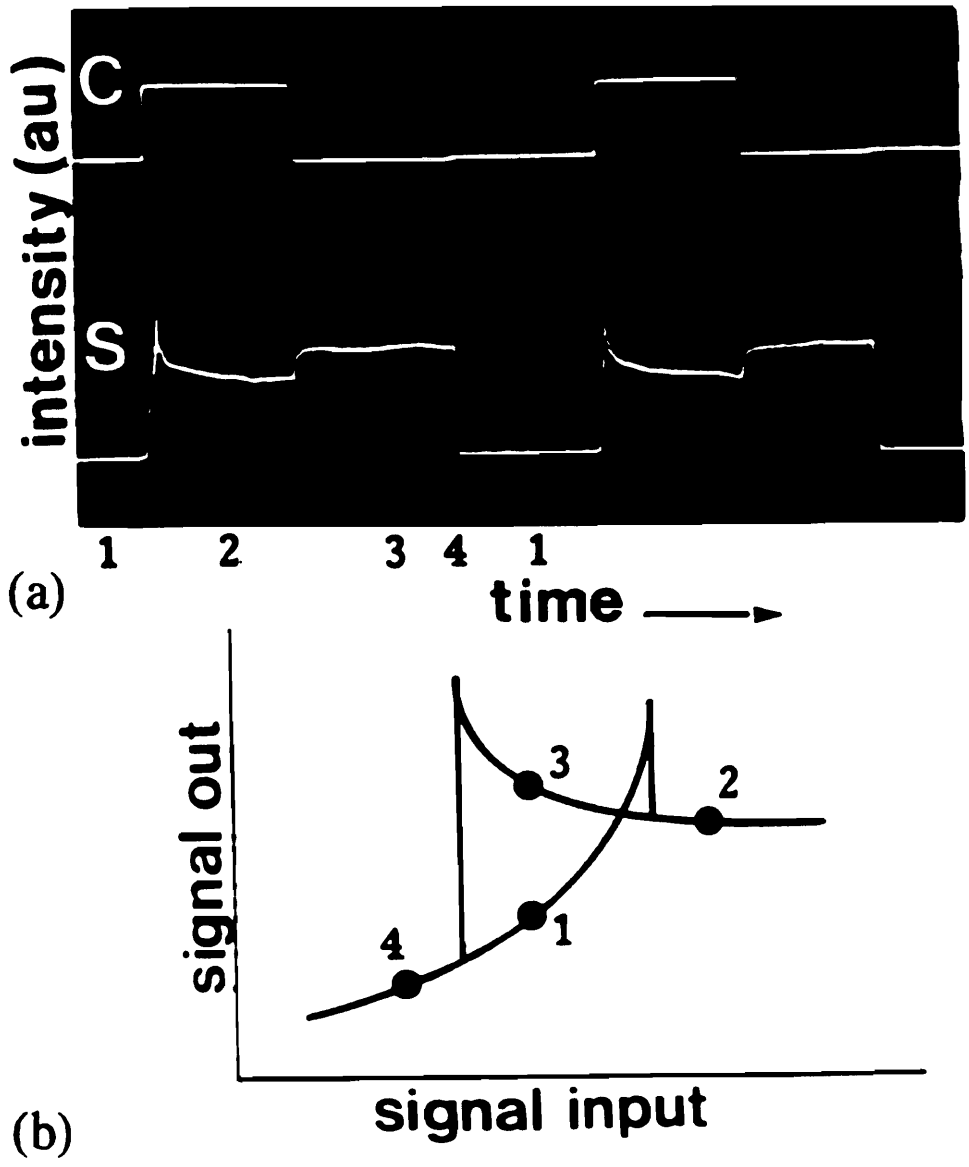

Figure 5.8: Example of a latch using orthogonally polarized clock and signal. (a) Clock C and signal S as a function of time. Reset (at point 4) is achieved by momentarily interrupting the signal. The switching frequency was of the order several Hz. (b) Hysteresis curve showing the various signal levels appearing in the switching sequence of (a).

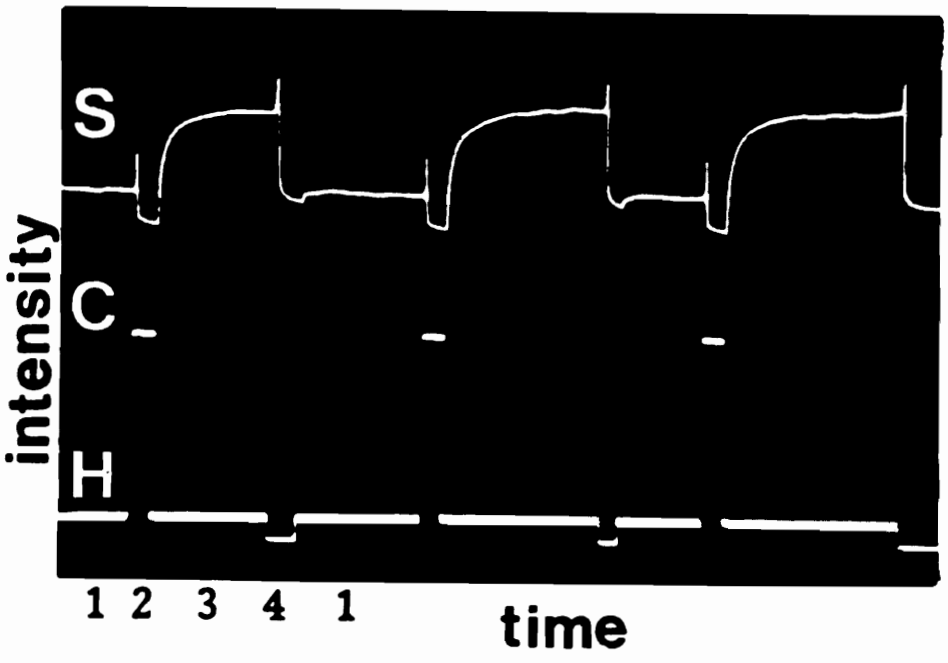

Figure 5.9: Latching similar to that shown in Fig.5.8 but with resetting achieved by momentarily interrupting a holding beam H added to the clock signal.

and the heating beam transmitted intensity change accordingly. When the modulatated signal beam and the heating beam are some distance apart, the switching of the signal beam produces a local change of temperature which, through heat diffusion, is still felt by the other beam. As the separation between the beams increases, the cross-talk effect decreases. When the heating beam and the modulating beams were more than 10 beam waists apart, the coupling between the beams was found to be negligible.

The switching intensity of the signal beam depends on the detuning of the cavity which is affected by the adjacent heating beam. It can be seen in Fig.5.11 that the increase in the adjacent heating beam intensity decreases the signal beam switching intensity proportionally.

Fig.5.12 shows how a modulated beam influences a heating beam held at 22mW. The two beams are two beam waists apart. The upper trace is the modulated beam output intensity and the lower trace is the heating beam output intensity. The maximum intensity of the modulated beam is 33mW. When the modulated beam was at zero intensity (a), the heating beam has a low transmission. When the modulated beam switches up at 24mW (b), the heating beam switches also. However, when the modulated beam switches down at 15.5mW upon decreasing intensity (c), the heating beam switches on. The heating beam remains in an on states state until the modulated beam drops to a very low value (d). This kind of induced switching could cause a problem in two dimensional optical switches. A switch can be turned on accidentally by a nearby switch. One way of minimizing this cross talk is to pixellate each switching element, i.e. each cavity can be made into small pixels which reduces the thermal conduction between elements.

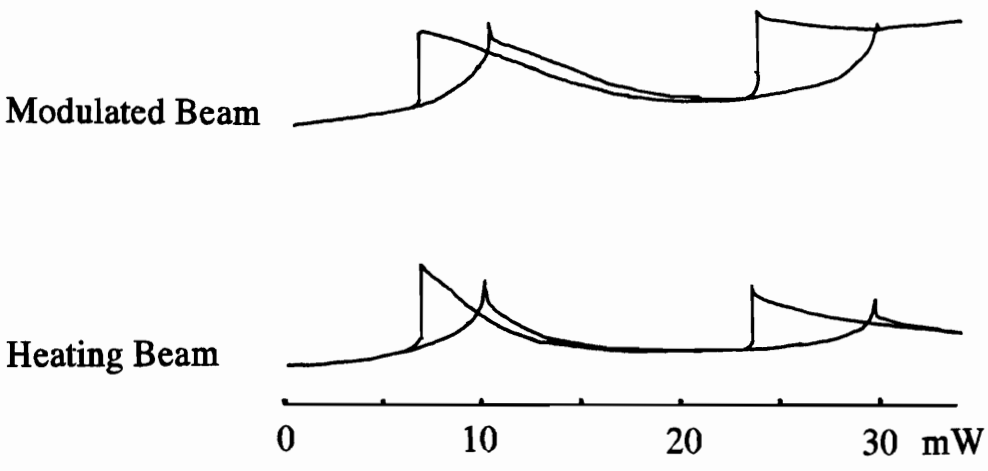

Figure 5.10: Switching curves of two colinear, orthogonally polarized beams. The upper curve is the signal beam modulated by a triangular waveform. The lower curve is the heating beam maintained at 1mW. The modulated beam scans a range of 33mW.

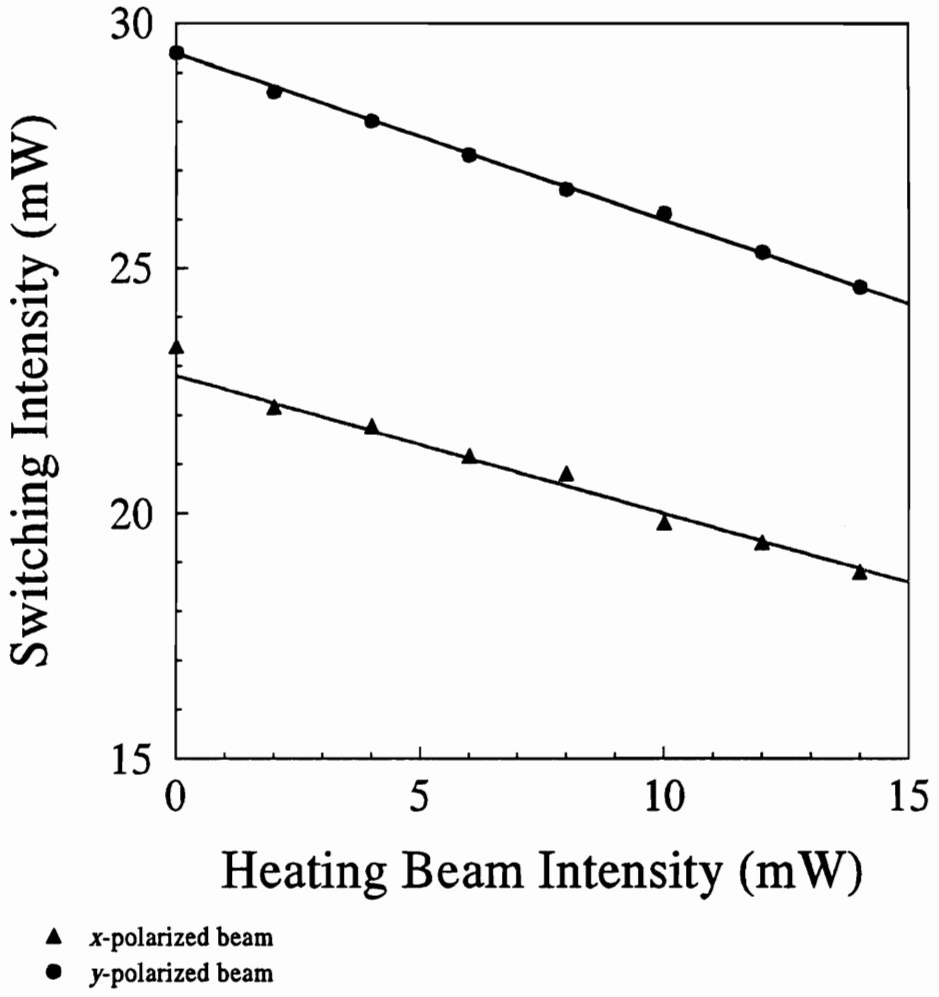

Figure 5.11: The switching intensity of a beam modulated with a triangular waveform decreases with the local temperature, which is affected by the presence of a constant adjacent heating beam.

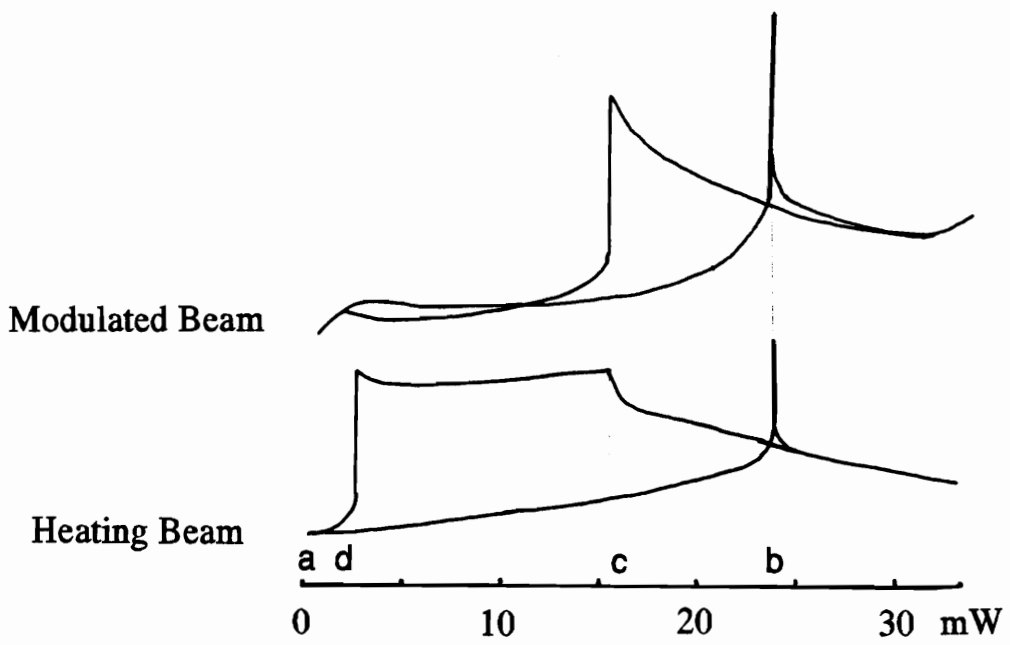

Figure 5.12: The modulated beam and the heating beam are two beam waists apart. The heating beam is held at 22mW. There is strong coupling between the beams. The switching of the modulated beam turns the heating beam on accidentally.

Chapter 6

Coupled Nonlinear Fabry-Perot – Steady State Case

The conventional way of switching on a bistable Fabry-Perot etalon by adding a positive pulse and switching it off by interrupting a bias (see chapter 3) is not conducive to high speed digital systems [30], where only positive pulses operations are preferred. It has been shown in chapter 4 that positive pulse switching utilizing polarization bistability in the steady state regime cannot be achieved with a single nonlinear birefringent Fabry-Perot cavity. The two polarization states in a single cavity are coupled by the total intensity trapped inside the cavity. This forces the two polarizations to switch simultaneously. Using different parts of the cavity to decouple the two polarization states does not solve the problem either as has been shown for the Korpel-Lohmann scheme. In this case, the output will eventually find itself 'locked' in a state from which it cannot be displaced by a positive pulse. In this chapter, we will examine the possibility of positive pulse switching in coupled systems of more than one nonlinear cavity.

6.1 Nonlinear Fabry-Perot with a Variable External Mirror

As seen from previous examples, the difficulty resides in achieving down switching with a positive pulse. With a single conventional cavity, a negative pulse, or a reduction of the incident intensity seems to be necessary. One way of reducing the total incident beam intensity applied to a NLFP is to use a variable beam-splitter in front of the NLFP to block the incoming beam when necessary. This is a trivial solution which is equivalent to changing the incident intensity directly and has the same drawbacks.

Another way of achieving the same result is to use an external mirror with variable reflectivity behind the NLFP. This will act as a variable feedback allowing one to control the total intensity incident on the NLFP. A schematic configuration is shown in Fig.6.1. It includes a feedback mirror M, the reflectivity of which can be controlled externally by some means. The Fabry-Perot etalon, NLFP, is filled with a homogeneous isotropic Kerr-type medium[1]. The reflectivity of the lossless dielectric mirrors of the Fabry-Perot etalon is R_1. During operation, NLFP is biased by two beams, the incident beam and the beam reflected by the external mirror M. Varying the reflectivity of M will change the bias of NLFP. The output I_o is the beam transmitted by the Fabry-Perot. The distance between M and NLFP is assumed to be large compared with the coherence length of the input beam. Under this condition, the mirror M will not form a resonant cavity with the back mirror of the NLFP. The total intensity trapped between the Fabry-Perot and the mirror can be found by summing up the contributions after each pass between the cavity and the mirror. The transmissivity and the reflectivity of the NLFP are given by

$$\mathcal{T}_1 = \frac{I_t}{I_i} = \frac{1}{1 + F \sin^2 \phi_1} \tag{6.1}$$

$$\mathcal{R}_1 = \frac{I_r}{I_i} = 1 - \mathcal{T} \tag{6.2}$$

where ϕ_1 is the round trip phase change inside the cavity.

[1]The index of refraction of a Kerr-type medium has the form $n(I) = n_0 + n_2 I$.

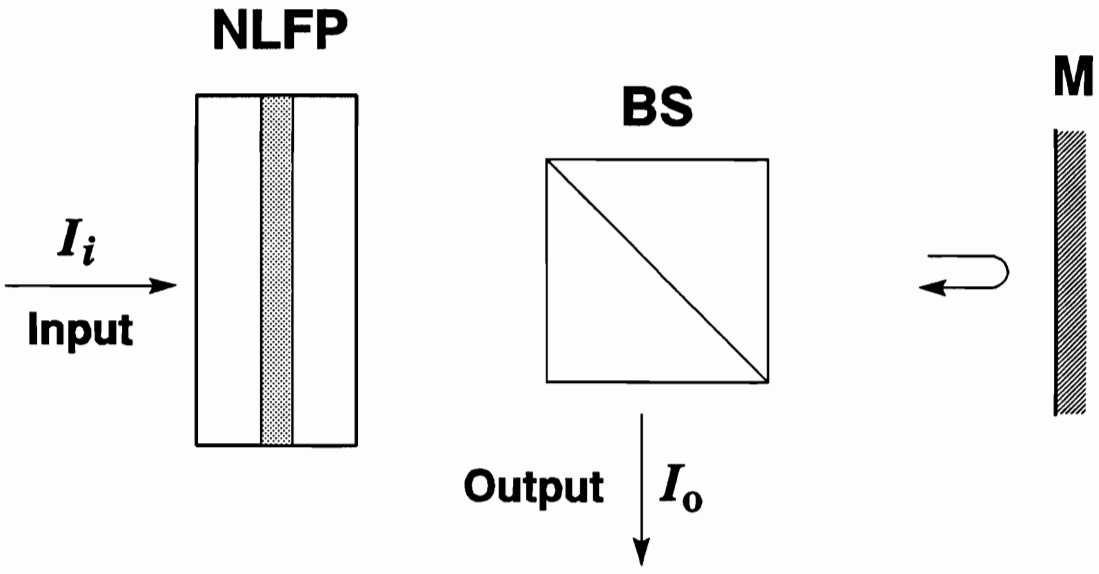

Figure 6.1: Configuration of an optical latch which consists of a NLFP and a mirror M with externally controlled reflectivity. NLFP : dielectric Fabry-Perot etalon filled with a nonlinear medium, BS : beam splitter.

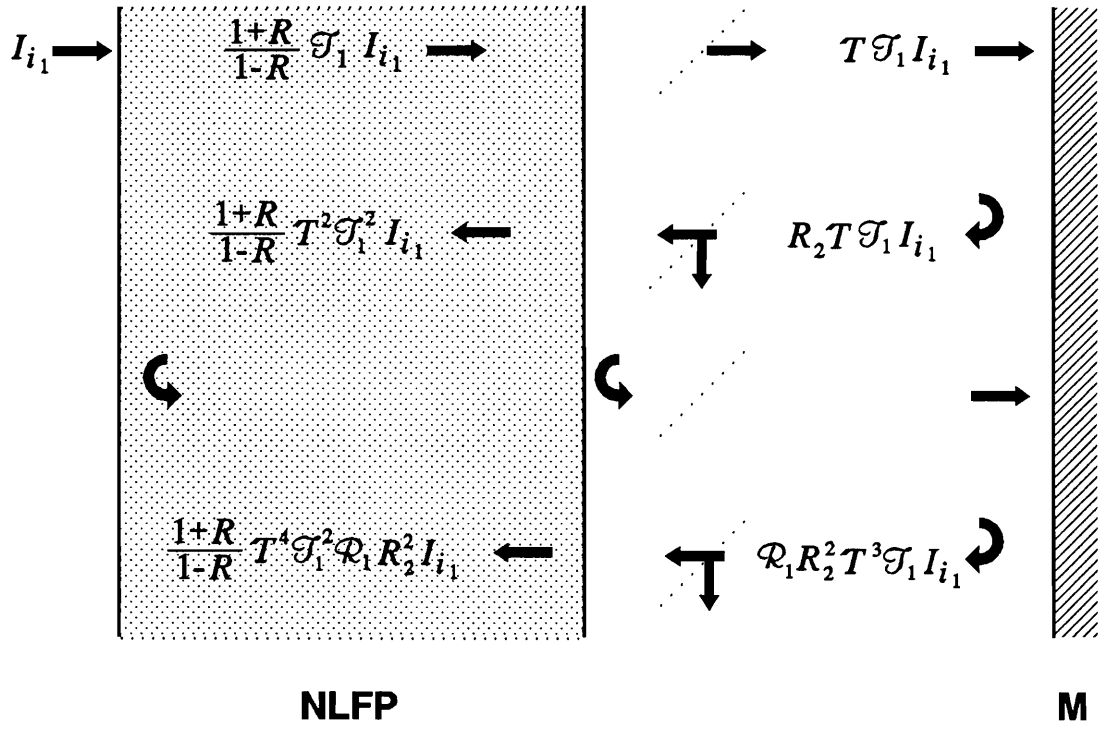

Figure 6.2: Intensity inside the cavity and between M and the cavity. The separation between NLFP and M is assumed to be large compared with the coherence length of the radiation.

Fig.6.2 shows the intensity after several passes between NLFP and M. Since the separation between NLFP and M is larger than the coherence length of the incident beam, the contributions sum up in intensity. The transmittance of the Fabry-Perot depends on the total intensity inside the cavity which itself depends on the total intensity reflected by M. Carrying out the infinite sum, the total intensity inside the cavity is found to be:

$$I = \frac{1+R_1}{1-R_1}\mathcal{T}_1 I_{i_1}\left\{1+\frac{T^2\mathcal{T}_1 R_2}{1-T^2\mathcal{R}_1 R_2}\right\}, \tag{6.3}$$

where T is the transmissivity of the beam splitter and R_2 is the reflectivity of the externally controlled mirror. Notice that the introduction of an external mirror causes an increase in the intensity inside the cavity. The intensity inside a nonlinear Fabry-Perot without the feedback mirror is

$$I = \frac{1+R_1}{1-R_1}\mathcal{T} I_i \,. \tag{6.4}$$

The intensity inside a Fabry-Perot with a feedback mirror is increased by the second factor in the brackets. This increase is controlled by the reflectivity of the feedback mirror which can thus be used to change the switching intensity of the cavity.

Increasing the reflectivity of the feedback mirror increases the feedback and thus reduces the switching intensity of the cavity. A graph of the hysteresis curves of a nonlinear Fabry-Perot with different values of the reflectivity of the feedback mirror is plotted in Fig.6.3.

It can be seen that the switching intensity changes with the reflectivity of M. Thus, if the reflectivity of M can be controlled by some external means, the output state of the system can also be controlled in the following way. The cavity is biased with a beam of intensity I_B as shown in Fig.6.3, and the reflectivity of the feedback mirror is set to 0.5. There are two possible stable output intensity, **a** and **b**, corresponding to this input intensity. The initial state is **a**, i.e. the Fabry-Perot is in a low transmission state, or an OFF state. If the reflectivity of M is increased to 0.9, the hysteresis curve shifts towards the left. When the up-switching point becomes smaller than the bias,

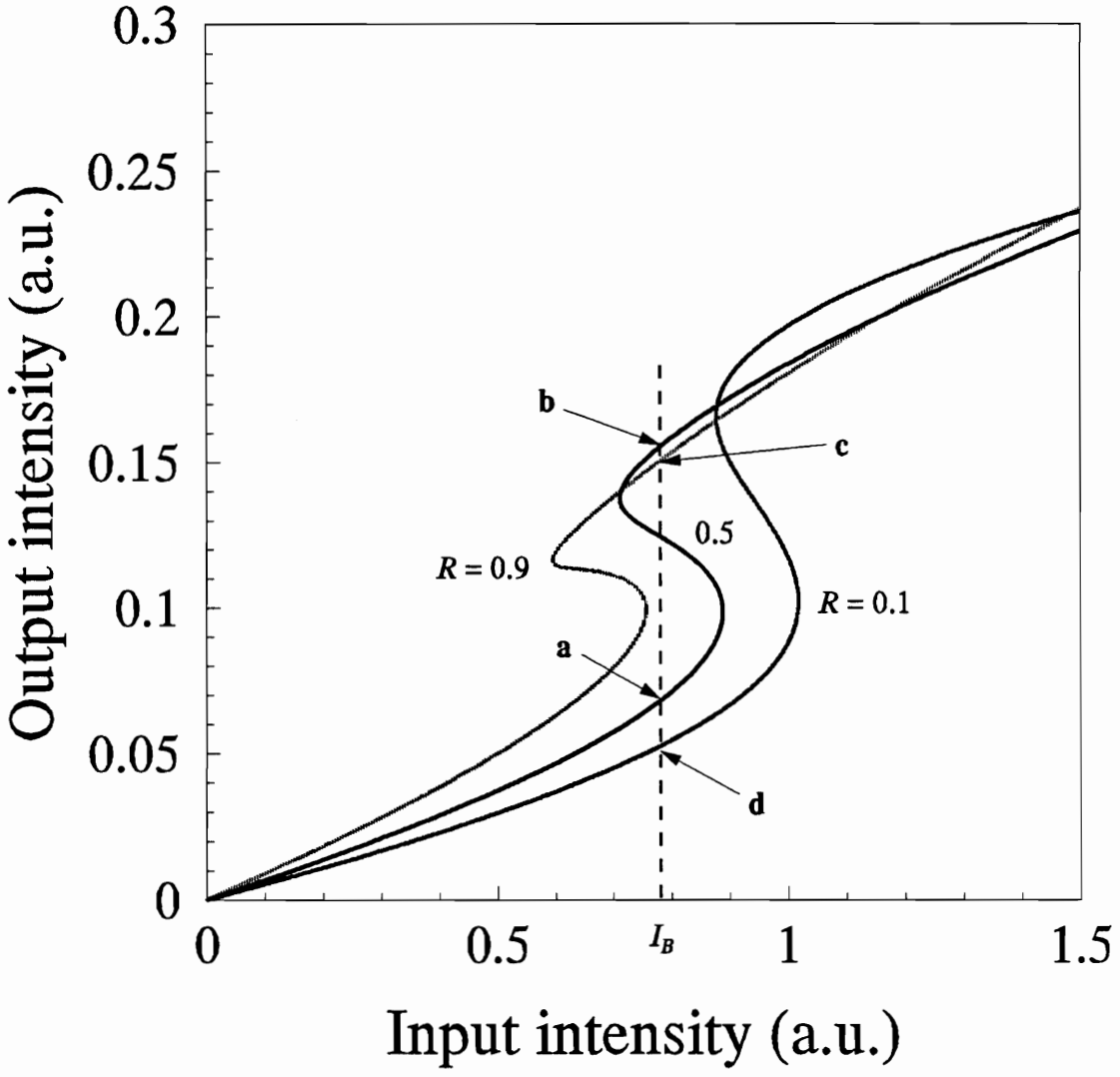

Figure 6.3: Output intensity of the NLFP with different values of the reflectivity of the feedback mirrors. The switching intensity decreases with increasing feedback.

the cavity switches to the upper branch of the hysteresis at **c**. Upon decreasing the reflectivity of M back to 0.5, the output stays at **b** which is the high transmission state of NLFP. The cavity is now ON. To turn the cavity OFF the reflectivity of the mirror needs to be reduced to a value such that the down-switching point of the hysteresis curve becomes higher than the biasing intensity I_B. If the reflectivity of the mirror drops to 0.1, for example, the output will switch down to **d** and upon restoring the reflectivity back to 0.5 the output will go to **a** and remain low.

It therefore appears possible to control the output state of a nonlinear Fabry-Perot cavity by using a variable reflectivity mirror as a feedback element. In fact, the nonlinear Fabry-Perot itself is a variable reflectivity mirror, the reflectivity of which can be controlled by an external beam. Fig.6.4 shows a plot of the reflectivity of a NLFP versus the intensity incident on the cavity. One can make use of this controllable reflectivity to implement a feedback element capable of turning another NLFP on or off with positive pulses.

6.2 Coupled Nonlinear Fabry-Perot Cavities

We saw in the last section that it is possible to switch the output of a nonlinear Fabry Perot cavity on and off with positive pulses if a mirror of variable reflectivity is being used. In this section we demonstrate, with numerical examples, that this idea can be realized in the steady state regime with two optically coupled nonlinear Fabry-Perot cavities. The coupled cavities can either be two separate cavities or two nonoverlapping regions of the same cavity. The model used to describe the cavities and its underlying assumptions are outlined in the next subsection. A simple model is chosen and the analysis is limited to the steady state regime. The dynamics of the system will be discussed in chapter 7. The response of the device is described in section 6.2.2 and demonstrated with numerical examples. Some of the limitations and requirements for positive pulse switching with this device are also discussed.

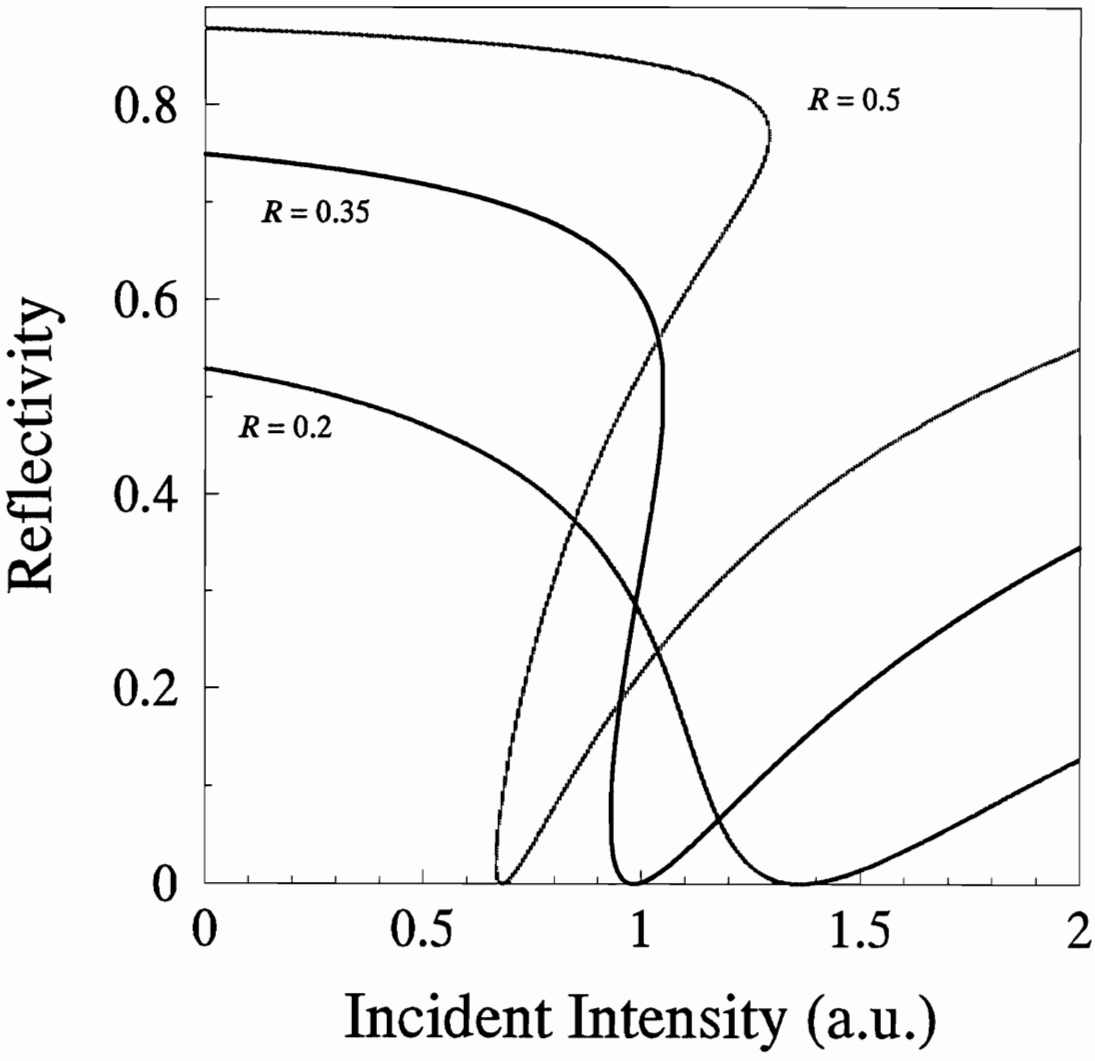

Figure 6.4: Reflectivity of a NLFP versus incident intensity. The reflectivity of a NLFP can be controlled by the intensity of the incident beam. The contrast is determined by the reflectivity R, of the mirror of the cavity.

6.2.1 Theoretical Model

Fig.6.5 shows the arrangement of the system. It consists of two nonlinear Fabry-Perot cavities FP1 and FP2 arranged in series. Each cavity is made of two dielectric lossless mirrors of reflectivity R_1 for FP1 and R_2 for FP2. The cavities are filled with homogeneous isotropic Kerr-type media having a long diffusion length (so that any local effect can be neglected and spatial averages can be used). As a result, the cavities are characterized by conventional hysteretic responses. The polarizer P is used to isolate FP1 from the control beam. The outputs, which derive only from the signal beam, are extracted by the beam splitter BS.

The round trip phase change in each cavity depends only on the average total intensity trapped inside. The round trip phase change in cavity j can thus be written as

$$\phi_j = 2kd_j(n_{o_j} + n_{2_j}I_j), \qquad j = 1, 2, \tag{6.5}$$

where $k = 2\pi/\lambda$ is the wave number in vacuum, λ is the wavelength, n_{o_j} is the linear index of refraction of the medium in the cavity j and n_{2_j} is the value of its nonlinear index, and I_j is the intensity trapped in cavity j.

There are two inputs to the system. Input I_{i_1} is called the signal beam and input I_{i_2} is called the control beam. The polarization of the two inputs are orthogonal. Three possible outputs can be used. I_{o_1}, which is the signal beam transmitted by FP1, I_{o_3}, which is complementary to I_{o_1}, or I_{o_2}, which has experienced an additional reflection on FP2. Because the polarizer isolates FP1 from I_{i_2}, the outputs derive entirely from the signal I_{i_1}. The geometry shown is chosen for the purpose of illustration. It does not rule out other folded geometries which may permit a better manipulation of the beams or more compact designs.

Isolating cavity FP1 from the control beam results in the simplest form of coupling between the two cavities. The control beam does not reach cavity FP1 and, therefore, does not affect it directly. The important point is that the control beam can change the reflectivity of FP2 which then can act as an external mirror of variable reflectivity

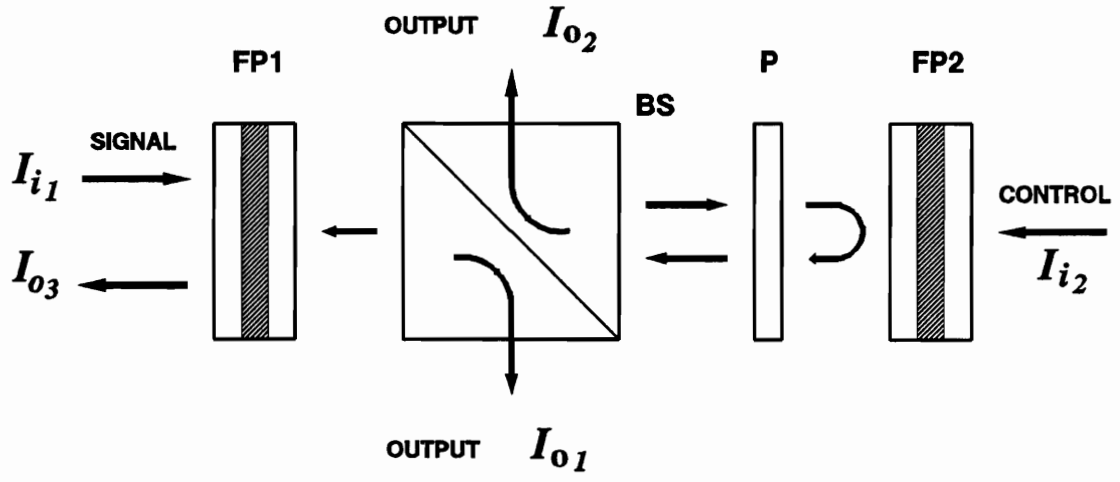

Figure 6.5: Arrangement of two of coupled cavities, FP1 and FP2. The two inputs I_{i_1} and I_{i_2} are orthogonally polarized. The polarizer P is used to isolate FP1 from the control beam. The beamsplitter BS is used to extract the outputs I_{o_1} and I_{o_2}. I_{o_3} is another possible output.

for FP1. This affects the total intensity incident on FP1, thus changing the shape of its hysteretic response curve and the value of its critical switching intensity.

It is further assumed that the two cavities are coupled incoherently. That is, the irradiance reflected by FP2 is fed back onto FP1, changing the total irradiance inside that cavity, but the reflected radiation does not interfere with the incident signal beam. This situation occurs when the coherence time of the radiation is shorter than the transit time between the cavities or if the spacing between the cavities does not form a resonant cavity because of misalignment or other mistuning.

There are four time scales in the system: τ_r is the cavity round trip time, τ_c the cavity life time, τ_m the medium response time and τ_p the rise and fall time of the input pulse. In the quasi steady state regime, the four time scales have to satisfy the following condition

$$\tau_r < \tau_c \ll \tau_m \ll \tau_p \, . \tag{6.6}$$

Assuming plane wave inputs, the average irradiance inside each cavity can be calculated by summing up the contributions after each round trip, giving the result:

$$I_1 = \frac{1+R_1}{1-R_1}\mathcal{T}_1 I_{i_1}\left(1+\frac{T^2\mathcal{T}_1\mathcal{R}_2}{1-T^2\mathcal{R}_1\mathcal{R}_2}\right), \tag{6.7}$$

$$I_2 = \frac{1+R_2}{1-R_2}\mathcal{T}_2 I_{i_2}\left(\mathcal{T}_2 I_{i_2}+\frac{T^2\mathcal{T}_1\mathcal{T}_2}{1-T^2\mathcal{R}_1\mathcal{R}_2}\right), \tag{6.8}$$

where $\mathcal{T}_j$ is the transmissivity of each cavity which is given by the usual Airy function :

$$\mathcal{T}_j = \frac{1}{1+F_j\sin^2\phi_j/2} \qquad j=1,2\,. \tag{6.9}$$

For lossless cavities, $\mathcal{R}_j = 1-\mathcal{T}_j$. F_j is the coefficient of finesse of cavity j. The round trip phase change ϕ_j is given in Eq.(6.5). T is the transmissivity of the beam splitter.

Equation (6.5) to (6.9) were solved numerically by searching for consistent solutions for the round trip phase shift ϕ_j in each cavity, for all pairs of input values I_{i_1} and I_{i_2}. The outputs were then calculated from

$$I_{o_1} = \frac{R\mathcal{T}_1}{1-T^2\mathcal{R}_1\mathcal{R}_2}I_{i_1}, \tag{6.10}$$

$$I_{o_2} = T\mathcal{R}_2 I_{i_1}, \tag{6.11}$$

where $R = 1 - T$ is the reflectivity of the beam splitter.

6.2.2 Numerical Results

There are two different modes of operation in which the output of the system can be switched on and off by positive pulses. In the first mode, the device is switched on and off by two control pulses of different magnitude while in the second mode, it is switched on by a signal pulse and switched off by a control pulse.

In both cases, the cavity FP1 is biased within its bistable region by the sum of a constant input signal beam and the reflection of that beam from cavity FP2. Cavity FP2 is not biased and acts as a mirror of variable reflectivity. The control pulses are used to change the reflectivity of FP2 and consequently switch the device.

Switching with Control Pulses of Different Magnitudes

In this mode of operation, cavity FP2 is chosen to be bistable. Control pulses of different magnitudes are used to change the reflectivity of FP2. This changes the total bias of FP1 and thus shifts the operating point on the hysteretic transfer function of the device. The end result is that the output will switch either on or off depending on the intensity of the control beam. Fig.6.6 shows different hysteresis curves of FP1 corresponding to different values of the reflectivity of FP2 resulting from different control beam intensities. The reflectivity of FP2, uncoupled, is shown in the insert. Curves 1, 2 and 3 correspond to the different reflectivity values shown in the insert. With no control beam, FP1 is biased within its bistable region at an intensity equal to 0.61 relative units. FP2 is unbiased and its reflectivity is 0.17.

Assuming that the output is initially in state A, the output can be turned on by a control pulse having a magnitude of approximately 10 units. As the intensity incident on FP2 increases to about 10 units, the reflectivity of FP2 increases to 0.81 (2 in the insert). This increases the feedback to FP1, shifting its hysteresis towards the left (curve 2), hence reducing the switching intensity. When the switch up point passes

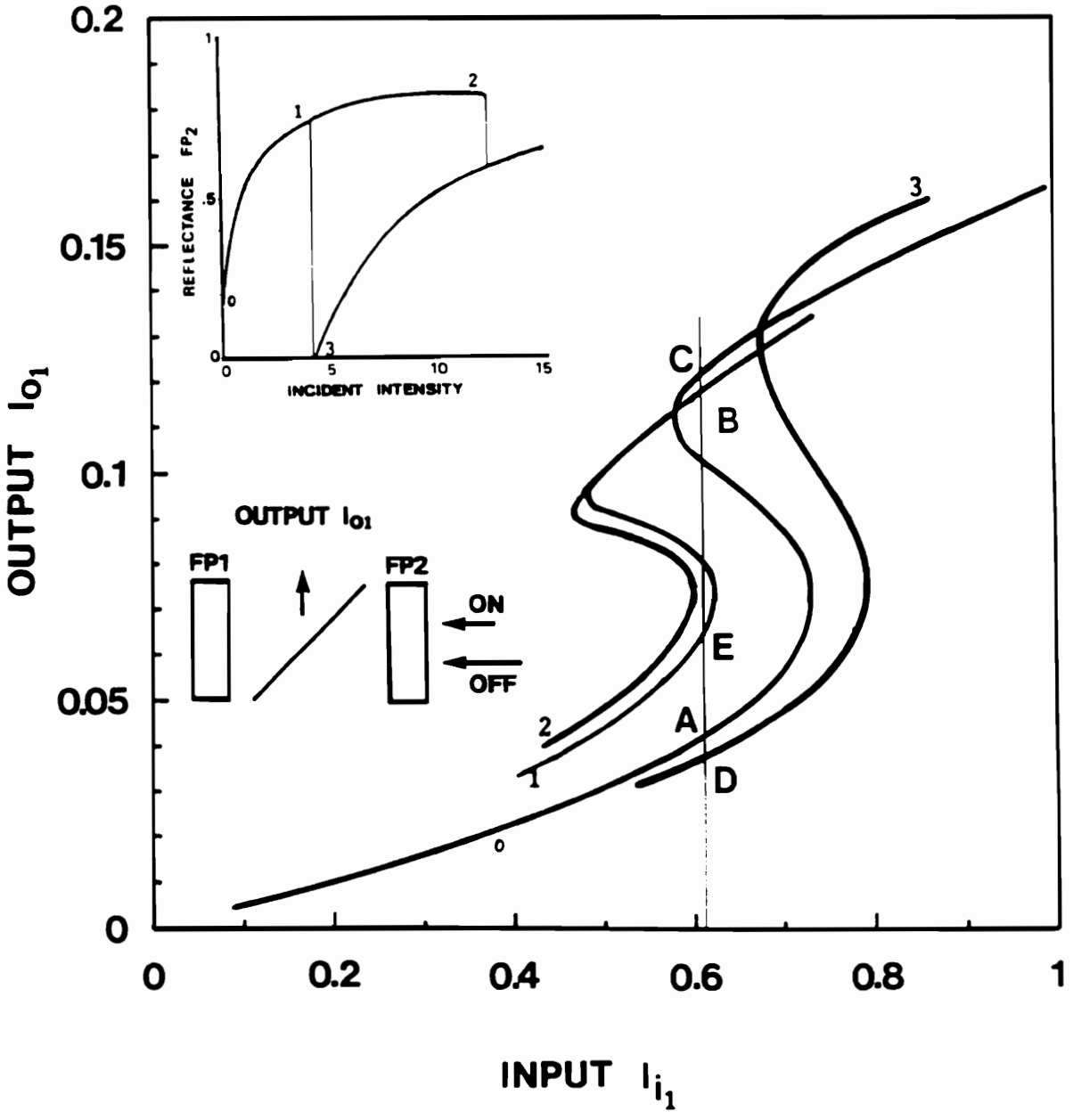

Figure 6.6: Switching a system of two coupled cavities on and off with positive pulses of different magnitudes incident on the control cavity. The reflectivity of the control cavity FP2 is shown in the insert. The hysteresis curves for different reflectivity of FP2 are is shown as curves 0, 1, 2 and 3.

the biasing intensity, the output switches up to point B. Upon decreasing the intensity incident on FP2, the output stays in the upper branch of the hysteresis curve. The output eventually reaches C as the intensity I_{i_2} goes back to zero. The output is then left in a high state.

To turn the output off, one need to bring the reflectivity of FP2 beyond its bistable region. Assuming that the output is now in state C, this can be accomplished by sending a pulse of magnitude larger than 12.8 units into FP2. The reflectivity of FP2 will then land on its lower branch. As the control pulse is removed, the reflectivity of FP2 decreases, shifting the hysteresis curve of FP1 towards the right (curve 3). This increases the switching intensity of the output. As the switch-down point passes the bias, the output is forced to switch down. The output is at D while the reflectivity of FP2 is at a minimum (point 3 in the insert). As the intensity on FP2 goes back to zero, the output will stay in the lower branch of the hysteresis curve and return to A The output corresponding to this switching sequence are shown in Fig.6.7.

Switching with Pulses Incident on Different Cavities

FP2 need not be bistable in this mode of operation, but it must have a nonlinear reflectivity that drops with incident intensity. As shown in Fig.6.8, the device is switched up by a pulse on FP1and switched down by a pulse on FP2. FP1 is biased at X, with a constant intensity of 0.56 unit, within the bistable region of the hysteresis curve 1. FP2 is unbiased. Fig.6.8. shows different hysteresis curves of FP1 for different values of the reflectivity of FP2. The reflectivity of FP2 (uncoupled) is shown in the insert. Curves 1, 2 and 3 correspond to the there different reflectivity values indicated in the insert.

Initially, the output is in state A. The output can be turned on by a pulse incident on FP1 which brings the input I_{i_1} beyond the bistable region. This carries the output from A to B. The output then stays at B after the pulse is removed. Switching off can be achieved by sending a pulse to the control cavity, FP2. Increasing the intensity incident on FP2 first increases its reflectivity which shifts the hysteresis curve of FP1

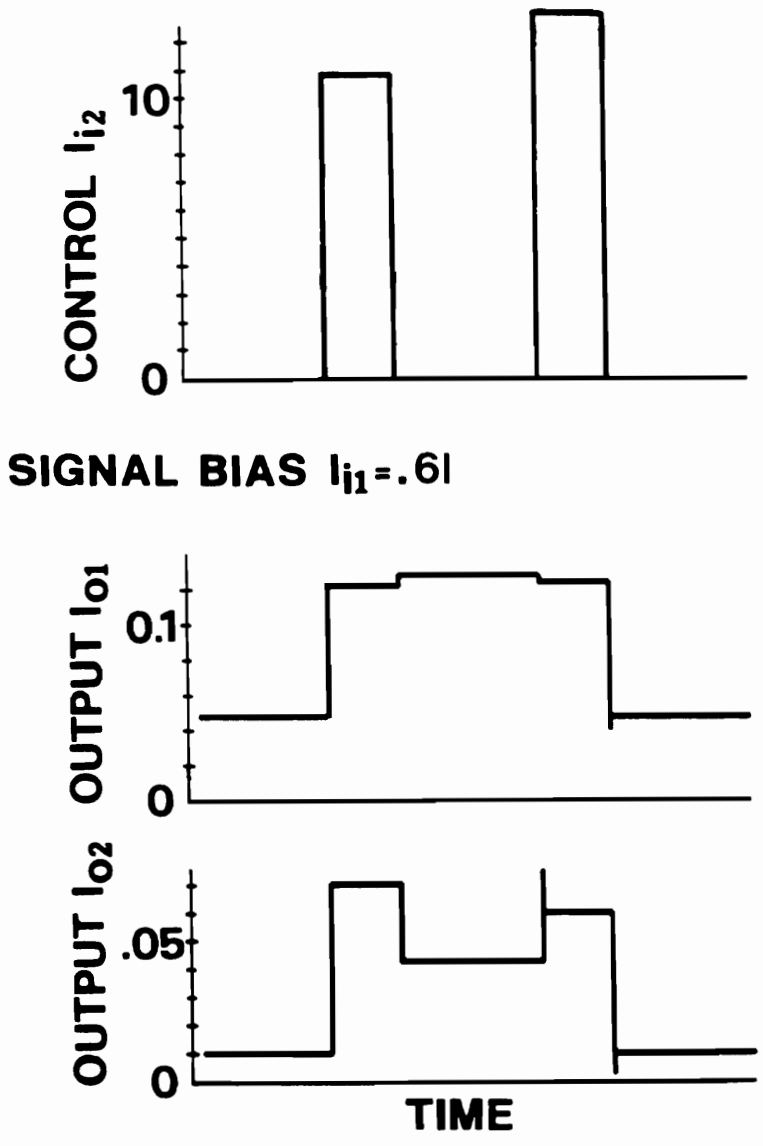

Figure 6.7: Switching sequence of the coupled cavity system of Fig.6.6. The outputs can be turned on and off by pulses of different magnitudes incident on FP2.

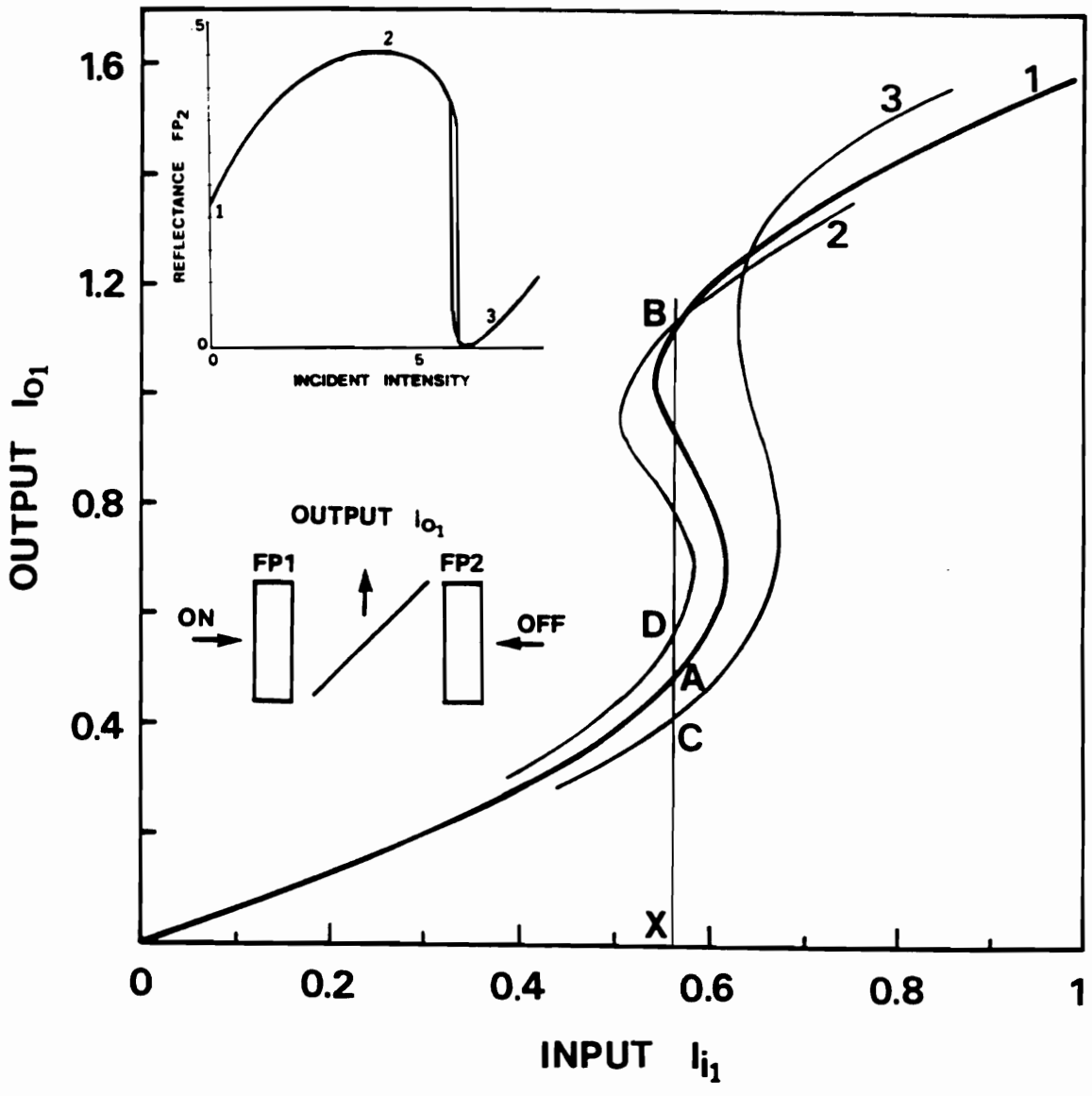

Figure 6.8: Switching a system of two coupled cavities on and off with pulses incident on different cavities. A pulse on FP1 switches the output to a high state (B). A pulse on FP2 shifts the hysteresis towards the right and 'forces' the output to a low state.

towards the left. The bias of FP1 must be such that the operating point stays in the bistable region when the reflectivity of FP2 is at a maximum. A further increase of the intensity incident on FP2 brings the reflectivity to a low value (3 in the insert of Fig.6.8). This increases the switch-down intensity of the output. The hysteresis curve moves to (3) and the output switches down to C as the down switching point passes the biasing intensity. As the control pulse is removed, the reflectivity traces back the same path. As the reflectivity approaches its maximum (2 in the insert), the output hysteresis shifts toward the left again. The output reaches D when the reflectivity is at maximum. Finally, the output goes back to A as the intensity incident on FP2 goes back to zero. The corresponding switching sequence is shown in Fig.6.9.

6.2.3 Discussions

Each of the two modes of operation discussed has its relative advantages and disadvantages. An advantage of the first mode of operation, in which the output is turned on and off by control pulses of different magnitudes is that the signal is totally isolated from the control. There is no need to mix the control beam and the signal beam. However, this mode of operation requires a tight control of the bias level. As seen in Fig.6.6, the biasing intensity has to be maintained between the switch-up points of the hysteresis curves 1 and 2 to prevent the system from switching back on when the pulse used to turn it off is removed and the reflectivity of FP2 goes through point 1 (Fig.6.6-insert). A disadvantage is that FP2 must be a high finesse cavity. Such cavities have a wide bistable region. Thus, the intensity required for the control beam to drive it beyond its bistable region is large. This limits the cascadability of the device.

One of the criteria for cascadability is that the output signal from a switching device must be able to switch on another device of the same kind. This implies that the difference in magnitude of the ON state and the OFF state of the output must be at least equal to the magnitude required for switching. This condition is illustrated in Fig.6.10. In practice, the output contrast has to be larger than the required switching

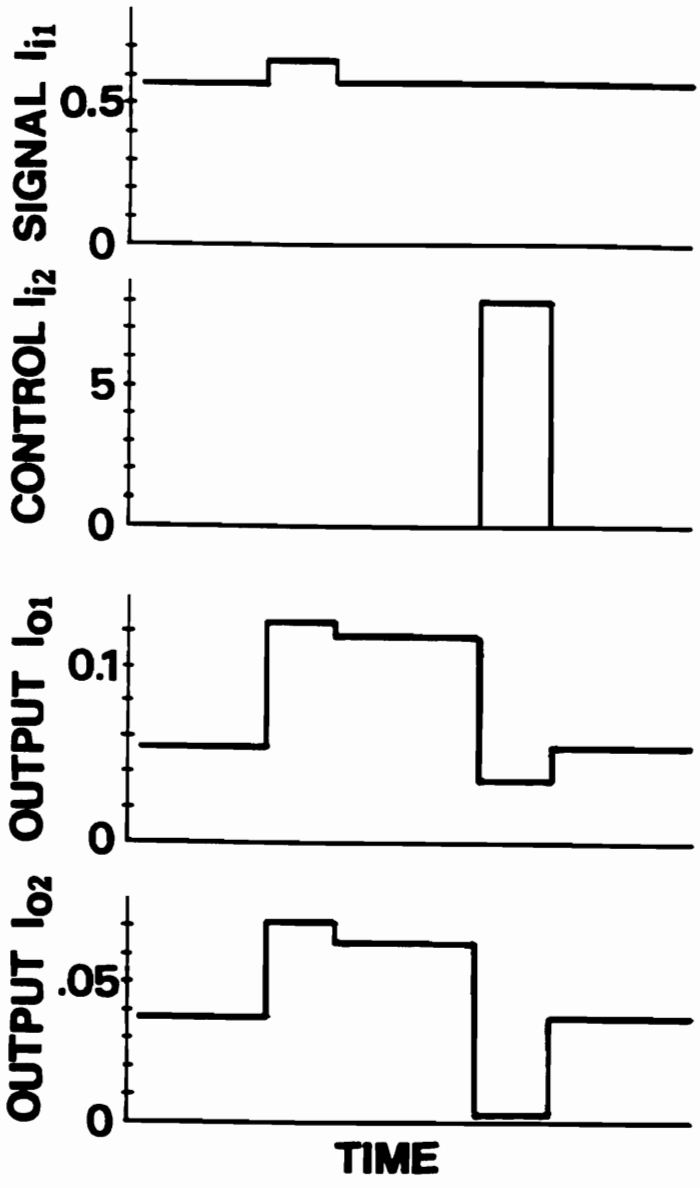

Figure 6.9: Switching sequence of the coupled cavities system of Fig.6.8. A small pulse on FP1 switches the outputs on and a larger pulse on FP2 turns the outputs off.

intensity in order to compensate for the energy losses of the signal as it propagates from one device to the next.

The second mode of operation does not have this disadvantage since FP2 does not need to be bistable, but a control beam must be mixed with the signal beam in order to turn the device on. Referring to Fig.6.8, FP1 can be biased at X with an intensity of about 0.56. FP2 can be biased at an intensity of 5.5 just before the region where the reflectivity drops sharply. A pulse of magnitude of less than 0.1 is then sufficient to turn the output on. This gives a 0.6 unit difference between the on and off states of the output I_{o_1}, which is more than sufficient to turn another device on. To turn the output off, a control pulse of approximately 0.5 unit is sufficient to bring the reflectivity of FP2 to its low value. Since the difference in output intensity is 0.6, this is also sufficient to switch another device of the same kind off.

In this chapter we have demonstrated numerically that it is possible to switch a system of two coupled nonlinear Fabry-Perot cavities with positive pulses in the steady state regime. The dynamic behavior of a system of two coupled cavities will be studied in the next chapter.

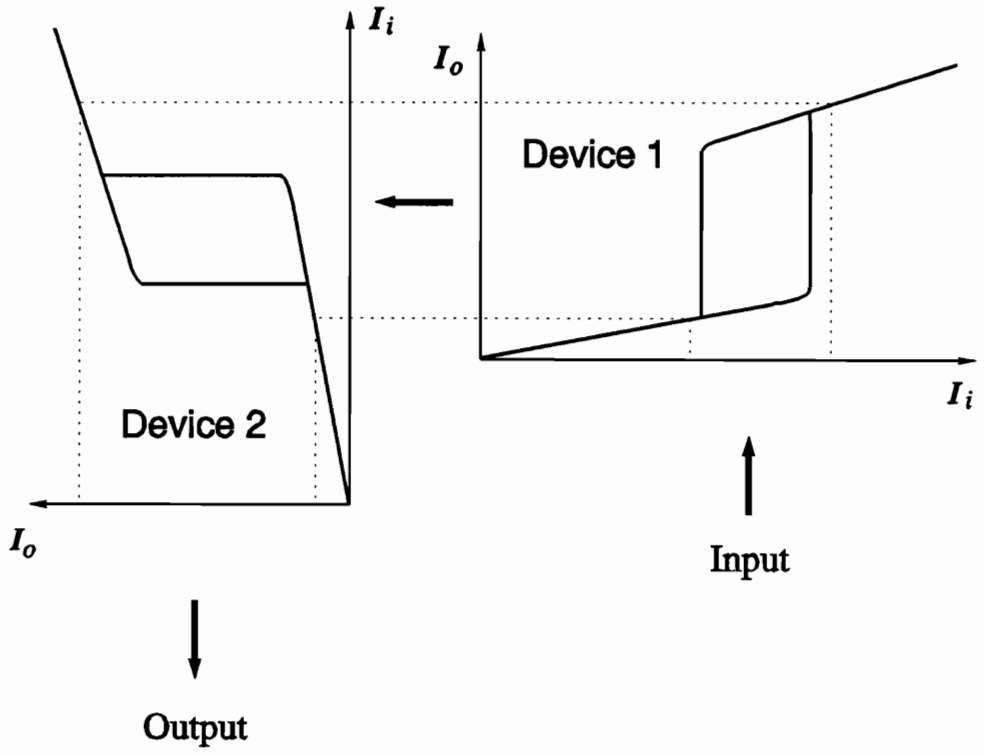

Figure 6.10: Criteria for cascadability of a switching device: the output from an element should be at equal to the minimum intensity required for switching the next element.

Chapter 7

Dynamics of Two Coupled Nonlinear Fabry-Perot Cavities

So far, our study of systems of coupled nonlinear Fabry-Perot cavities has been restricted to the steady state case. For practical devices, however, where speed is one of the most important factors, it is crucial to understand the transient and dynamic response of the Fabry-Perot. The ability to control one light beam with another relies entirely on the interaction of the nonlinear material with light. The response time of nonlinear media can vary greatly depending upon the nature of the interaction. Nonlinear responses due to electronic interaction are the fastest while responses due to thermal interaction are slower and orientational effects are even slower. An optical cavity has properties similar to those of an electrical capacitor. As a capacitor, an optical cavity does not respond instantly to an incoming signal. The characteristic response time of an optical cavity depends on its length and on the index of refraction of the medium filling it.

Bischofberger and Shen reported the first experiment describing the dynamical behavior of a nonlinear Fabry-Perot [39]. Their results show remarkable agreement with the predicted behavior [40]. The theoretical framework is simple: the contributions to the electric field inside the cavity are summed up, the resulting field is made

to interact with the medium and this changes the transmitted field.

In all practical situations, the cavity length is short (from a few wavelengths to some thousands of wavelengths). As a consequence, for common pulse rise and fall times ($\sim$ psec), the change of the incident field intensity during one round-trip remains small. Goldstone and Garmire made use of this approximation and derived a simpler model to describe the dynamics of a nonlinear Fabry-Perot cavity [41]. The computation time required by the Goldstone/Garmire algorithm is also considerably shorter than that required by the Bischofberger/Shen algorithm.

This chapter is divided into three parts. First, we review the model of Goldstone and Garmire for a single nonlinear Fabry-Perot. Next, the model is extended to the case of a system of two coupled nonlinear Fabry-Perot cavities. Finally, we discuss the possibility of switching this coupled system with positive pulses in the dynamic mode. Numerical example are given, showing that a system of two coupled cavities can be switched on and off with positive pulses in the dynamic regime as well as in the steady state regime.

7.1 Dynamic Theory of a Nonlinear Fabry-Perot

The model is derived from a set of difference equations for the electric field inside a Fabry-Perot cavity containing a refractive nonlinear medium. The medium has a response time τ_m. The round-trip time is proportional to the intra-cavity spacing and to the instantaneous refractive index of the medium. The analysis is carried out to first order in time and space. Two differential equations are derived from the difference equations. One describes the evolution of the transmitted field and the other describes the evolution of the refractive index of the nonlinear medium.

The fields inside the cavity at some time are defined as follow:

$$\begin{aligned} \mathcal{E}_i(t) &= E_i(t)e^{-i\omega t} \\ \mathcal{E}_\pm(t) &= E_\pm(z,t)\exp\{i(k_\pm(z,t)z - \omega t)\} \end{aligned}$$

$$\mathcal{E}_T(t) = E_T(t)\exp\{i(kd-\omega t)\}\ , \tag{7.1}$$

where $\mathcal{E}_i(t)$ is the incident field. $\mathcal{E}_\pm(t)$ are the forward and backward propagating fields and $\mathcal{E}_T(t)$ is the field transmitted by the cavity at time t, as shown in Fig.7.1(a). The incident field $\mathcal{E}_i(t)$ and the transmitted field $\mathcal{E}_T(t)$ are defined at the entrance ($z=0$) and exit ($z=d$) mirror, respectively. The forward and backward propagating fields as well as the wavenumber inside the cavity are functions of position and time because of the presence of the nonlinear medium.

The forward propagating field at time t is the sum of the forward propagating field at time $t-\tau_c$ and the transmitted incident field at time $t-\Delta t_0^z$, (see Fig.7.1(b)), where τ_c is the round-trip time and Δt_0^z is the time for the incident field $\mathcal{E}_i(t)$ to propagate from $z=0$ to z. Defining the notations for the transit time as follow:

$\Delta t_{z_1}^{z_2}$ = actual transit time from z_1 to z_2
τ_c = actual round-trip time starting at t
τ_c' = round-trip time with cavity parameters frozen at their values at t
$\delta t(z) = \Delta t_z^d + \Delta t_d^0$ = actual transit time from z to d to 0,

we have

$$\begin{aligned}\mathcal{E}_+(z,t) &= R\mathcal{E}_+(z,t-\tau_c)+\sqrt{T}\mathcal{E}_i(t-\Delta t_0^z)\\ \mathcal{E}_+(z,t+\tau_c) &= R\mathcal{E}_+(z,t)+\sqrt{T}\mathcal{E}_i(t+\delta t).\end{aligned} \tag{7.2}$$

Substituting Eq.(7.1) into Eq.(7.2) and canceling the common factor $e^{-i\omega t}$ gives

$$\begin{aligned}E_+(z,t+\tau_c) &= RE_+(z,t)\exp\{ik_+(z,t)z-ik_+(z,t+\tau_c)z+i\omega\tau_c\}\\ &\quad +\sqrt{T}E_i(t+\delta t)\exp\{-i\omega\delta t-ik_+(z,t+\tau_c)z+i\omega\tau_c\}.\end{aligned} \tag{7.3}$$

The difference $k_+(z,t+\tau_c)z-k_+(z,t)z$ can be approximated by $\tau_c\frac{\partial k_+(z,t)}{\partial t}z$, which gives

$$\begin{aligned}E_+(z,t+\tau_c) &= RE_+(z,t)\exp\left\{i\left[\omega\tau_c-\tau_c\frac{\partial k_+(z,t)}{\partial t}z\right]\right\}\\ &\quad +\sqrt{T}E_i(t+\delta t)\exp\left\{i\left[\omega(\tau_c-\delta t)-k_+(z,t+\tau_c)z\right]\right\}.\end{aligned} \tag{7.4}$$

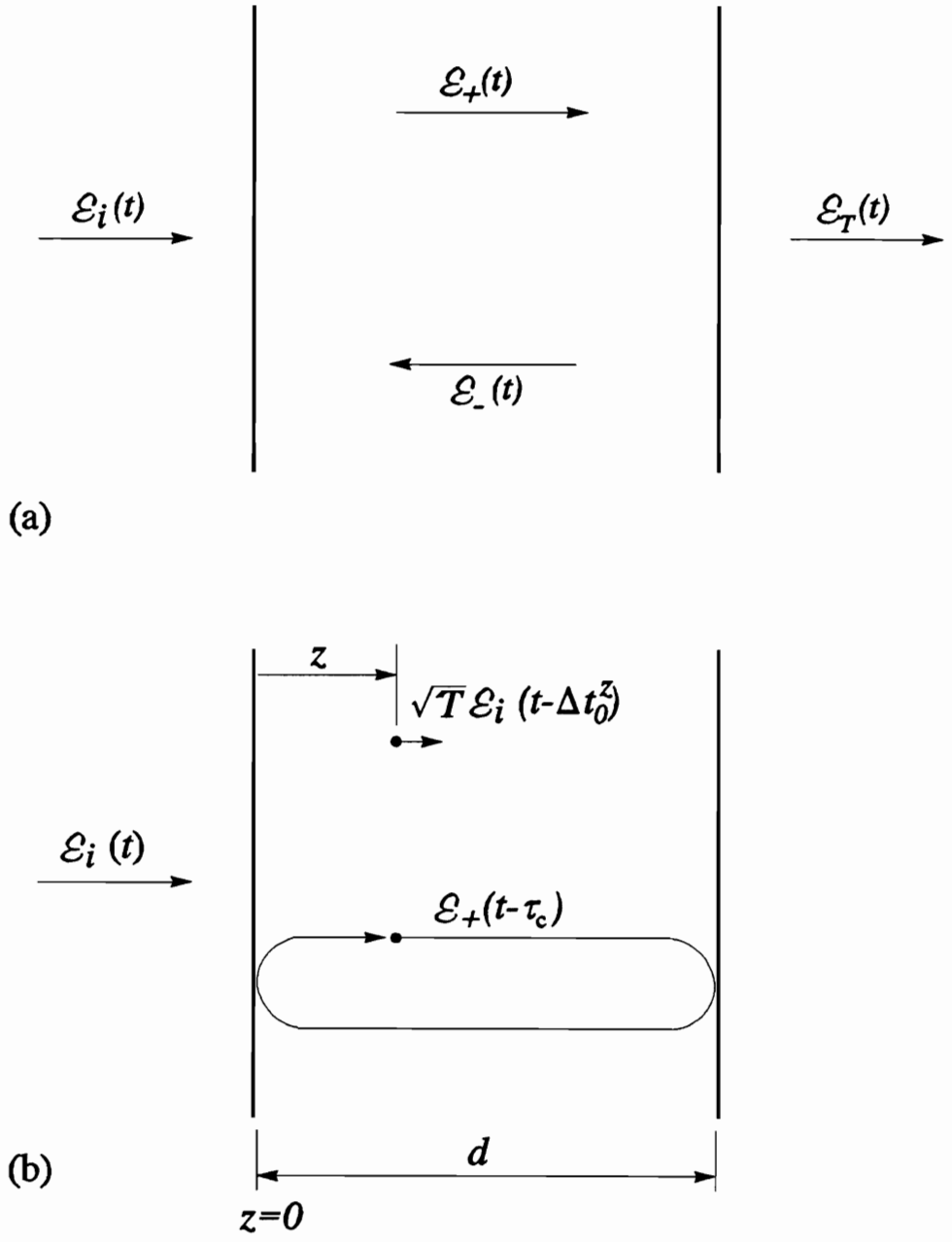

Figure 7.1: (a) Geometry of the nonlinear Fabry-Perot cavity. (b) The electric field inside the cavity at time t is the sum of the forward propagating field a round-trip time ago and the incident field.

At the exit mirror, $z = d$, the transmitted field differs from the forward propagating field by a constant factor $\sqrt{T}$: $\sqrt{T}\mathcal{E}_+(d,t) = \mathcal{E}_T(t)$. $\delta t(d)$ is half the round-trip time τ_c. Therefore, we can write Eq.(7.4) as

$$\begin{aligned} E_T(t+\tau_c) &= RE_T(t)\exp\left\{i\left[\omega\tau_c - \tau_c\frac{\partial k_+(d,t)}{\partial t}d\right]\right\} \\ &\quad + TE_i(t+\tau_c/2)\exp\left\{i\left[\omega\tau_c/2 - k_+(d,t+\tau_c)d\right]\right\}. \end{aligned} \tag{7.5}$$

Expanding the actual round-trip time τ_c from the round-trip time τ_c' with parameter frozen at time t, we have

$$\tau_c \simeq \tau_c' + \frac{\tau_c'}{2}\frac{\partial\tau_c'}{\partial t} \tag{7.6}$$

$$\omega\tau_c \simeq \overline{\phi} + \frac{\tau_c'}{2}\frac{\partial\overline{\phi}}{\partial t}. \tag{7.7}$$

Where the round-trip phases ϕ and $\overline{\phi}$ are defined as

$$\phi = \omega\tau_c \tag{7.8}$$

$$\overline{\phi} \equiv \omega\tau_c' \tag{7.9}$$

$$= 2\overline{k}d\,. \tag{7.10}$$

$\overline{\phi}$ is the round-trip phase shift at t with the cavity parameters frozen and $\overline{k}$ is the wave vector averaged over one round-trip starting at t. Note that $\overline{k}$ differs from $k_+(d,t)$ by a first order correction in $\partial k_+/\partial t$. Therefore, to first order approximation, we have

$$\begin{aligned} \frac{\partial k_+}{\partial t} &= \frac{\partial\overline{k}}{\partial t} + \mathrm{O}\left(\frac{\partial^2\overline{k}}{\partial t\partial z}\right) \\ &\simeq \frac{\partial\overline{k}}{\partial t}\,, \end{aligned} \tag{7.11}$$

$$\begin{aligned} \tau_c\frac{\partial k_+}{\partial t}d &\simeq \tau_c'\frac{\partial\overline{k}}{\partial t}d \\ &= \frac{\tau_c'}{2}\frac{\partial\overline{\phi}}{\partial t}\,. \end{aligned} \tag{7.12}$$

Making use of Eq.(7.7) and Eq.(7.12), the argument of the first exponential function in Eq.(7.5) can be written as

$$\omega\tau_c - \tau_c\left(\frac{\partial k_+}{\partial t}d\right) \simeq \overline{\phi}. \tag{7.13}$$

Since the change of the incident field is assumed to be small during one cavity round-trip time, the change in round-trip phase will also remain small. Therefore, to first order approximation, the argument of the second exponential function in Eq.(7.5) is zero:

$$\begin{aligned} \omega\tau_c/2 - k_+(d, t+\tau_c)d &= \phi/2 - k_+ d - \tau_c \frac{\partial k_+}{\partial t} d \\ &\simeq 0. \end{aligned} \tag{7.14}$$

Since the difference between τ_c, τ_c' and the linear round-trip time $\overline{\tau_c}$ is small in one round-trip time, we can neglect the difference between them outside the exponents. Expanding the term $E_T(t+\tau_c)$ in Eq.(7.5) ,rearranging and replacing τ_c as the linear round-trip time $\overline{\tau_c}$, we have

$$\overline{\tau_c}\frac{\partial E_T(t)}{\partial t} + \{1 - Re^{i\overline{\phi}(t)}\}E_T(t) = TE_i(t + \overline{\tau_c}/2). \tag{7.15}$$

This field evolution equation is coupled to the equation for the time dependent refractive index which is assumed to obey a Debye relaxation equation. Thus, the round-trip phase $\overline{\phi} = 2\overline{n}k_0 d$, where k_0 is the wavenumber in vacuum, $\overline{n}$ is the index of refraction of the medium at time t, follows an equation of the form

$$\tau_m \frac{\partial \overline{\phi}}{\partial t} + \overline{\phi} = \alpha + \beta |E_T|^2 \,, \tag{7.16}$$

where $\alpha = \phi_0$ is the initial detuning of the cavity and $\beta = 2n_2 k_0 d\frac{1+R}{1-R}$, n_2 is the nonlinearity of the refractive index and R is the reflectivity of the mirrors. Eq.(7.15) and Eq.(7.16) are solved numerically to predict the behavior of the cavity.

7.2 Dynamics of a Linear Fabry-Perot

Eq.(7.15) and Eq.(7.16) can be solved to obtain the dynamics of the switching. Some general questions that one might ask are: "How fast can a device of this kind switch?" or "What parameters determine the dynamics of the switching?".

To answer these questions, it is necessary to understand how each parameter affects the dynamics of the nonlinear Fabry-Perot. As a starting point, we look at

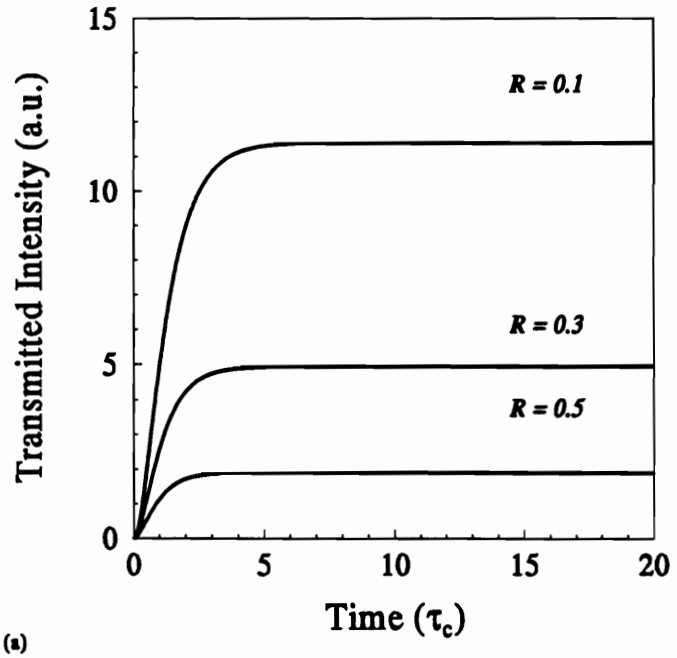

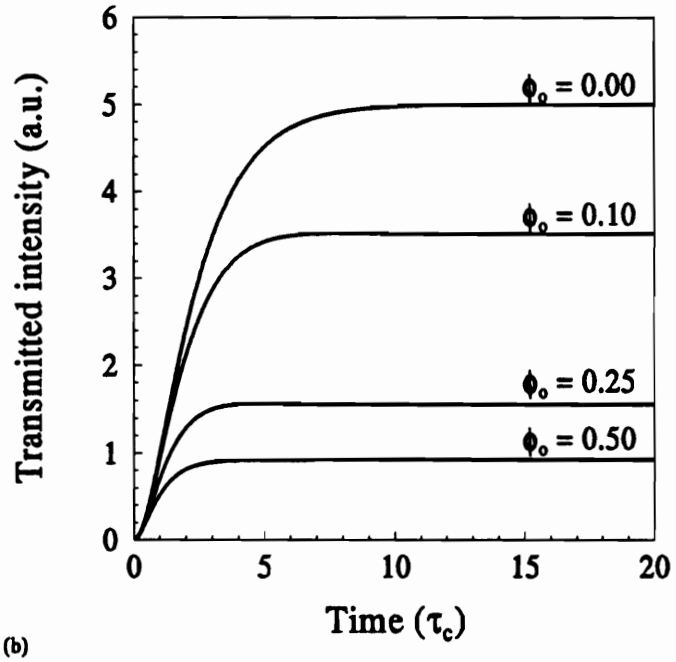

Figure 7.2: Dynamics of a linear Fabry-Perot. The rise-time of the output depends on (a) the reflectivity of the mirrors and (b) the initial detuning of the cavity. The cavity parameters for (a) are: $n_0 = 1.56$, $d = 292.505\lambda$ where $\lambda = 514$nm and for (b) are: $n_0 = 1.56$ and $R = 0.4$.

an empty Fabry-Perot. As mentioned in the previous section, an empty Fabry-Perot acts as a capacitor in an optical circuit. When an incoming field enters the Fabry-Perot, one part of the wave is transmitted through the front mirror and the other part is reflected. The portion that enters the cavity travels the exit mirror, where it is partially reflected back into the cavity. This wave is reflected back and forth between the entrance and the exit mirror. Each time the wave hits the exit mirror, a portion of the wave is added to the transmitted field. The transmitted intensity is found by squaring the sum of all the contributions to the field. The length of the cavity determines the time of flight of the wave between the mirrors and the reflectivity of the mirrors determines how fast the sum converges. Therefore, the buildup time of a linear cavity is determined by the optical length of the cavity and the reflectivity of the mirrors.

In an empty or a linear cavity, ϕ is a constant, $\phi(t) = \phi_0$ where ϕ_0 is the initial detuning. Rewriting Eq.(7.15) for a Fabry-Perot with a linear medium, we have:

$$\tau_c \frac{\partial E_T(t)}{\partial t} + \{1 - Re^{i\phi_0}\} E_T(t) = T E_i(t + \tau_c/2) \ , \tag{7.17}$$

which can be directly compared to the equation for the current in a RC series circuit, i.e.:

$$R\frac{\partial I(t)}{\partial t} + \frac{1}{C} I(t) = I_0(t). \tag{7.18}$$

The time constant of a linear Fabry-Perot cavity can then be written as $\tau_c/(1 - Re^{i\phi_0})$. Notice that the round-trip time is proportional to the the round-trip phase, $\tau_c = \phi/kc$, where c is the speed of light in vacuum. Therefore, the rise-time of a linear Fabry-Perot cavity is seen to depend on the detuning of the cavity and on the reflectivity of the mirrors. Solving Eq.(7.17) gives the dynamic response of a linear Fabry-Perot. For a step input starting at $t = 0$ we find:

$$E_T(t) = \frac{T\mathcal{E}_o}{1 - Re^{i\phi_0}} \left\{ 1 - \exp[-(\frac{1 - Re^{i\phi_0}}{\tau_c})t] \right\}. \tag{7.19}$$

The effect of the mirror reflectivity is shown in Fig.7.2(a). For equal cavity detuning, the rise-time is proportional to the reflectivity of the mirrors. The effect of

the initial detuning is shown in Fig.7.2(b). From the graphs, it is seen that the cavity buildup time is of the order of a few cavity round-trip time.

7.3 Dynamics of a Nonlinear Fabry-Perot

Fig.7.3 shows two steady state response curves of a dielectric Fabry-Perot filled with a Kerr-type medium. In Fig.7.3(a), the cavity is initially tuned to a high transmission state and in Fig.7.3(b) it is tuned to a low transmission state. The mistuning is 0.01π in each case. The steady-state switch-up intensity for (a) is approximately 4.07 units and for (b) it is approximately 16.7 units.

The method used to compute the solutions of the differential equations (7.15) and (7.16), employs a variable step size control iteration. It was found that a small mistuning of the cavity will sizeably reduce the computation time. Some results are shown in the following figures.

The temporal evolution of the transmitted intensity and of the change in round-trip phase ($\Delta\phi = \phi - \phi_0$) in the cavity is shown in Fig.7.4(a) and (Fig.7.4(b)), respectively. The cavity is initially tuned close to a minimum transmission state (Fig.7.3(a)). The cavity is excited by a plane wave of magnitude approximately equal to the minimum steady state switching intensity (4.07 units). The response of the cavity filled with materials of different response time is depicted. For a material with a response time equal to one round-trip time ($\tau_m/\tau_c = 1$), the cavity switches after about 25 round-trips. Materials with a slower response time take a longer time to switch. Notice that there is always a finite time delay before the cavity switches. As seen from the graph, the switch up time is much longer than the cavity build up time of the corresponding linear cavity which was found to be of the order of a few round-trip times. This slowing down of the cavity response occurs when the incident intensity is approximately equal to the critical switching intensity. This effect is called *critical slowing down.* As a result, the response of the cavity is much slower than what could be expected from the steady state analysis. The transmitted intensity and the

change in round-trip phase have similar dynamic responses.

Fig.7.5 is a similar plot for a cavity which is initially tuned close to a maximum transmission state. Fig.7.5(b) and Fig.7.4(b) show that the dynamics of the change in round-trip phase is basically the same in both cases and the same delay in switching is observed in both cases. The transmitted intensity behaves somewhat differently from that in Fig.7.4(a). The sharp peak seen at about $2\tau_c$ is due to the sweeping of the transmission peak of the cavity through a peak transmission when the phase of the cavity is momentarily equal to an integral multiple of 2π.

The magnitude of the slowing down increases with the medium response time. Fig.7.6 shows a plot of the switch-up time versus the medium response time. It shows that the switch-up time is directly proportional to the medium response time. The switch-up time measured in units of round-trip time is found to be 10 times larger than the medium response time.

The critical slowing down effect depends on the excess of incident intensity above the critical switching intensity and can be reduced by increasing the incident intensity. The closer the incident intensity is to the critical value, the longer the slowing down. Consequently, practical switching devices have to be switched with pulses of magnitude considerably larger than the critical switching intensity. Fig.7.7 shows the dynamic response of a nonlinear Fabry-Perot cavity, for different values of the incident intensity. It can be seen that the switching time increases drastically as the incident intensity gets closer to the critical switching intensity.

7.4 Dynamic Theory of Coupled Fabry-Perot Cavities

In this section, the dynamic theory of a nonlinear cavity is extended to the case of two coupled cavities. The goal is to determine the circumstances under which this system can be switched with positive pulses in the dynamic regime. The model and its underlying assumptions are described in appendix A. The schematic configuration of the two coupled cavities is shown in Fig.7.8. The system under consideration

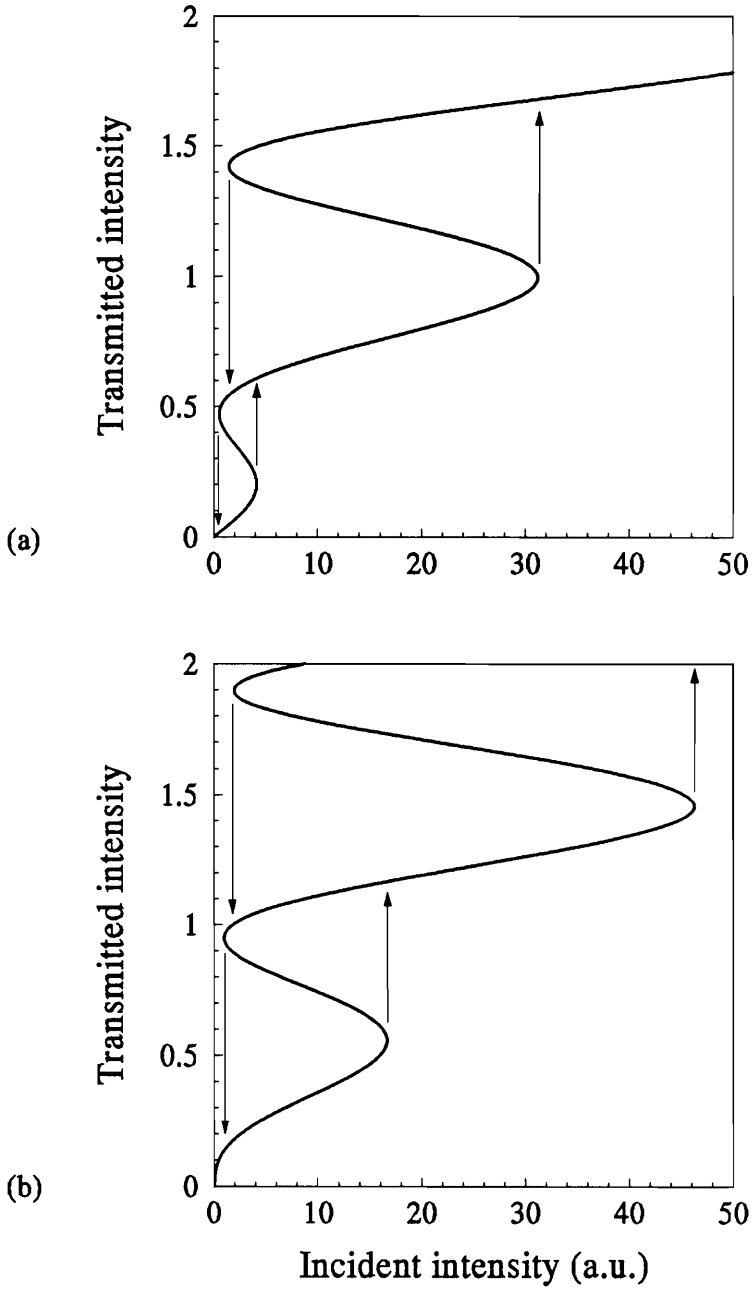

Figure 7.3: Steady state response of a nonlinear Fabry-Perot cavity. The cavity parameters are : $R = 0.7$, $n_0 = 1.56$, $n_2 = 10^{-3}$. The initial detuning is (a) 0.01π, (b) 1.01π. The slight mistuning of 0.01π is added to decrease the computation time when calculating the dynamics of the cavity.

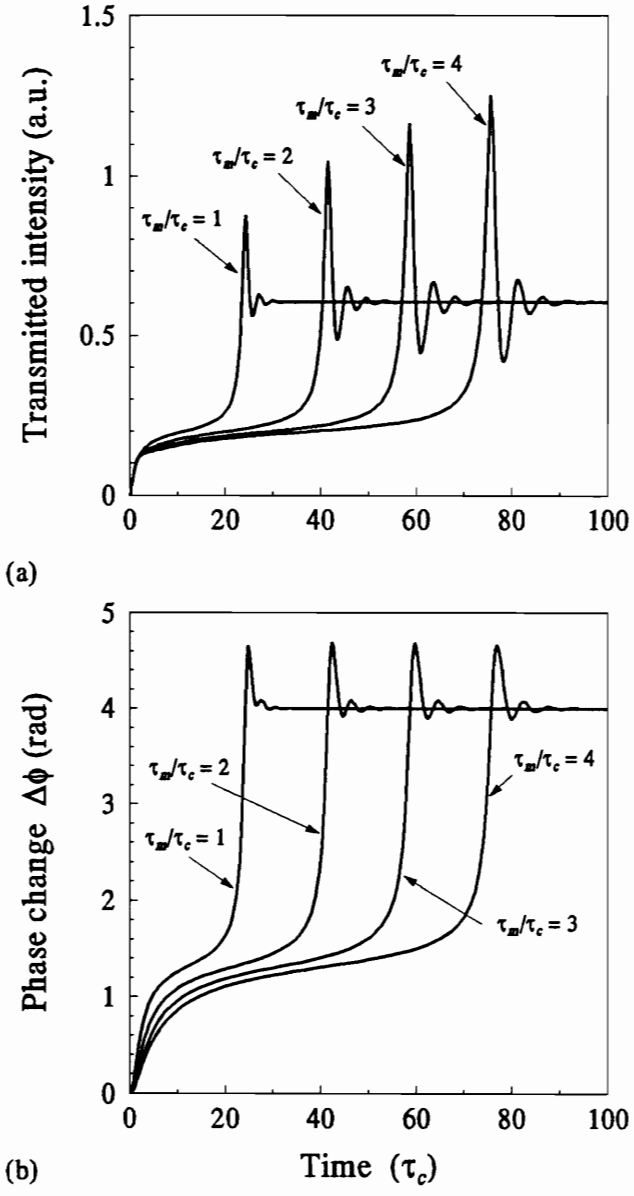

Figure 7.4: Dynamic response of a nonlinear Fabry-Perot cavity for various ratios of medium response time to cavity round-trip time. (a) transmitted intensity, (b) change in round-trip phase. The cavity is initially tuned close to a minimum transmission state. Critical slowing down occurs when the incident intensity is approximately equal to the critical switching intensity.

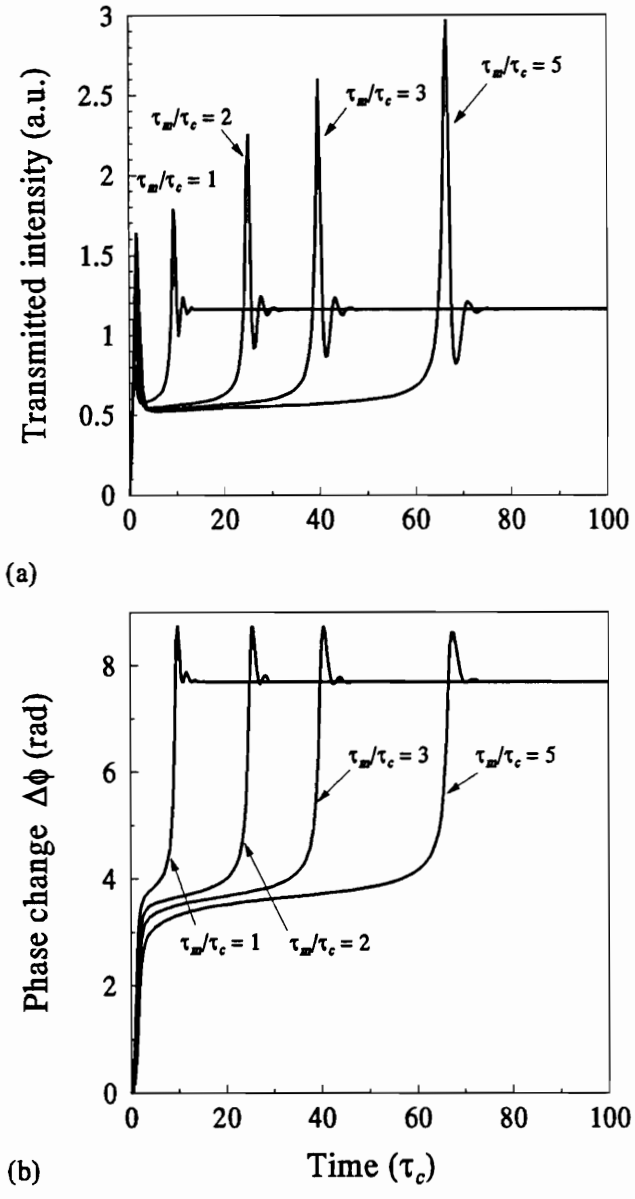

Figure 7.5: Dynamic response of a nonlinear Fabry-Perot cavity for various ratios of medium response time to cavity round-trip time.(a) transmitted intensity, (b) change in round-trip phase. The cavity is initially tuned close to a maximum transmission state. Critical slowing down occurs when the incident intensity is approximately equal to the critical switching intensity. The first peak in (a) is due to the rapid sweeping of the phase of the cavity through an integral multiple of 2π.

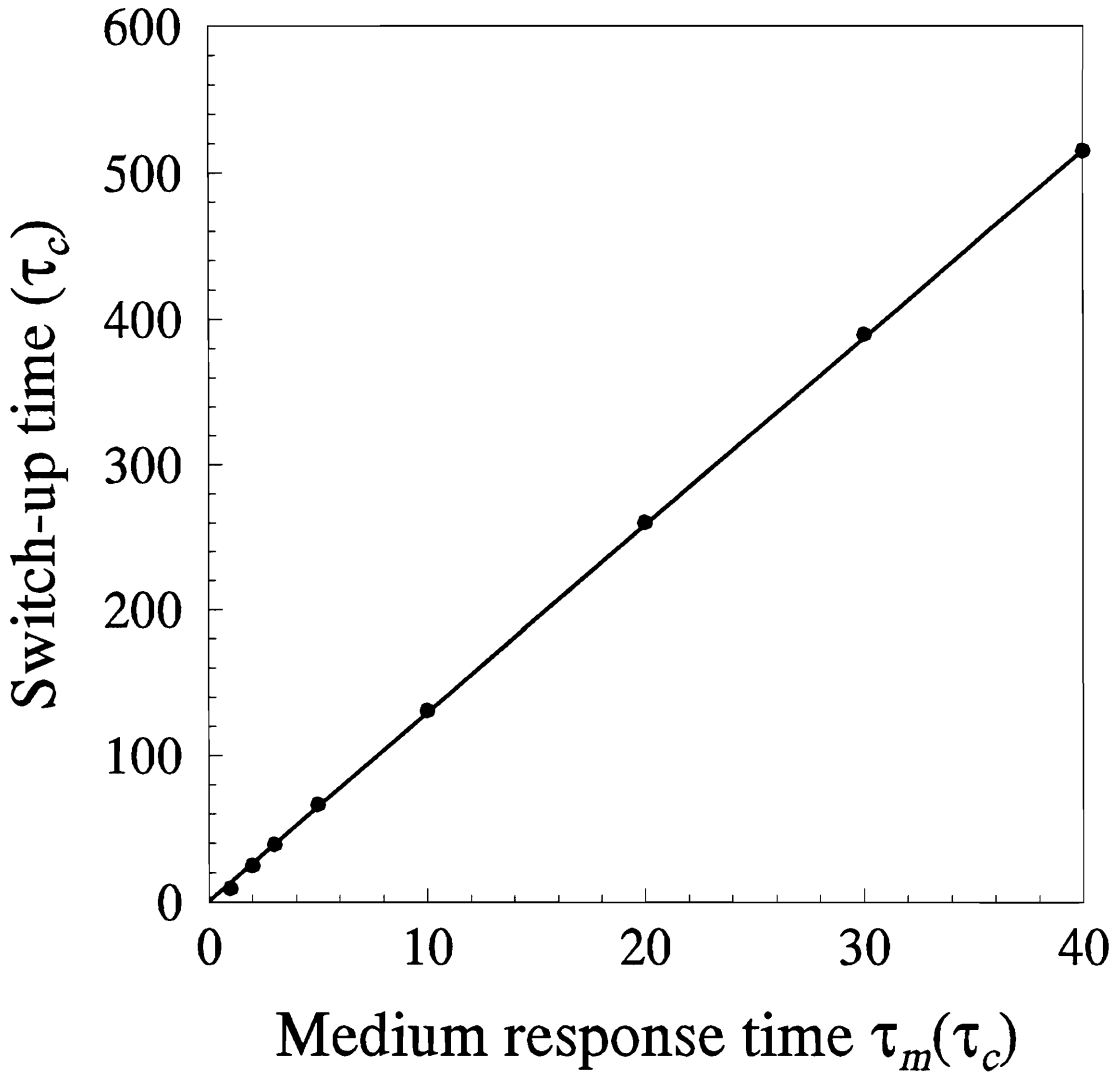

Figure 7.6: Switch-up time of a nonlinear cavity against the medium response time. The cavity is excited by a step function input with the same incident intensity but is with materials having different response times. The incident intensity is approximately equal to the critical switching intensity. The switch-up time measured in units of cavity round-trip time is 10 times larger than the medium response time.

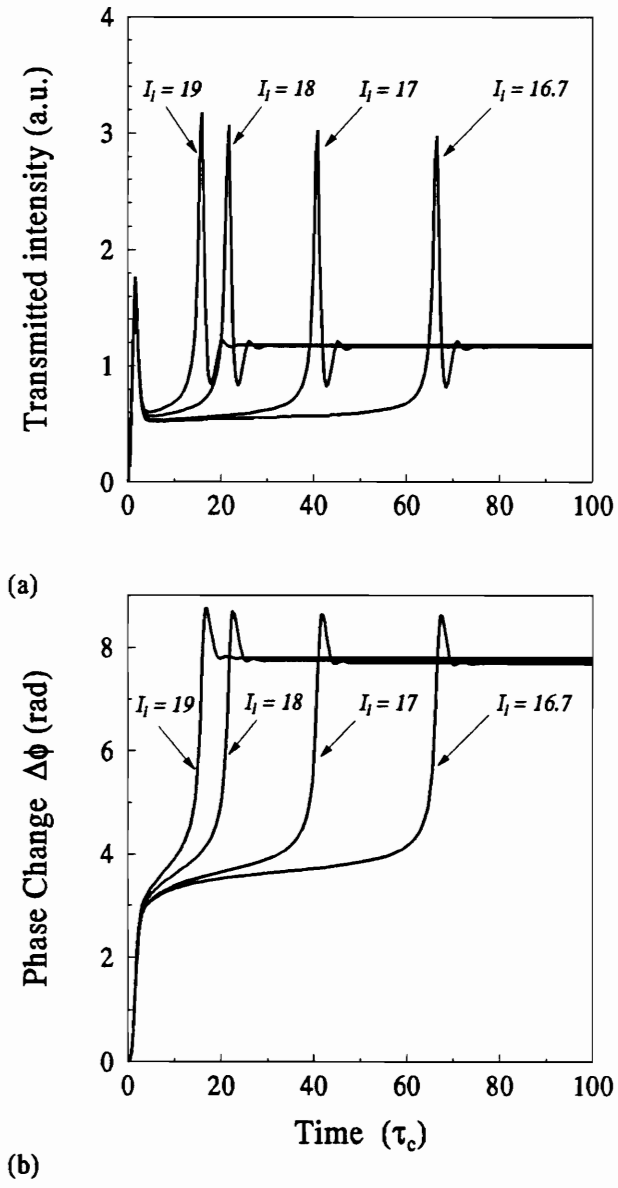

Figure 7.7: The critical slowing down depends on the difference between the incident intensity and the critical switching intensity. The smaller the difference, the slower the switching time is. The graphs show the response of a nonlinear Fabry-Perot cavity filled with a fast medium $\tau_m/\tau_c = 1$. A step input is applied to the cavity at $t = 0$. The critical switching intensity is approximately 16.7 units. At $I_i = 16.7$ the switching time is approximately $70\tau_c$. Increasing I_i to 19 units reduces the switching time to less than $20\tau_c$. (a) Transmitted intensity, (b) phase change in the cavity.

is similar to the one described in chapter 6. This coupled cavity system actually consists of three cavities, two nonlinear and one linear. The cavities at both ends are nonlinear and the space between them forms a linear Fabry-Perot cavity. The intra-cavity spacings are d_1, d_2 and d_3, as shown in the figure. The transmission and reflection coefficients of the mirrors are t_j and r_j respectively (where $j = 1$ to 4).

There are two inputs to the system, $E_{i_1}(t)$ and $E_{i_2}(t)$. $E_{i_1}(t)$ and $E_{i_2}(t)$ are orthogonally polarized. A polarizer P is used to isolate cavity 1 from $E_{i_2}(t)$. Thus, the analysis can be split into two parts, one concerning the input $E_{i_1}(t)$ and the other concerning the input $E_{i_2}(t)$. The main point is that E_{i_1} affects both nonlinear media in cavity 1 and in cavity 3 directly, while E_{i_2} affects only cavity 3 directly. Since E_{i_1} and E_{i_2} are orthogonally polarized, the fields do not interact with each other. The refractive index in cavity 1 is thus affected by E_{i_1} directly and by the field reflected from cavity 3. It is not affected by E_{i_2} directly. The refractive index in cavity 3 is affected by E_{i_2} directly and by the beam transmitted by cavity 1 and the polarizer.

The equations describing the fields inside each cavity can be easily established. For an input E_{i_1} alone, the evolution of the right-going field E_5 in cavity 3 can be described by the following equation:

$$\begin{aligned} & \overline{\tau_3}\frac{\partial E_5(C,t)}{\partial t} + \{1 - r_3 r_4 e^{i\overline{\phi_3}(t)}\}E_5(C,t) \\ = \; & it_3 E_3(B, t + \overline{\tau_3}/2) \\ \simeq \; & it_3\left\{E_3(B,t) + \frac{\overline{\tau_3}}{2}\frac{\partial E_3(B,t)}{\partial t}\right\}, \end{aligned} \tag{7.20}$$

where $\overline{\tau_3}$ is the average round-trip time of cavity 3. It can be seen that the rate of change of E_5 at $z = C$ depends on the electric field E_3, entering cavity 3. Eq.(7.20) is identical to Eq.(7.15), which describes the response of a single nonlinear cavity. The left-going field E_6 also depends on E_3, with some phase change:

$$\overline{\tau_3}\frac{\partial E_6(B,t)}{\partial t} + \{1 - r_3 r_4 e^{i\overline{\phi_3}(t)}\}E_6(B,t) = it_3 r_4 E_3(B,t)e^{i\overline{\phi_3}(t)} . \tag{7.21}$$

The extra factor r_4 on the right hand side comes from the additional reflection of E_3 on M4.

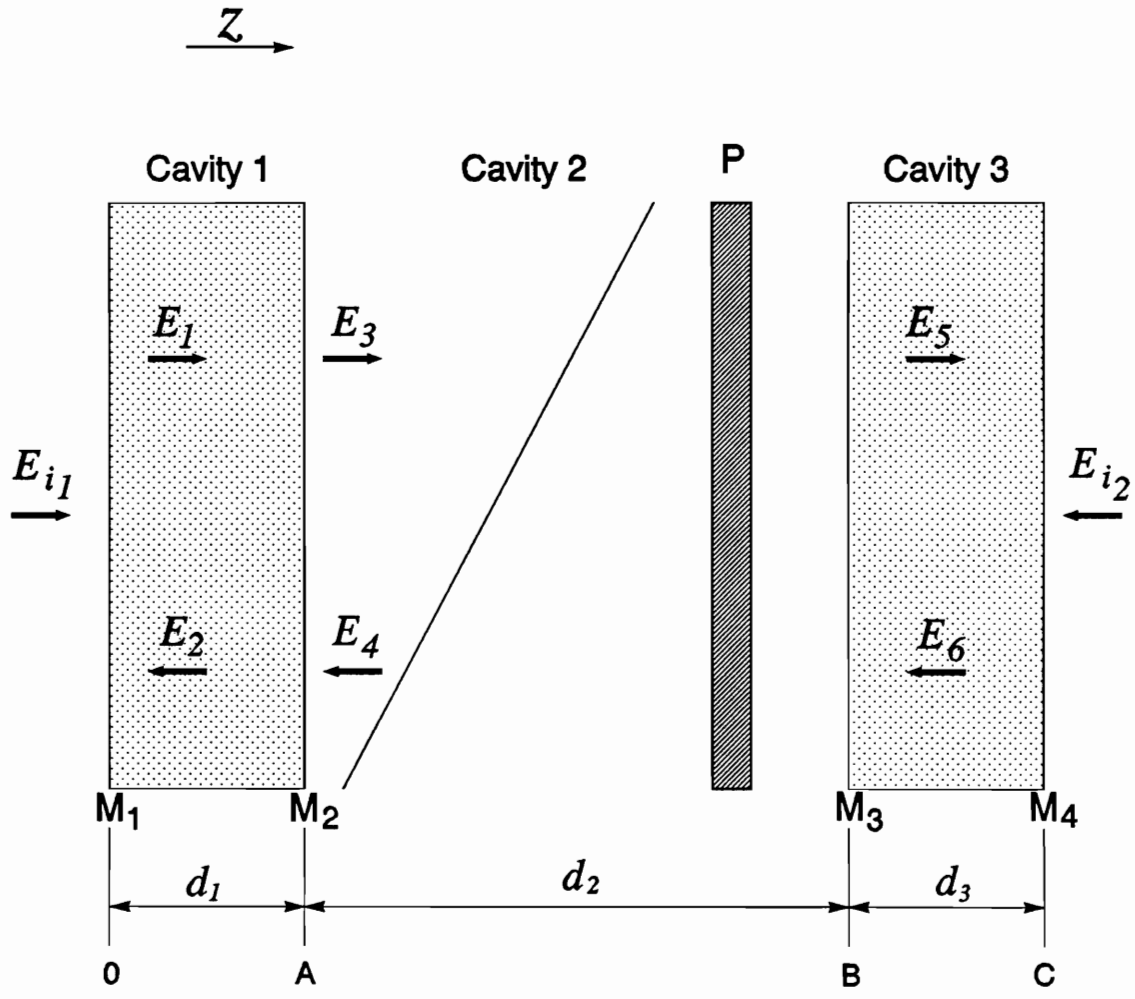

Figure 7.8: Schematic configuration of two coupled nonlinear Fabry-Perot cavities. Cavity 1 and cavity 3 are nonlinear Fabry-Perots. The space between these nonlinear Fabry-Perots forms a linear Fabry-Perot cavity 2. M1, M2, M3 and M4 are dielectric mirrors with reflection coefficients r_1, r_2, r_3 and r_4 respectively. The input E_{i_1} and E_{i_2} are orthogonally polarized. The polarizer P transmits E_{i_1} and blocks E_{i_2}. It is used to isolate cavity 1 from the input E_{i_2}. The intra-cavity spacings are d_1, d_2 and d_3. E_1 to E_6 are the fields inside the cavities.

For cavity 1, there is an additional input to the cavity, namely E_4, the left-going field inside cavity 2. The equation for E_1 and E_3 are found to be

$$\begin{aligned} & \overline{\tau_1}\frac{\partial E_1(A,t)}{\partial t} + \{1 - r_1 r_2 e^{i\overline{\phi_1}(t)}\}E_1(A,t) \\ = \; & i r_1 t_2 E_4(A,t) e^{i\overline{\phi_1}(t)} + i t_1 E_{i1}(t + \overline{\tau_1}/2) \, , \end{aligned} \tag{7.22}$$

and similarly,

$$\begin{aligned} & \overline{\tau_1}\frac{\partial E_2(0,t)}{\partial t} + \{1 - r_1 r_2 e^{i\overline{\phi_1}(t)}\}E_2(0,t) \\ = \; & i t_2 E_4(A, t + \overline{\tau_1}/2) e^{i\overline{\phi_1}(t)} + i t_1 r_2 E_{i1}(t) e^{i\overline{\phi_1}(t)} \\ \simeq \; & i t_2 \left\{ E_4(A,t) + \frac{\overline{\tau_1}}{2}\frac{\partial E_4(A,t)}{\partial t} \right\} e^{i\overline{\phi_1}(t)} + i t_1 r_2 E_{i1}(t) e^{i\overline{\phi_1}(t)}. \end{aligned} \tag{7.23}$$

Notice that E_2 is evaluated at 0 and E_4 is evaluated at A. The term $\frac{\overline{\tau_1}}{2}\frac{\partial E_4(A,t)}{\partial t}$ reflects the advance in time between O and A. In a similar fashion, E_3 and E_4 can be expressed as follow:

$$\begin{aligned} & \tau_2\frac{\partial E_3(B,t)}{\partial t} + \{1 - r_2 r_3 e^{i\phi_2}\}E_3(B,t) \\ = \; & i t_2 \left\{ E_1(A,t) + \frac{\tau_2}{2}\frac{\partial E_1(A,t)}{\partial t} \right\} + i r_2 t_3 E_6(B,t) e^{i\phi_2} \, , \end{aligned} \tag{7.24}$$

$$\begin{aligned} & \tau_2\frac{\partial E_4(A,t)}{\partial t} + \{1 - r_2 r_3 e^{i\phi_2}\}E_4(A,t) \\ = \; & i t_3 \left\{ E_6(B,t) + \frac{\tau_2}{2}\frac{\partial E_6(B,t)}{\partial t} \right\} e^{i\phi_2} + i t_2 r_3 E_1(A,t) e^{i\phi_2} \, . \end{aligned} \tag{7.25}$$

Eq.(7.20) to Eq.(7.25) describe the dynamics of the six fields in the coupled cavities system with one input E_{i_1}. The next step is to incorporate the second input E_{i_2} into the model. Since the inputs are orthogonally polarized and the media respond only to the total intensity of the radiation, the response of the refractive index of each cavity can be computed using the total intensity of the radiation inside each cavity. Therefore, we can separate the system as follow. First, for the input $E_{i_1}(t)$, the system is treated as a coupled cavities system with one input. Next, for the input $E_{i_2}(t)$,

the situation is the same as for a single cavity with one input since the polarizer isolates cavity 1 from E_{i_2}. Notice that the equations describing these two situations are coupled by the nonlinear media inside cavity 1 and 3. Although the fields can be consider separately in each case for each input, their equations of motion have to be solved consistently, together with the medium response equations, in order to obtain the coupled response of the entire system.

Since the response of cavity 3 due to the input E_{i_2} can be considered as a single cavity case, we can use the result of section 7.1 to describe the evolution of the fields in cavity 3. For the second input, $E_{i_2}(t)$, the left-going field E_{T2} transmitted by cavity 3 and blocked by the polarizer is given by

$$\overline{\tau_3}\frac{\partial E_{T2}(t)}{\partial t} + \{1 - r_3 r_4 e^{i\overline{\phi_3}(t)}\}E_{T2}(t) = -t_3 t_4 E_{i2}(t + \overline{\tau_3}/2)\ , \tag{7.26}$$

The index of refraction of the medium in cavity 1 depends only on E_{i_1}. Assuming a Debye relaxation equation with a time constant τ_{m1} for the nonlinear index of refraction in cavity 1, the equation for the detuning in cavity 1 can then be written as

$$\tau_{m1}\frac{\partial\overline{\phi_1}}{\partial t} + \overline{\phi_1} = \alpha_1 + \beta_1|E_1|^2\ , \tag{7.27}$$

where α_1 is the initial detuning of cavity 1 and β_1 depends on the reflectivity of the mirrors of cavity 1 and on the nonlinearity n_{12} of the refractive index of the medium. The index of refraction of the medium in cavity 3 depends on the field transmitted from cavity 1 to cavity 2 and also depend on the input $E_{i_2}(t)$. The equation for the detuning in cavity 3 can be written as

$$\tau_{m3}\frac{\partial\overline{\phi_3}}{\partial t} + \overline{\phi_3} = \alpha_2 + \beta_2\left\{|E_5|^2 + \frac{1 + r_3 r_4}{1 - r_3 r_4}|E_{T2}|^2\right\}\ , \tag{7.28}$$

where τ_{m2}, α_2 and β_2 have the same meanings as for cavity 1.

7.5 Numerical Results

One of the main goal of this numerical study is to verify that positive pulse switching, which was shown to be feasible in the steady-state model of chapter 6, is also

possible in the dynamic regime. The possibility of positive pulse switching is demonstrated in this section, for both cases described in section 6.2.2 i.e.: switching on and off with two pulses of different magnitudes incident on the same cavity and switching on and off with two pulses on different cavities.

The dynamic response of the coupled cavities system is found by solving the seven differential equations describing the fields inside the cavities (Eq.(7.20) to Eq.(7.25) coupled with the two Debye relaxation equations governing the evolution of the indices of refraction of the nonlinear media and thus governing the cavity detunings (Eq.(7.27) and Eq.(7.28)). Each of the seven equations governing the electric fields were split into two equations, one for the real part and one for the imaginary part of each field. These fourteen differential equations were then solved numerically, together with the two material equations. Two numerical methods were used: the adaptive stepsize control for the Runge-Kutta method and the Bulirsch-Stoer method. The two different approaches were used in order to check the integrity of the two methods and to ensure that the results obtained with each technique agreed with each other.

As an additional check of the validity of the results, the reflectivity of the mirrors of each cavity were made to be zero, in turn. The system was then subjected to different inputs (step, pulse and triangular) of different magnitude, and the response was recorded. The results show that when the reflectivity of the mirrors of either one of the two cavities were set to zero, the response of the system is identical to that of a single cavity.

7.5.1 Positive Pulse Switching by Control Pulses Incident on Different Cavities

To demonstrate positive pulse switching in the dynamic regime, a system of two coupled cavities containing fast media is used. With fast media, the computation time is reduced. In addition, the inter-cavity spacing d_2 is made to be small. This reduces the time taken for the information of one cavity to propagate to the other,

which further reduces the computation time. In short, the cavity media are assumed to respond quasi-instantly and the response of one cavity is immediately felt by the other one.

In order to verify the prediction that the output of the system can be turned on and off by positive pulses sent into different cavities, the cavity parameters were chosen according to the criteria described in section 6.2.2 for the steady state regime. In the steady state regime (Fig.6.8) it was found that in order to turn the system on and off with pulses incident on cavity 1 and 3 respectively, cavity 1 should be bistable and cavity 3 needs to have a region in which the reflectivity decreases upon increasing its incident intensity. Cavity 3 should then be biased near its region of negative slope. This way, one can reduce the amount of radiation feedback to cavity 1 by increasing the incident radiation on cavity 3 and consequently switching the output off. The system can then be turned back on with a pulse incident on cavity 1.

The steady-state characteristics of the individual, uncoupled cavities are shown in Fig.7.9. These curves are guidelines helping in the understanding of the switching process. It must be stressed that the response of each individual cavity in the coupled system can be quite different from the individual, uncoupled response. To avoid possible misinterpretations, the intensity axis is not labeled in Fig.7.9 since these labels would not correspond to the intensity values given in the description of the switching of the coupled system.

Fig.7.9 (b) shows that cavity 3 is not bistable and is tuned very close to resonance ($\phi_0 = 0.1\pi$). The reflectivity of cavity 3 is thus very low (less than 0.05 as seen in Fig.7.9(d)). During operation, cavity 1 is biased within its bistable region near the down-switching point (I_B in Fig.7.9(a)).

The dynamic response of the coupled system is shown in Fig.7.10 and Fig.7.11. Fig.7.10 shows the change in round-trip phases in the cavities as the system is being turned on by a pulse I_{i_1} and turned off by a pulse I_{i_2}. In the figure, the labels $\Delta\phi_1$ and $\Delta\phi_2$ are used to distinguish between ϕ_1 and ϕ_2. $\Delta\phi_j = \phi_j - \phi_{0j}$ where $j = 1, 2$. These are the actual changes in the round-trip phase in each the cavity. The round-

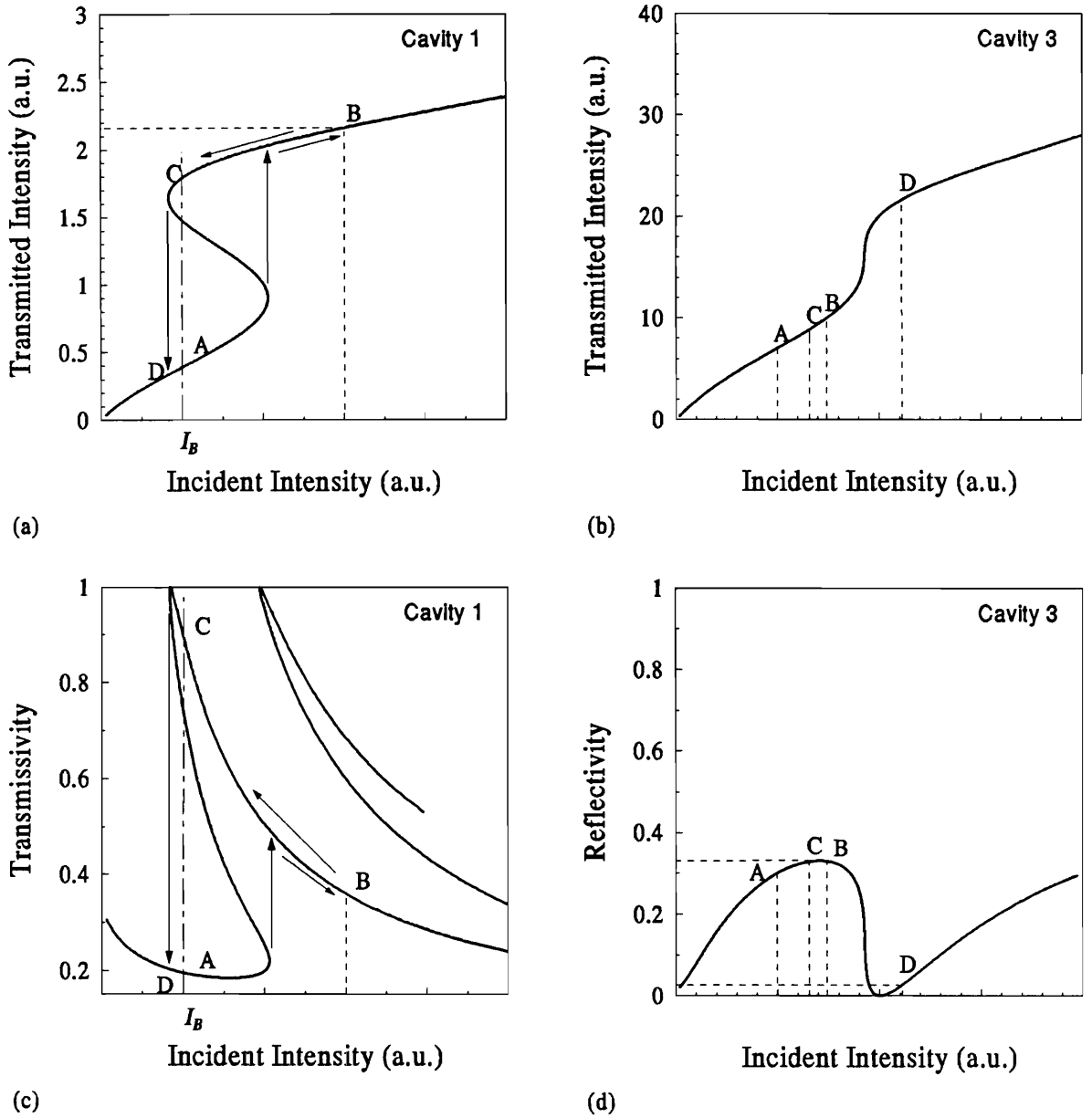

Figure 7.9: Individual, uncoupled response curves of the two cavities used in the coupled system. (a),(c) : transmitted intensity against incident intensity for cavity 1 and 3. (b),(d) : transmissivity and reflectivity of cavity 1 and 2 respectively. The parameters for the cavities are, for cavity 1 : $R = 0.4$, $n_0 = 1.5$, $n_2 = 10^{-3}$, $\phi_0 = 0.48\pi$; for cavity 3 : $R = 0.4$, $n_0 = 1.5$, $n_2 = 2 \times 10^{-4}$, $\phi_0 = 0.1\pi$.

trip phase change is the most fundamental parameter describing the state of a cavity. It is proportional to the change in refractive index of the cavity.

There are two inputs to the system, I_{i_1} and I_{i_2}. I_{i_1} is biased with a constant beam of 2 units and I_{i_2} is unbiased. The turn on pulse I_{i_1} starts at $40\tau_1$ and has an amplitude of 4 units. The turn off pulse I_{i_2} starts at $250\tau_1$ and has a magnitude of 6 units. The changes in round-trip phase in cavity 1 and 3 are shown as $\Delta\phi_1$ and $\Delta\phi_3$. The response is separated in five regions labeled A to D. These labels are matched with the corresponding labels in Fig.7.9.

The change in round-trip phases in cavity 1 and 3 is shown in Fig.7.10. At point A in Fig.7.9(b) and (d), cavity 1 is in a low transmission state and cavity 3 is in a high reflection state. When the input I_{i_1} is increased to a value of 6 units in region B (Fig.7.10), the round-trip phase of cavity 1 and the intensity transmitted by that cavity increases drastically. The system switches on. Cavity 3 is affected by this increase of the intensity transmitted by cavity 1 and shows an increase in its round-trip phase. When the input I_{i_1} is reduced to the value of the bias in region C, cavity 1 stays in a high state. Its round-trip phase remains high. It should be noted that although $\Delta\phi_3$ and $\Delta\phi_1$ show similar dynamics in region A and B, cavity 3 has not switched. The change in round-trip phase in cavity 3 is an induced effect due to the increase in the intensity transmitted by cavity 1.

At $t = 250\tau_1$, the input I_{i_2} rises from zero to an intensity of 6 units. This increase in intensity decreases the reflectivity of cavity 3 (Fig.7.9(d) region D) thus reducing the feedback on cavity 1. This leads to an immediate decrease of the round-trip phase of cavity 1. While the input I_{i_2} increases to a value of 6 units in region D, cavity 1 has already switched to a low transmission state (point D in Fig.7.9(b)). Although the feedback is restored when the pulse I_{i_2} is removed, in region A, after $t = 330\tau_1$, cavity 1 does not return to a high transmission state but instead stays in a low transmission state. In this scheme, I_{i_2} serves as a control pulse to turn cavity 1 off.

In this example, it is shown that the state of cavity 1 can be controlled by two input pulses I_{i_1} and I_{i_2}. The output can be taken from either the right propagating field I_3

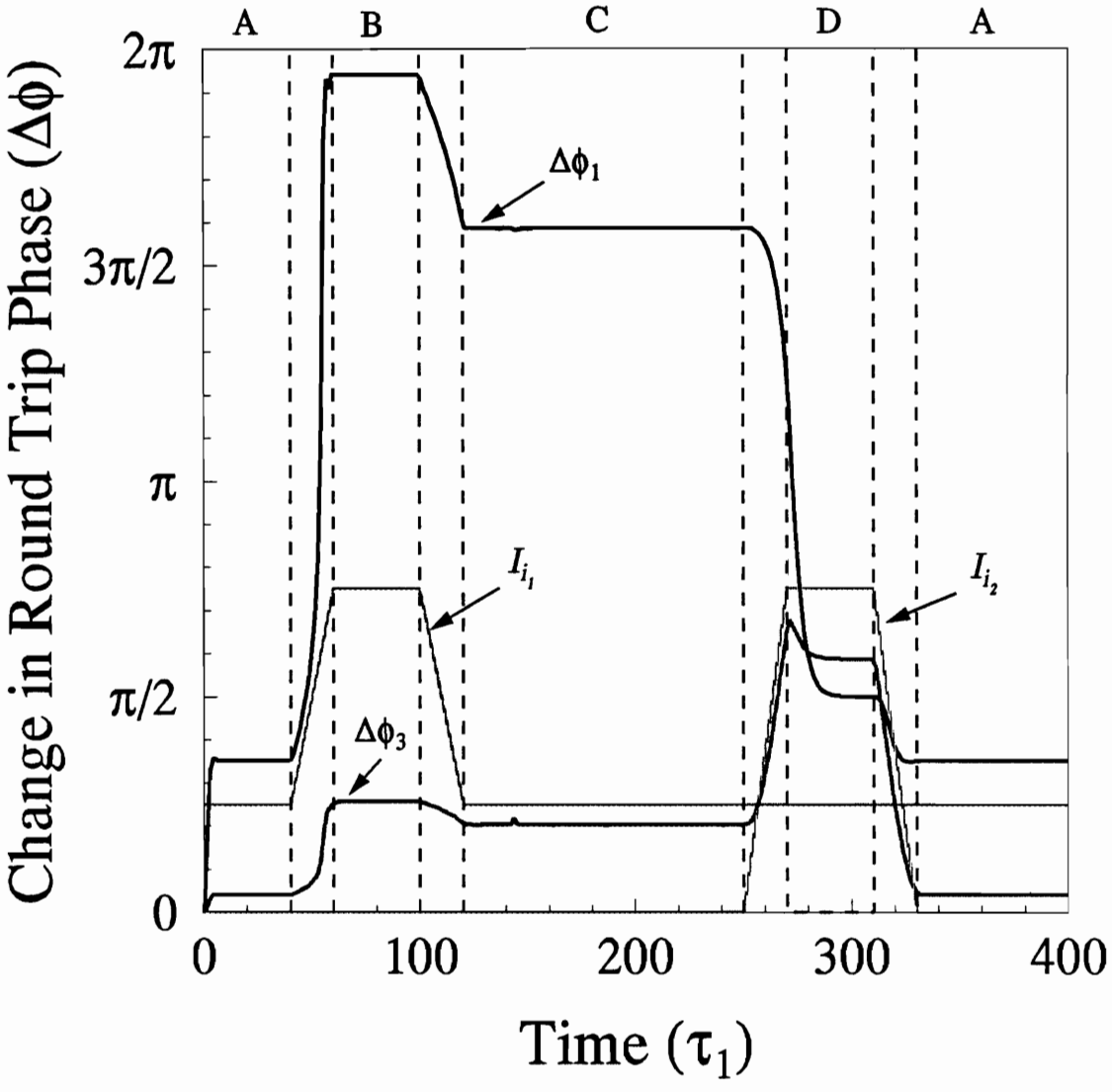

Figure 7.10: $\Delta\phi_1 = \phi_1 - \phi_{01}$, $\Delta\phi_3 = \phi_3 - \phi_{03}$ are the changes in round-trip phase in cavity 1 and 3. A pulse I_{i_1} of 4 units incident on cavity 1 is used to turn the system on. A pulse I_{i_2} of 6 units incident on cavity 3 is used to turn the system off. Cavity 1 is biased with a constant intensity of 2 units and cavity 3 is unbiased.

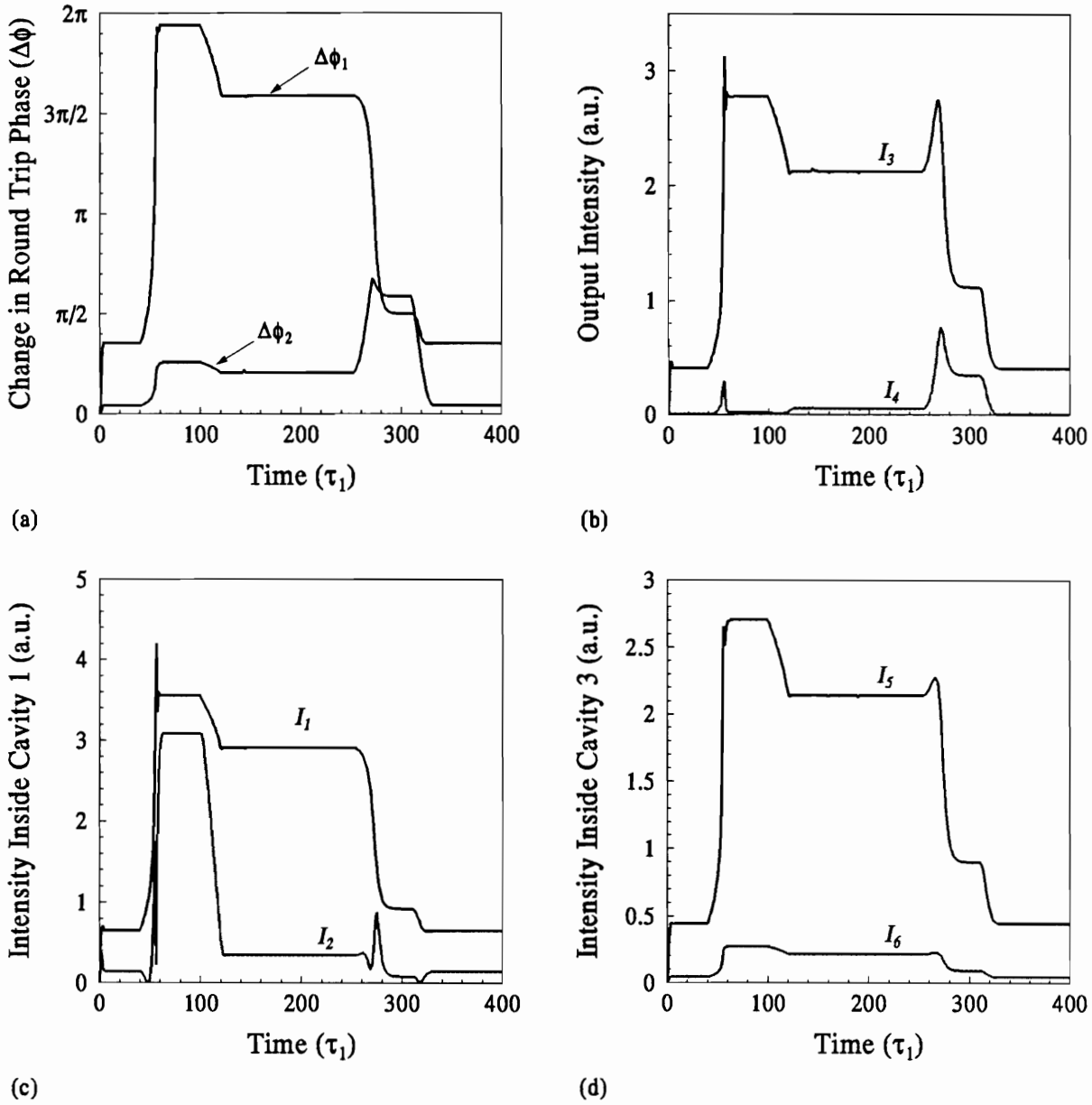

Figure 7.11: Positive pulse switching by pulses incident on different cavities. The dynamic response of (a) the change in round-trip phases in cavity 1 and 3, (b) the output intensities I_3 and I_4, (c) the intensities of the left and right propagating fields in cavity 1 and (d) the intensities in cavity 3.

or the left propagating field I_4(see Fig.7.8). The dynamic response of the outputs I_3 and I_4 is shown in Fig.7.11(b). Although the intensities of the right propagating and the left propagating fields differ by a large amount, it can be seen that both outputs can be turned on and off by positive input pulses. The individual intensities in each cavity are shown in Fig.7.11(c) and (d).

7.5.2 Positive Pulse Switching by Control Pulses of Different Magnitude on One Cavity

In the steady-state model of the coupled cavities system, it was shown that the output of the system could be switched on and off by control pulses of different magnitude incident on cavity 3. This prediction can also be verified numerically in the dynamic regime.

The steady state solution for this mode of operation is shown in Fig.6.6. An important attribute of this configuration is that cavity 3 must be bistable and must be tuned very close to a resonance so that the reflectivity increases rapidly for very small intensities. The characteristic steady-state response curves for the individual cavities, uncoupled are shown in Fig.7.12.

Both cavities are made with mirrors having the same reflectivity, $R = 0.4$ and filled with the same nonlinear medium, $n_0 = 1.5$; $n_2 = 10^{-3}$, but the detuning of the cavities are different. The detuning of cavity 1 is 0.48π and that of cavity 3 is 0.04π.

The dynamics of the change in round-trip phase is shown in Fig.7.13. Cavity 1 is biased within its bistable region by a constant intensity of 0.56 unit and cavity 3 is unbiased (point A in Fig.7.12). A pulse of magnitude 0.8 units enters cavity 3 at time $t = 40\tau_1$, increases the reflectivity of cavity 3 and immediately increases the feedback to cavity 1. The switch up point of cavity 1 shifts to a lower value and the output is switched on. Due to critical slowing down, the cavity does not switch during the rise time of the control beam (from $40\tau_1$ to $60\tau_1$), but with a delay. Cavity 1 switches completely at $t = 80\tau_1$ (point B in Fig.7.12). It is worth mentioning that cavity 3 has

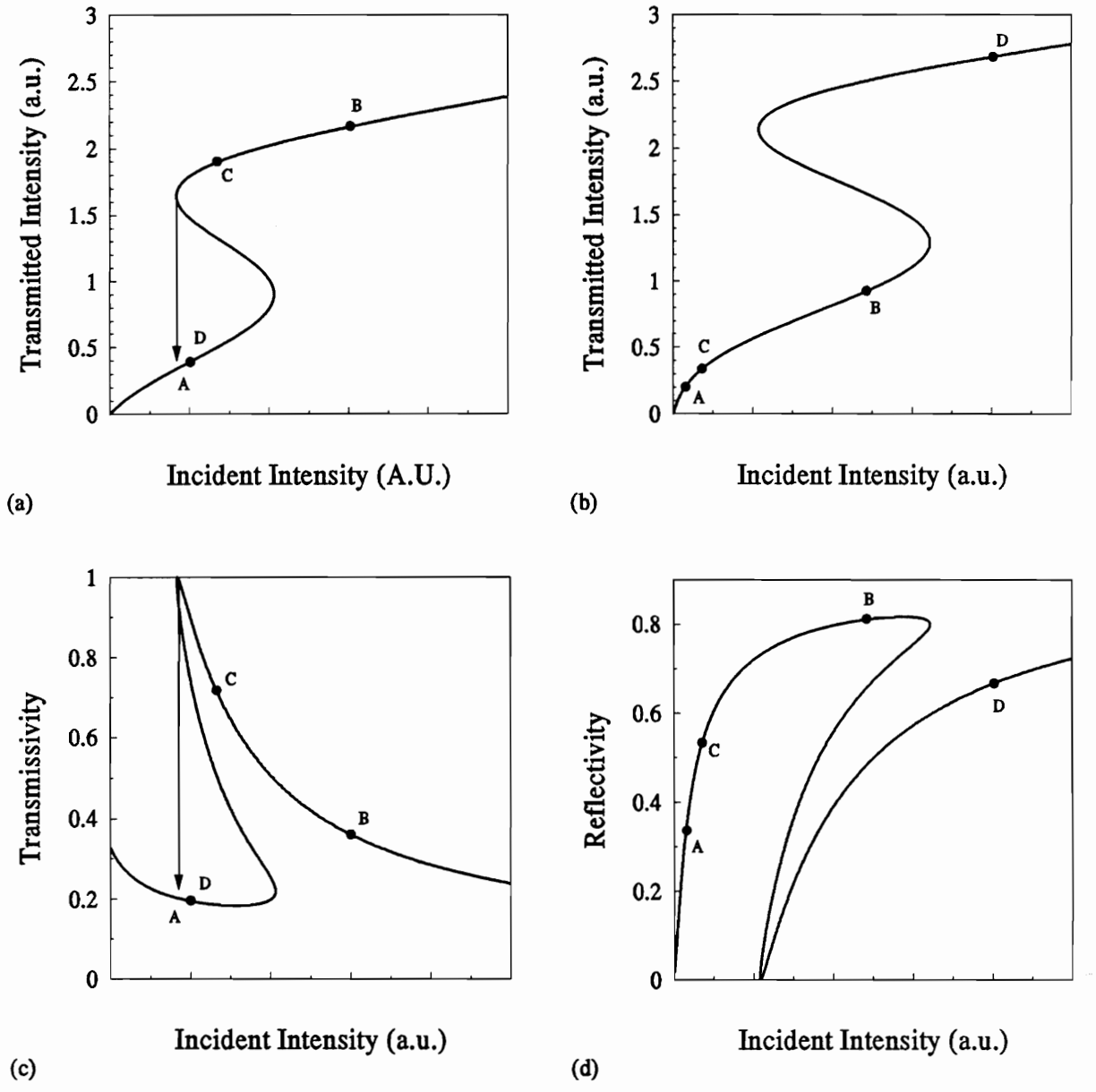

Figure 7.12: Characteristic steady-state response curves for the two individual, uncoupled cavities used in the coupled cavities system. (a),(c) : transmitted intensity versus incident intensity for cavity 1, and 3. (b),(d) : transmissivity and reflectivity of cavity 1 and 3, respectively. The parameters for the cavities are, for cavity 1 : $R = 0.4$, $n_0 = 1.5$, $n_2 = 10^{-3}$, $\phi_0 = 0.48\pi$; for cavity 3 : $R = 0.4$, $n_0 = 1.5$, $n_2 = 10^{-3}$, $\phi_0 = 0.04\pi$.

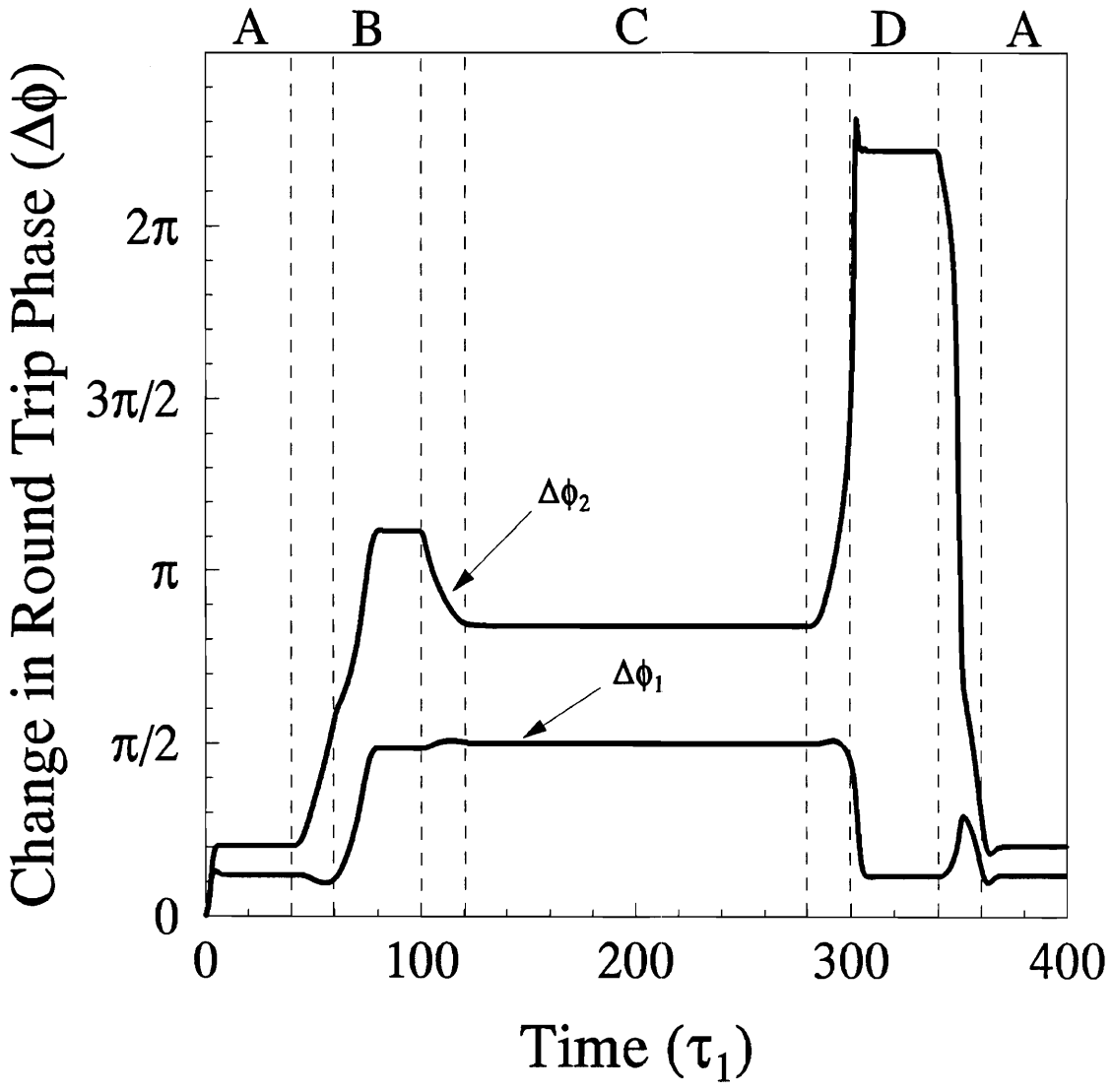

Figure 7.13: Cavity 1 can be turned on and off by pulses of different magnitude incident on cavity 3. Initially, cavity 1 is biased with an intensity of 0.56 unit. A pulse of magnitude 0.8 unit turns the cavity on and a pulse of magnitude 1.6 units turns the cavity off.

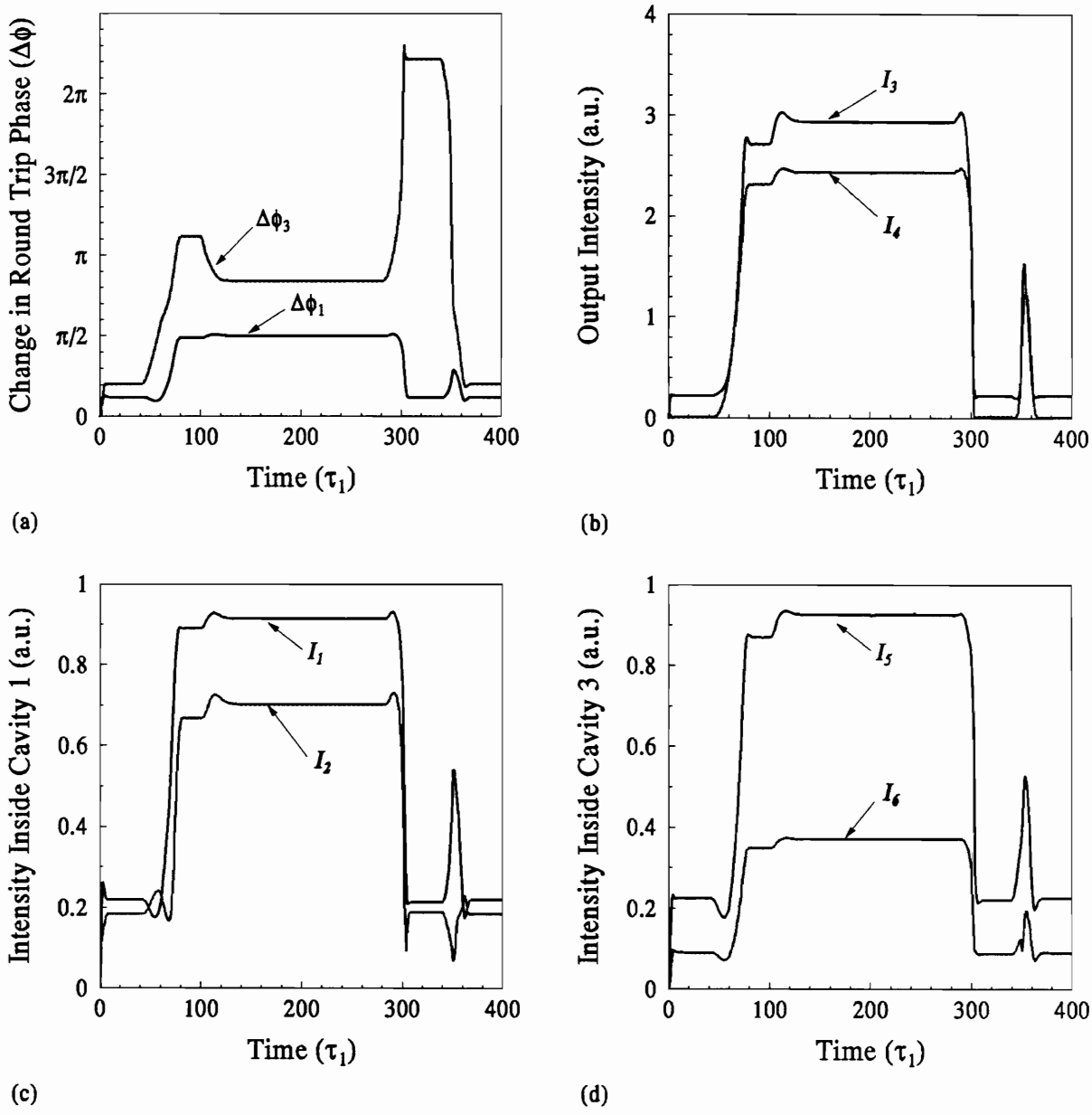

Figure 7.14: Positive pulse switching with pulses of different magnitudes incident on one cavity. The dynamic response of (a) the change in round-trip phases in cavity 1 and 3, (b) the output intensities I_3 and I_4, (c) the intensities of the left and right propagating fields in cavity 1 and (d) the intensities in cavity 3.

not yet switched (point C in Fig.7.12(b) and (d)) although its reflectivity increases because of the higher bias.

At $t = 280\tau_1$, a pulse of magnitude 1.6 units switches cavity 3, causing the reflectivity of cavity 3 to drop to a low value, thus decreasing the feedback to cavity 1. This decrease in the feedback causes cavity 1 to switch off. Since cavity 3 is not biased, it switches off and goes back to its original state when the control pulse is removed. The two outputs and the intensities in cavity 1 and 3 are plotted in Fig.7.14(b)-(d). The outputs I_3 and I_4 is seen to be turned on and off, respectively, by pulses of different magnitudes incident on cavity 3

As mentioned in chapter 6, the switching scheme using pulses incident on the same cavity requires an accurately maintained bias. This drawback is illustrated in Fig.7.15. In Fig.7.15(a), cavity 1 is biased at an intensity of 0.8 units, which is too far off from the down-switching intensity of cavity 1. This makes it impossible to switch the cavity off by a decrease of the feedback from cavity 3. In Fig.7.15(b); the bias is too low. With a bias outside the bistable region, switching on is impossible.

We have verified numerically that a system of two coupled nonlinear Fabry-Perot cavities can be switched with positive pulses in the dynamic regime. Devices based on such concepts could thus be used to implement optical switches that are compatible with present digital circuitry; namely, devices that use monopolar pulses.

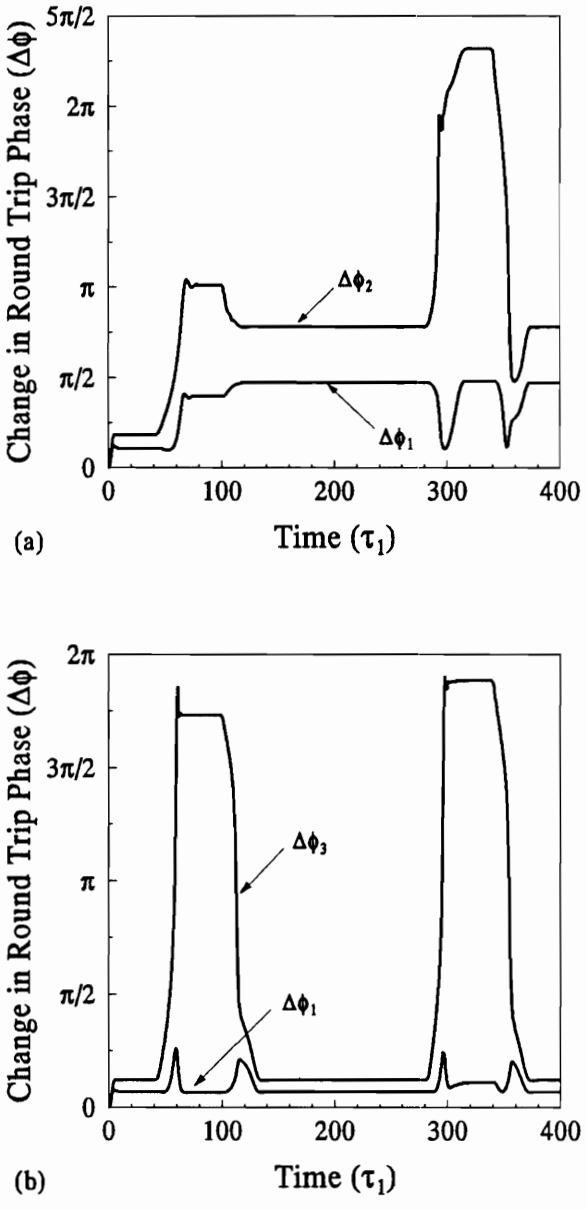

Figure 7.15: Turning the output on and off with positive pulses on the same cavity requires accurate bias. (a) Cavity 1 is biased too far within the bistable region (at an intensity of 0.8 unit). This causes cavity 1 to be locked in a high transmission state. (b) Cavity 1 is biased before its bistable region (biasing level 0.2 units), locking it in a low state.

Chapter 8

Conclusion

The search for an optical latch based on a system of coupled nonlinear Fabry-Perots and compatible with digital circuits was successful. The Nonlinear Fabry-Perot has been a valuable candidate for an optical switch for a long time but in order to be compatible with digital circuit, it must be switched on and off with positive pulses. Conventional Fabry-Perots need a "negative pulse" to be switched off. Korpel and Lohmann had proposed to use the two eigen-polarization states in a nonlinear birefringent Fabry-Perot as an additional design parameter to implement optical switches that can be switched on and off with positive pulses. We studied this proposal in details and showed that it could not work as proposed by the authors. What had been overlooked is that the device could be switched on and off once but then will be locked in a state from which it can only be dislodged by a "negative" pulse. Although a single nonlinear birefringent cavity was shown not to be the solution for positive-pulse switching, we were nevertheless able to utilize the coupling between the orthogonal polarization states to demonstrate experimentally other types of optical switches.

Having disproved the Korpel and Lohmann's scheme, we turned to the study of a system of coupled cavities as a possible means of achieving positive-pulse switching. We chose a simple coupling configuration in which one cavity serves as an optically

bistable element and the other serves as a variable feedback mirror which controls the bistable cavity. This configuration differs from an electronic latch in the sense that it is not symmetrical.

A steady-state model was developed and we showed that positive-pulse switching of this coupled device is feasible in the steady-state regime. We then looked in more details at the possible modes of operations of the device and demonstrated two different schemes of switching. In the first scheme, the output is turned on and off by pulses of different magnitudes incident on the control cavity. This scheme suffers from the disadvantage of needing a narrow biasing range. In the second scheme, the output is turned on by a pulse incident on the bistable cavity and it can be turned off by a pulse of the same magnitude incident on the control cavity. This scheme afford a more relaxed biasing requirement.

Both switching schemes have their own advantages and disadvantages, but they are both compatible with digital switching circuitry, namely, they can be switched on and off with positive pulses.

Having proven the feasibility of the coupled cavities in the steady-state regime, it became crucial to show that positive-pulse switching was also achievable in the dynamic regime. To this end, we extended the dynamic model of Goldstone and Garmire for a single cavity and one input, to the case of a system of two coupled cavities and two inputs. The possibility of positive-pulse switching was tested using the dynamic model. The parameters used in the numerical simulation were chosen according to the criteria found in the steady-state case. The result confirmed the predictions of the steady-state analysis with remarkable accuracy. Both switching modes demonstrated in the steady-state regime were found to exist in the dynamic model, also.

8.1 Future Work

Although the steady-state prediction of positive-pulse switching was verified in the dynamic case, it is by no means the only use one could make of the model. Many interesting phenomena occur in a nonlinear cavity in the dynamic regime. For example, bifurcations and chaos have been shown to occur in a nonlinear Fabry-Perot. These phenomena will surely occur also in a coupled cavities system, but the coupling of the cavities may reveal some different or unexpected features in the dynamics.

Another area that definitely needs to be further investigated is the transverse dynamics of the switching. Our model is a plane-wave model. Introducing a transverse gradient term in the field equations changes the temporal problem to a spatio-temporal one and increases the computational effort required by many orders of magnitudes.

As far as practical devices are concerned, the need to search for more efficient ways of switching still exists. It may be possible to find a switching scheme in the dynamic regime which is not predicted by the steady-state model.

Numerical simulations are helpful for predicting the behavior of a system of coupled nonlinear Fabry-Perots in a variety of cases but certainly, actual experiments are necessary to verify these predictions.

Appendix A

Derivation of the dynamics of a coupled cavities system

Let us consider a coupled cavities system which consists of two nonlinear dielectric Fabry-Perot cavities as shown in Fig.A.1. Cavity 1 and cavity 3 are nonlinear cavities while the space between the nonlinear cavities forms a linear Fabry-Perot. The intracavity spacing are given by d_1, d_2 and d_3 respectively (see Fig.A.1). The reflection coefficients and transmission coefficients of the mirrors are given by r_i and t_i ($i = 1$ to 4) respectively for mirrors M1 to M4.

There are two inputs to the system, $\mathcal{E}_{i1}(t)$ and $\mathcal{E}_{i2}(t)$. $\mathcal{E}_{i1}(t)$ and $\mathcal{E}_{i2}(t)$ are orthogonally polarized. A polarizer P is used to isolate cavity 1 from $\mathcal{E}_{i2}(t)$. Thus, the analysis can be split into two parts, one concerning the input $\mathcal{E}_{i1}(t)$ and the other concerning the input $\mathcal{E}_{i2}(t)$. In this appendix, the equations governing the evolution of the fields for the case of one input is derived.

The dynamics of the fields inside the cavities can be derived from a set of difference equations. First, let us look at the electric fields inside cavity 3. At time t, the forward propagating field inside cavity 3, $\mathcal{E}_5$, is the sum of the forward propagating field at time $t - \tau_3$ and the transmitted incident field at $t - \Delta t_B^z$ where τ_3 is the actual round-

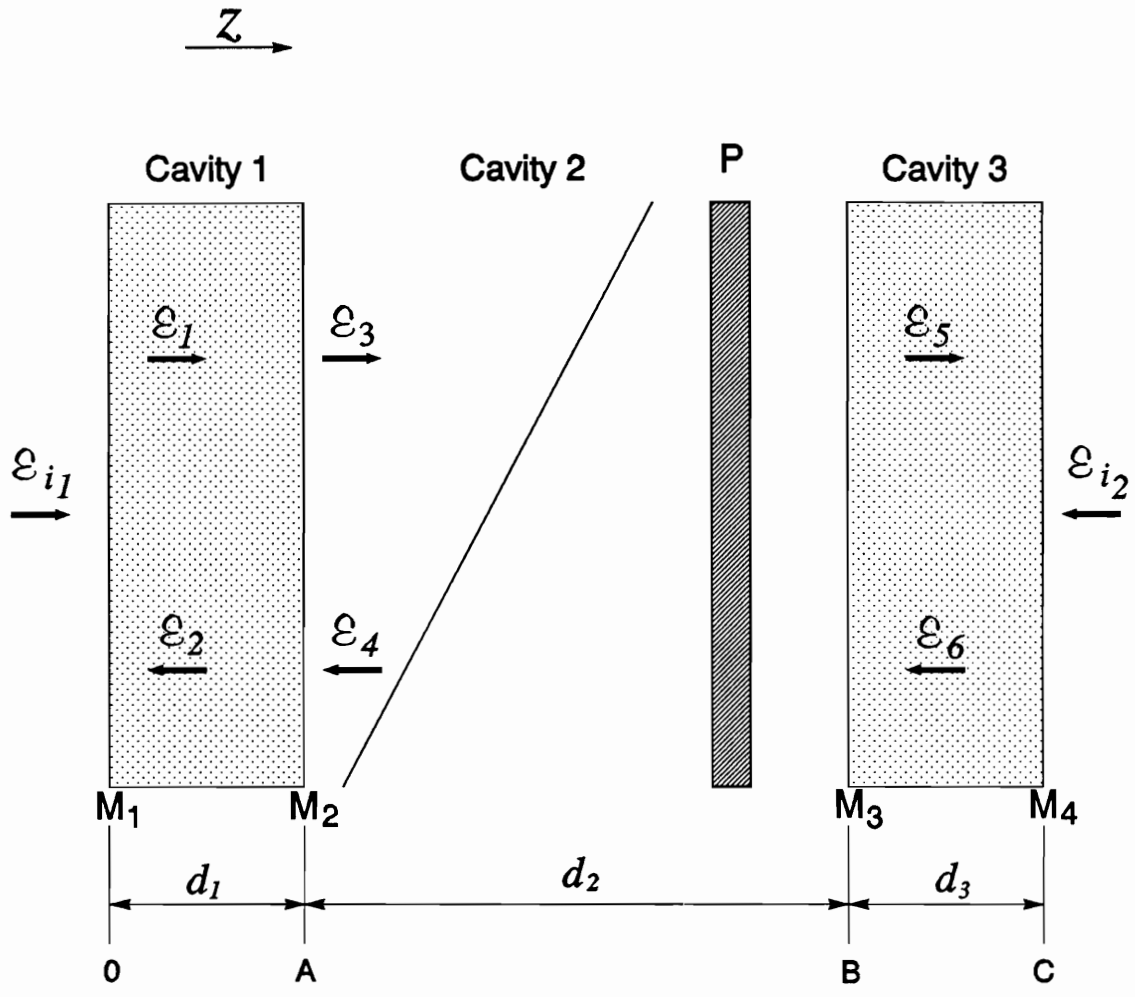

Figure A.1: Schematic configuration of two coupled nonlinear Fabry-Perot cavities. Cavity 1 and cavity 3 are nonlinear Fabry-Perots. The space between these mirrors with reflection coefficients r_1, r_2, r_3 and r_4 respectively. The input $\mathcal{E}_{i1}$ and $\mathcal{E}_{i2}$ are orthogonally polarized. The polarizer P transmits $\mathcal{E}_{i1}$ and blocks $\mathcal{E}_{i2}$. It is used to isolate cavity 1 from the input $\mathcal{E}_{i2}$. The intra-cavity spacings are d_1, d_2 and d_3. $\mathcal{E}_1$ to $\mathcal{E}_6$ are the fields inside the cavities.

trip time of cavity 3 starting at t and Δt_B^z is the time for the incident field $\mathcal{E}_{i1}(t)$ to propagate from $z = B$ to z:

$$\mathcal{E}_5(z,t) = r_3 r_4 \mathcal{E}_5(z, t-\tau_3) + i t_3 \mathcal{E}_3(B, t - \Delta t_B^z) \,, \tag{A.1}$$

where r_3, r_4 are the transmission coefficients of mirrors M_3 and M_4. The first term on the right hand side is the field $\mathcal{E}_5$ a round-trip time ago. This field is reflected by mirrors M_3 and M_4. The second term is the right going field in cavity 2 and incident on cavity 3, evaluated at some time $t - \Delta t_B^z$ ago. Shifting the origin of time by τ_3 in the above equations, we have

$$\mathcal{E}_5(z, t+\tau_3) = r_3 r_4 \mathcal{E}_5(z,t) + i t_3 \mathcal{E}_3(B, t - \Delta t_z^C + \Delta t_C^B) \,. \tag{A.2}$$

We have used the same notation as in chapter 7 with the following definitions:

$$\begin{aligned}
\Delta t_{z_1}^{z_2} &= \text{actual transit time from } z_1 \text{ to } z_2, \\
\tau_j &= \text{actual round-trip time starting at } t \text{ for cavity } j, \\
\tau_j' &= \text{round-trip time with cavity parameters fixed at their values at } t.
\end{aligned}$$

Splitting the complex electric field $\mathcal{E}_5$ into its amplitude and phase factors, we have:

$$\begin{aligned}
& E_5(z, t+\tau_3) \exp\{ i[\phi_1(t+\tau_3)/2 + \phi_2(t+\tau_3)/2 \\
& + k_5(z, t+\tau_3)(z-B) - \omega(t+\tau_3)]\} \\
= \; & r_3 r_4 E_5(z,t) \exp\{ i[\phi_1(t)/2 + \phi_2(t)/2 + k_5(z,t)(z-B) - \omega t]\} \\
& + i t_3 E_3(B, t + \Delta t_z^C + \Delta t_C^B) \exp\Big\{ i[\phi_1(t + \Delta t_z^C + \Delta t_C^B)/2 \\
& + \phi_2(t + \Delta t_z^C + \Delta t_C^B)/2 - \omega[t + \Delta t_z^C + \Delta t_C^B]]\Big\} \,.
\end{aligned} \tag{A.3}$$

Cancelling the ωt term in the above expression, rearranging and writing the difference of the wave vector k_5 at two different times as a differential:

$$k_5(z,t)(z-B) - k_5(z, t+\tau_3)(z-B) = \tau_3 \frac{\partial k_5(t)}{\partial t}(z-B), \tag{A.4}$$

we find:

$$
\begin{aligned}
& E_5(z,t+\tau_3) \\
= \; & r_3 r_4 E_5(z,t)\exp\{i[\phi_1(t)/2-\phi_1(t+\tau_3)/2+\phi_2(t)/2-\phi_2(t+\tau_3)/2 \\
& -\tau_3(z-B)\frac{\partial k_5(t)}{\partial t}+\omega\tau_3]\} \\
& +it_3E_3(B,t+\Delta t_z^C+\Delta t_C^B)\exp\Big\{i[\phi_1(t+\Delta t_z^C+\Delta t_C^B)/2-\phi_2(t+\tau_3)/2 \\
& +\omega[\tau_3-\Delta t_z^C-\Delta t_C^B]-k_5(z,t+\tau_3)(z-B)-\phi_2(t+\tau_3)/2 \\
& +\phi_2(t+\Delta t_z^C+\Delta t_C^B)/2]\Big\}\ . \qquad \text{(A.5)}
\end{aligned}
$$

Writing the difference in ϕ's in differential form and evaluating the fields at $z=C$, $\Delta_z^C=0$, we find

$$
\begin{aligned}
& E_5(C,t+\tau_3) \\
= \; & r_3 r_4 E_5(C,t)\exp\left\{i[-\frac{\tau_3}{2}\frac{\partial\phi_1(t)}{\partial t}-\frac{\tau_3}{2}\frac{\partial\phi_2(t)}{\partial t}-\tau_3 d_3\frac{\partial k_5(t)}{\partial t}+\omega\tau_3]\right\} \\
& +it_3E_3(B,t+\frac{\tau_3}{2})\exp\left\{i[\phi_1(t+\frac{\tau_3}{2})/2-\phi_1(t+\tau_3)/2\right. \\
& \left.+\phi_2(t+\frac{\tau_3}{2})/2-\phi_2(t+\tau_3)/2-k_5(C,t+\tau_3)d_3+\omega\frac{\tau_3}{2}]\right\}\ . \qquad \text{(A.6)}
\end{aligned}
$$

Since cavity 2 is linear, $\phi_2(t)=\phi_2$. Using the same approximation as described in section 7.1 i.e.:

$$\tau \simeq \overline{\tau'}+\frac{\tau'}{2}\frac{\partial\overline{\tau'}}{\partial t} \qquad \text{(A.7)}$$

$$\omega\tau \simeq \overline{\phi}+\frac{\tau'}{2}\frac{\partial\overline{\phi}}{\partial t} \qquad \text{(A.8)}$$

$$\tau\frac{\partial k}{\partial t}d \simeq \frac{\tau'}{2}\frac{\partial\overline{\phi}}{\partial t}\ , \qquad \text{(A.9)}$$

where d_j is the cavity spacing, the argument of the first exponential function in Eq.(A.6) can be simplified as follow:

$$
\begin{aligned}
& -\frac{\tau_3}{2}\frac{\partial\phi_1(t)}{\partial t}-\frac{\tau_3}{2}\frac{\partial\phi_2(t)}{\partial t}-\tau_3 d_3\frac{\partial k_5(t)}{\partial t}+\omega\tau_3 \\
= \; & -\frac{\tau_3}{2}\frac{\partial\overline{\phi_1}(t)}{\partial t}-\frac{\tau_3'}{2}\frac{\partial\overline{\phi_3}(t)}{\partial t}+\frac{\tau_3'}{2}\frac{\partial\overline{\phi_3}(t)}{\partial t}+\overline{\phi_3} \\
= \; & \overline{\phi_3}(t)-\frac{\tau_3}{2}\frac{\partial\overline{\phi_1}(t)}{\partial t}\ . \qquad \text{(A.10)}
\end{aligned}
$$

APPENDIX A.

The argument of the second exponential function in Eq.(A.6) can be expressed as

$$\begin{aligned}
& \phi_1(t+\frac{\tau_3}{2})/2 - \phi_1(t+\tau_3)/2 + \phi_2(t+\frac{\tau_3}{2})/2 - \phi_2(t+\tau_3)/2 - k_5(C,t+\tau_3)d_3 \\
& +\omega\tau_3/2 \\
= & -\frac{\tau_3}{4}\frac{\partial\phi_1(t)}{\partial t} - k_5(C,t)d_3 - \tau_3\frac{\partial k_5(C,t)}{\partial t}d_3 + \phi_3/2 \\
= & -\frac{\tau_3}{4}\frac{\partial\overline{\phi_1}(t)}{\partial t} - \phi_3/2 - \tau_3 d_3\frac{\partial k_5(C,t)}{\partial t} + \phi_3/2 \\
= & -\frac{\tau_3}{4}\left\{\frac{\partial\overline{\phi_1}(t)}{\partial t} + 2\frac{\partial\overline{\phi_3}(t)}{\partial t}\right\} . \qquad \text{(A.11)}
\end{aligned}$$

Therefore, the equation for E_5 can finally be written as

$$\begin{aligned}
& \tau_3\frac{\partial E_5(t)}{\partial t} + \left\{1 - r_3 r_4 \exp i[\overline{\phi_3}(t) - \frac{\tau_3}{2}\frac{\partial\overline{\phi_1}(t)}{\partial t}]\right\} E_5(C,t) \\
= & \; it_3 E_3(B,t+\tau_3/2)\exp\left\{-i\frac{\tau_3}{4}[\frac{\partial\overline{\phi_1}(t)}{\partial t} + 2\frac{\partial\overline{\phi_3}(t)}{\partial t}]\right\} . \qquad \text{(A.12)}
\end{aligned}$$

For the backward propagating field E_6 in cavity 3 we have:

$$\begin{aligned}
\mathcal{E}_6(z,t) &= r_3 r_4 \mathcal{E}_6(z,t-\tau_3) + it_3 r_4 \mathcal{E}_3(B,t-\Delta t_z^C + \Delta t_C^B) \\
\mathcal{E}_6(z,t+\tau_3) &= r_3 r_4 \mathcal{E}_6(z,t) + it_3 r_4 \mathcal{E}_3(B,t-\Delta t_z^B) , \qquad \text{(A.13)}
\end{aligned}$$

or, after separating amplitude and phase factors

$$\begin{aligned}
& E_6(z,t_+\tau_3)\exp\{i[\phi_1(t+\tau_3)/2 + \phi_2(t+\tau_3)/2 + k_6(z,t+\tau_3)(z-B) \\
& -\omega(t+\tau_3)]\} \\
= & \; r_3 r_4 E_6(z,t)\exp\{i[\phi_1(t)/2 + \phi_2(t)/2 + k_6(z,t)(z-B) - \omega t]\} \\
& +it_3 r_4 E_3(B,t+\Delta t_z^B)\exp\left\{i[\phi_1(t+\Delta t_z^B)/2 + \phi_2(t+\Delta t_z^B)/2\right. \\
& \left.-\omega(t+\Delta t_z^B)]\right\} . \qquad \text{(A.14)}
\end{aligned}$$

Evaluating the field at $z = B$, $\Delta t_z^B = 0$, and writing the differences as differentials, we have

$$\begin{aligned}
& E_6(B,t+\tau_3) \\
= & \; r_3 r_4 E_6 \exp\left\{i[-\frac{\tau_3}{2}\frac{\partial\overline{\phi_1}(t)}{\partial t} + \phi_3(t)]\right\} \\
& +it_3 r_4 E_3(B,t+\Delta t_z^B)\exp\left\{i[-\frac{\tau_3}{2}\frac{\partial\overline{\phi_1}(t)}{\partial t} + \phi_3(t)]\right\} . \qquad \text{(A.15)}
\end{aligned}$$

APPENDIX A.

Writing $\phi_3(t) = \overline{\phi_3} + \frac{\tau_3}{2}\frac{\partial\overline{\phi_3}}{\partial t}$ as before, we have

$$\tau_3\frac{\partial E_6(B,t)}{\partial t} + \left\{1 - r_3r_4\exp\left\{i[-\overline{\phi_3} - \frac{\tau_3}{2}\left(\frac{\partial\overline{\phi_1}(t)}{\partial t} - \frac{\partial\overline{\phi_3}(t)}{\partial t}\right)]\right\}\right\} E_6(B,t)$$
$$= it_3r_4E_3(B,t)\exp\left\{i[-\frac{\tau_3}{2}\left(\frac{\partial\overline{\phi_1}(t)}{\partial t} - \frac{\partial\overline{\phi_3}(t)}{\partial t}\right) + \overline{\phi_3}(t)]\right\} E_6(B,t)\ . \qquad \text{(A.16)}$$

Assuming that the change of input intensity during a round-trip time is small, $\frac{\partial\phi_1}{\partial t} \simeq \frac{\partial\phi_3}{\partial t} \simeq 0$. Outside the exponent, the difference between τ's, τ''s and the linear round-trip time $\overline{\tau}$'s can then be ignored. Eq.(A.12) and Eq.(A.16) can then be simplified as

$$\begin{aligned}\overline{\tau_3}\frac{\partial E_5(C,t)}{\partial t} + \{1 - r_3r_4e^{i\overline{\phi_3}(t)}\}E_5(C,t) \\ = it_3E_3(B,t+\overline{\tau_3}/2) \\ = it_3\left\{E_3(B,t) + \frac{\overline{\tau_3}}{2}\frac{\partial E_3(B,t)}{\partial t}\right\}\ ,\end{aligned} \qquad \text{(A.17)}$$

$$\overline{\tau_3}\frac{\partial E_6(B,t)}{\partial t} + \{1 - r_3r_4e^{i\overline{\phi_3}(t)}\}E_6(B,t) = it_3r_4E_3(B,t)e^{i\overline{\phi_3}(t)}\ . \qquad \text{(A.18)}$$

The same procedure is repeated for cavity 2 to give:

$$\begin{aligned}\mathcal{E}_3(z,t) &= r_2r_3\mathcal{E}_3(z,t-\tau_2) + it_3r_2\mathcal{E}_6(B,t-\Delta t_B^A - \Delta t_A^z) \\ &\quad + it_2\mathcal{E}_1(A,t-\Delta t_A^z)\end{aligned} \qquad \text{(A.19)}$$

Cancelling ωt from each phase term, the amplitude of $\mathcal{E}_3$ is found to be

$$\begin{aligned}&E_3(z,t+\tau_2) \\ &= r_2r_3E_3(z,t)\exp\left\{i[-\tau_2\frac{\partial k_3(z,t)}{\partial t}(z-A) + \omega\tau_2 + \phi_1(t)/2 - \phi_1(t+\tau_2)/2]\right\} \\ &\quad + ir_2t_3E_6(B,t+\Delta t_z^B)\exp\left\{i[\phi_1(t+\Delta t_z^B)/2 + \phi_2(t+\Delta t_z^B)/2 + \omega(\tau_2 - \Delta t_z^B)\right. \\ &\quad \left. - k_3(z,t+\tau_2)(z-A) - \phi_1(t+\tau_2)/2]\right\} \\ &\quad + it_2E_1(A,t+\Delta t_z^B + \Delta t_B^A)\exp\left\{i[\phi_1(t+\Delta t_z^B + \Delta t_B^A)/2 - \phi_1(t+\tau_2)/2\right. \\ &\quad \left. - k_3(z,t+\tau_2)(z-A) + \omega(\tau_2 - \Delta t_z^B - \Delta t_B^A)]\right\}\ .\end{aligned} \qquad \text{(A.20)}$$

APPENDIX A.

Since cavity 2 is linear, $\frac{\partial k_2}{\partial t} = 0$ and $\phi_2(t) = \phi_2 = \omega\tau_2$. At $z = B$, $\Delta t_z^B = 0$ and using $\Delta t_B^A = \frac{\tau_2}{2}$, the first term in the argument of the exponential function is found to be

$$\phi_2 - \phi_1(t)/2 - \phi_1(t+\tau_2)/2 = \phi_2 - \frac{\tau_2}{2}\frac{\partial\overline{\phi_1}(t)}{\partial t} . \tag{A.21}$$

The second and the third term in the argument of the expontial function are

$$\begin{aligned} & \phi_1(t)/2 + \phi_2 + \omega\tau_2 - k_3(B, t+\tau_2)d_2 - \phi_1(t+\tau_2)/2 \\ = \;& \phi_2 - \frac{\tau_2}{2}\frac{\partial\overline{\phi_1}(t)}{\partial t} \\ \simeq \;& \phi_2 , \end{aligned} \tag{A.22}$$

$$\begin{aligned} & \phi_1(t+\frac{\tau_2}{2})/2 - \phi_1(t+\tau_2)/2 - k_3(B, t+\tau_2)d_2 - \omega\tau_2/2 \\ = \;& -\frac{\tau_2}{4}\frac{\partial\overline{\phi_1}(t)}{\partial t} \\ \simeq \;& 0. \end{aligned} \tag{A.23}$$

Therefore, the equation for E_3 can be written as

$$\begin{aligned} & \tau_2\frac{\partial E_3(B,t)}{\partial t} + \{1 - r_2 r_3 e^{i\phi_2}\}E_3(B,t) \\ = \;& it_2\left\{E_1(A,t) + \frac{\tau_2}{2}\frac{\partial E_1(A,t)}{\partial t}\right\} + ir_2 t_3 E_6(B,t)e^{i\phi_2} , \end{aligned} \tag{A.24}$$

Likewise, the equation for E_4 has the following form

$$\begin{aligned} & \tau_2\frac{\partial E_4(A,t)}{\partial t} + \{1 - r_2 r_3 e^{i\phi_2}\}E_4(A,t) \\ = \;& it_3\left\{E_6(B,t) + \frac{\tau_2}{2}\frac{\partial E_6(B,t)}{\partial t}\right\}e^{i\phi_2} + it_2 r_3 E_1(A,t)e^{i\phi_2} . \end{aligned} \tag{A.25}$$

Evaluating E_1 at $z = A$ and E_2 at $z = 0$ and using the same approximations as before, E_1 and E_2 are found to be govened by the following equations:

$$\begin{aligned} & \overline{\tau_1}\frac{\partial E_1(A,t)}{\partial t} + \{1 - r_1 r_2 e^{i\overline{\phi_1}(t)}\}E_1(A,t) \\ = \;& ir_1 t_2 E_4(A,t)e^{i\overline{\phi_1}(t)} + it_1 E_{i1}(t + \overline{\tau_1}/2). \end{aligned} \tag{A.26}$$

$$\begin{aligned}
& \overline{\tau_1}\frac{\partial E_2(0,t)}{\partial t} + \{1 - r_1 r_2 e^{i\overline{\phi_1}(t)}\}E_2(0,t) \\
= \; & it_2 E_4(A, t + \overline{\tau_1}/2)e^{i\overline{\phi_1}(t)} + it_1 r_2 E_{i1}(t)e^{i\overline{\phi_1}(t)} \\
= \; & it_2 \left\{ E_4(A,t) + \frac{\overline{\tau_1}}{2}\frac{\partial E_4(A,t)}{\partial t} \right\} e^{i\overline{\phi_1}(t)} + it_1 r_2 E_{i1}(t)e^{i\overline{\phi_1}(t)}. \qquad \text{(A.27)}
\end{aligned}$$

The set of coupled equations (A.17) to (A.18) and (A.24) to (A.27) model the system of two nonlinear Fabry-Perot cavities.

REFERENCES

[1] S.L.McCall, H.M.Gibbs, G.G.Chruchill, and T.N.C.Venkatesan, "Optical transistor and bistability," *Bull. Am. Phys. Soc.*, **20**, p. 636, 1975.

[2] S. D. Smith, "On the Physical Limits of Digital Optical Switching and Logic Elements," *Bell Syst. Tech. J.*, **61**, pp. 1975–1993, 1982.

[3] J.L.Jewell, M.C.Rushford, and H.M.Gibbs, "Use of a single nonlinear Fabry-Perot etalon as optical logic gates," *Appl. Phys. Lett.*, **44**, no. 5, pp. 172–174, 1984.

[4] D.A.B.Miller, D.S.Chemla, and T.C.Damen, "Novel Hybrid optically bistable switch: The quantum well self-electro-opcic effect device," *Appl. Phys. Lett.*, **45**, no. 1, pp. 13–15, 1984.

[5] A.L.Lentine and H.S.Hinton, "Symmetric self-electro-opcic effect device: Optical set-reset latch," *Appl. Phys. Lett.*, **52**, no. 17, pp. 1419–1421, 1988.

[6] J.L.Jewell, A.Scherer, S.L.McCall, A.C.Gossard, and J.H.English, "GaAs-AlAs monolithic microresonator arrays," *Appl. Phys. Lett.*, **51**, no. 2, pp. 94–96, 1987.

[7] H.M.Gibbs, S.S.Tarng, and J.K.Jewell, "Room-temperature excitonic optical bistability in GaAs etalons," *Postdeadline paper FL6 in Conference on laser and electro-optics technical digest*, 1982.

[8] D.A.B.Miller, A.C.Gossard, and W.Wiegmann, "Optical bistability due to increasing absorption," *Opt. Lett.*, no. 9, pp. 162–164, 1984.

[9] D.A.B.Miller, "Optical bistability and differential gain resulting from absorption increasing with excitation," *J. Opt. Soc. of Am. B*, **1**, no. 6, pp. 857–864, 1984.

[10] H. M. Gibbs, *Progress toward practical optical bistable devices.* Quantum Electronic, 1979.

REFERENCES

[11] N.Peyghambarian, H.M.Gibbs, M.C.Rushford, D.Sarid, and D.A.Weinberg, "Experimental and theoretical investigations of the biexciton optical nonlinearity and bistability in CuCl," *J. Opt. Soc. of Am.*, **73**, p. 1863, 1983.

[12] M.Dagenais and W.F.Sharfin, "Optical hysteresis in fast transient experiments near the band gap of cadium sulfide," *Appl. Phys. Lett.*, **45**, p. 210, 1984.

[13] G.R.Olbright, N.Peyghambarian, H.M.Gibbs, H.A.Macleod, and F. Milligen, "Microsecond room-temperature optical hysteresis and crosstalk studies in ZnS and ZnSe interference filters with visible light and milliwatt powers," *Appl. Phys. Lett.*, **45**, p. 1031, 1984.

[14] J.G.H.Mathew, D.Craig, and A.Miller, "Optical switching in a CdHgTe etalon at room temperature," *Appl. Phys. Lett.*, **46**, p. 128, 1985.

[15] J. E. Midwinter, "Digital Optics, Smart Interconnect or Optical Logics?," *Phys. Tech.*, **19**, pp. 101–108, 1988.

[16] S. D. Smith, "Optical Bistability, Photonic Logic, and Optical Computation," *Appl. Opt.*, **25**, pp. 1550–1564, 1986.

[17] A.Huang, "Architectural consideration involved in the design of an optical digital computer," *Proc. IEEE*, **72**, p. 780, 1984.

[18] H. S. Stone, "Parallel Processing with the Perfect Shuffle," *IEEE Trans. Comput.*, **C-3**, p. 153, 1971.

[19] J. W. Goodman, "Optical Interconnections for VLSI Systems," *Proc. IEEE*, **72**, p. 850, 1984.

[20] M. E. Marhic, "Combinational Star Couplers for Single-Mode Optical Fibers," *FOC/LAN*, **84**, p. 175, 1984.

[21] G. Eichmann, "Compact Optical Generalized Perfect Shuffle," *Appl. Opt.*, **26**, pp. 1167–1169, 1987.

[22] K. H. Brenner, "Optical implementations of Symbolic Substitution," *J. Opt. Soc. of Am. A*, **1**, p. 1292, 1984.

[23] D. A. Miller, D. S. Chemla, and T. C. Damen, "Novel hybrid optially bistable switch: The quantum well self-electro-optic effect device," *Appl. Phys. Lett.*, **45**, no. 1, pp. 13–15, 1984.

[24] P.W.Smith, W.J.Tomlinson, P.J.Maloney, and J.P.Hermann, "Experimental studies of a nonlinear interface," *IEEE J. Quantum Electron*, **QE-17**, pp. 340–348, 1978.

[25] P.W.Smith, J.P.Hermann, W.J.Tomlinson, and P.J.Maloney, "Optical bistability at a nonlinear interface," *Appl. Phys. Lett.*, **35**, p. 846, 1979.

[26] N.G.Basv, "Methods of realization of an optical processor with variable operators," *Sov. J. Quantum Elec.*, **8**, pp. 307–312, 1978.

[27] A.Huang, Y.Tsunoda, J.W.Goodman, and S.Ishihar, "Optical compution using residue arithmetic," *Appl. Opt.*, **18**, pp. 149–162, 1979.

[28] K. C. Ho, "Coupling of orthogonal polarization states in a nonlinear birefringent cavity," *Appl. Opt.*, **29**, pp. 206–209, 1990.

[29] A.D.Lloyd, "Polarisation optical bistability in nematic liquid crystals," *Opt. Comm.*, **64**, pp. 302–306, 1987.

[30] A. Korpel and A. Lohmann, "Polarization and optical bistability," *Letter to the Editor,Applied Optics*, **25**, no. 10, pp. 1528–1529, 1986.

[31] Lohmann, "private communication,".

[32] S.S.Tarng, K.Tai, J.L.Jewell, H.M.Gibbs, A.C.Gossard, and S.L.Macall.., "External off and on switching of a bistable optical device," *Appl. Phys. Lett.*, **40**, p. 205, 1982.

[33] M. Born and E. Wolf, *Principle of Optics.* 1970.

[34] D. C. Hutchings, A. D. Lloyd, I. Janossy, and B. S. Wherrett, "Theory of optical bistability in metal mirrored Fabry-Perot cavities containing thermo-optic materials," *Optics Communications*, **61**, no. 5, pp. 345–350, 1987.

[35] I. F. Stower and H. G. Patton, "Cleaning Optical Surfaces," *SPIE*, **140**, pp. 16–31, 1978.

[36] J. Cognard, *Alignment of nematic liquid crystals and their mixtures.* Gordon and Breach Science Publishers, 1982.

[37] P.G.deGennes, *The Physics of Liquid Crystals.* Clarendon Press, 1975.

[38] S. Puang-ngern, *Nonlinear Optical Effects in Nematic Liquid Crystals.* PhD thesis, Virginia Polytechnic Institute and State University, 1985.

[39] T.Bischofberger and Y.R.Shen, "Transient behavior of a nonlinear Fabry-Perot," *Appl. Phys. Lett.*, **32**, p. 156, 1978.

[40] T.Bischofberger and Y.R.Shen, "Theoretical and experimental study of the dynamic behavior of a nonlinear Fabry-Perot interferometer," *Phys. Rev. A*, **19**, p. 169, 1979.

REFERENCES

[41] J.A.Goldstone and E.M.Garmire, "On the dynamic response of nonlinear Fabry-Perot interferometers," *IEEE J. Quantum Electron*, **QE-17**, no. 3, pp. 366–374, 1981.